Nuclear Magnetic Resonance and Molecular Orbital Studies of the Solvent and Substituent Dependence of the Internal Rotational Potentials in Some Symmetrically Fluorinated Benzyl Fluorides

by

Robert W. Schurko

A Thesis

Submitted to the Faculty of Graduate Studies

in Partial Fulfilment of the Requirements for

the Degree of

MASTER OF SCIENCE

Department of Chemistry

University of Manitoba

Winnipeg, Manitoba, Canada

August 1994

ISBN 0-315-99061-9

Name Robert Schurko

Dissertation Abstracts International is arranged by broad, general subject categories. Please select the one subject which most nearly describes the content of your dissertation. Enter the corresponding four-digit code in the spaces provided.

Chemistry, Physical
SUBJECT TERM

0494
SUBJECT CODE

U·M·I

Subject Categories

THE HUMANITIES AND SOCIAL SCIENCES

COMMUNICATIONS AND THE ARTS
Architecture 0729
Art History 0377
Cinema 0900
Dance 0378
Fine Arts 0357
Information Science 0723
Journalism 0391
Library Science 0399
Mass Communications 0708
Music 0413
Speech Communication 0459
Theater 0465

EDUCATION
General 0515
Administration 0514
Adult and Continuing 0516
Agricultural 0517
Art 0273
Bilingual and Multicultural 0282
Business 0688
Community College 0275
Curriculum and Instruction 0727
Early Childhood 0518
Elementary 0524
Finance 0277
Guidance and Counseling 0519
Health 0680
Higher 0745
History of 0520
Home Economics 0278
Industrial 0521
Language and Literature 0279
Mathematics 0280
Music 0522
Philosophy of 0998
Physical 0523
Psychology 0525
Reading 0535
Religious 0527
Sciences 0714
Secondary 0533
Social Sciences 0534
Sociology of 0340
Special 0529
Teacher Training 0530
Technology 0710
Tests and Measurements 0288
Vocational 0747

LANGUAGE, LITERATURE AND LINGUISTICS
Language
- General 0679
- Ancient 0289
- Linguistics 0290
- Modern 0291

Literature
- General 0401
- Classical 0294
- Comparative 0295
- Medieval 0297
- Modern 0298
- African 0316
- American 0591
- Asian 0305
- Canadian (English) 0352
- Canadian (French) 0355
- English 0593
- Germanic 0311
- Latin American 0312
- Middle Eastern 0315
- Romance 0313
- Slavic and East European 0314

PHILOSOPHY, RELIGION AND THEOLOGY
Philosophy 0422
Religion
- General 0318
- Biblical Studies 0321
- Clergy 0319
- History of 0320
- Philosophy of 0322

Theology 0469

SOCIAL SCIENCES
American Studies 0323
Anthropology
- Archaeology 0324
- Cultural 0326
- Physical 0327

Business Administration
- General 0310
- Accounting 0272
- Banking 0770
- Management 0454
- Marketing 0338

Canadian Studies 0385
Economics
- General 0501
- Agricultural 0503
- Commerce-Business 0505
- Finance 0508
- History 0509
- Labor 0510
- Theory 0511

Folklore 0358
Geography 0366
Gerontology 0351
History
- General 0578
- Ancient 0579
- Medieval 0581
- Modern 0582
- Black 0328
- African 0331
- Asia, Australia and Oceania 0332
- Canadian 0334
- European 0335
- Latin American 0336
- Middle Eastern 0333
- United States 0337

History of Science 0585
Law 0398
Political Science
- General 0615
- International Law and Relations 0616
- Public Administration 0617

Recreation 0814
Social Work 0452
Sociology
- General 0626
- Criminology and Penology ... 0627
- Demography 0938
- Ethnic and Racial Studies 0631
- Individual and Family Studies 0628
- Industrial and Labor Relations 0629
- Public and Social Welfare 0630
- Social Structure and Development 0700
- Theory and Methods 0344

Transportation 0709
Urban and Regional Planning 0999
Women's Studies 0453

THE SCIENCES AND ENGINEERING

BIOLOGICAL SCIENCES
Agriculture
- General 0473
- Agronomy 0285
- Animal Culture and Nutrition 0475
- Animal Pathology 0476
- Food Science and Technology 0359
- Forestry and Wildlife 0478
- Plant Culture 0479
- Plant Pathology 0480
- Plant Physiology 0817
- Range Management 0777
- Wood Technology 0746

Biology
- General 0306
- Anatomy 0287
- Biostatistics 0308
- Botany 0309
- Cell 0379
- Ecology 0329
- Entomology 0353
- Genetics 0369
- Limnology 0793
- Microbiology 0410
- Molecular 0307
- Neuroscience 0317
- Oceanography 0416
- Physiology 0433
- Radiation 0821
- Veterinary Science 0778
- Zoology 0472

Biophysics
- General 0786
- Medical 0760

EARTH SCIENCES
Biogeochemistry 0425
Geochemistry 0996
Geodesy 0370
Geology 0372
Geophysics 0373
Hydrology 0388
Mineralogy 0411
Paleobotany 0345
Paleoecology 0426
Paleontology 0418
Paleozoology 0985
Palynology 0427
Physical Geography 0368
Physical Oceanography 0415

HEALTH AND ENVIRONMENTAL SCIENCES
Environmental Sciences 0768
Health Sciences
- General 0566
- Audiology 0300
- Chemotherapy 0992
- Dentistry 0567
- Education 0350
- Hospital Management 0769
- Human Development 0758
- Immunology 0982
- Medicine and Surgery 0564
- Mental Health 0347
- Nursing 0569
- Nutrition 0570
- Obstetrics and Gynecology .. 0380
- Occupational Health and Therapy 0354
- Ophthalmology 0381
- Pathology 0571
- Pharmacology 0419
- Pharmacy 0572
- Physical Therapy 0382
- Public Health 0573
- Radiology 0574
- Recreation 0575
- Speech Pathology 0460
- Toxicology 0383

Home Economics 0386

PHYSICAL SCIENCES
Pure Sciences
Chemistry
- General 0485
- Agricultural 0749
- Analytical 0486
- Biochemistry 0487
- Inorganic 0488
- Nuclear 0738
- Organic 0490
- Pharmaceutical 0491
- Physical 0494
- Polymer 0495
- Radiation 0754

Mathematics 0405
Physics
- General 0605
- Acoustics 0986
- Astronomy and Astrophysics 0606
- Atmospheric Science 0608
- Atomic 0748
- Electronics and Electricity 0607
- Elementary Particles and High Energy 0798
- Fluid and Plasma 0759
- Molecular 0609
- Nuclear 0610
- Optics 0752
- Radiation 0756
- Solid State 0611

Statistics 0463

Applied Sciences
Applied Mechanics 0346
Computer Science 0984
Engineering
- General 0537
- Aerospace 0538
- Agricultural 0539
- Automotive 0540
- Biomedical 0541
- Chemical 0542
- Civil 0543
- Electronics and Electrical 0544
- Heat and Thermodynamics ... 0348
- Hydraulic 0545
- Industrial 0546
- Marine 0547
- Materials Science 0794
- Mechanical 0548
- Metallurgy 0743
- Mining 0551
- Nuclear 0552
- Packaging 0549
- Petroleum 0765
- Sanitary and Municipal 0554
- System Science 0790

Geotechnology 0428
Operations Research 0796
Plastics Technology 0795
Textile Technology 0994

PSYCHOLOGY
General 0621
Behavioral 0384
Clinical 0622
Developmental 0620
Experimental 0623
Industrial 0624
Personality 0625
Physiological 0989
Psychobiology 0349
Psychometrics 0632
Social 0451

NUCLEAR MAGNETIC RESONANCE AND MOLECULAR ORBITAL STUDIES OF THE SOLVENT AND SUBSTITUENT DEPENDENCE OF THE INTERNAL ROTATIONAL POTENTIALS IN SOME SYMMETRICALLY FLUORINATED BENZYL FLUORIDES

BY

ROBERT W. SCHURKO

A Thesis submitted to the Faculty of Graduate Studies of the University of Manitoba in partial fulfillment of the requirements for the degree of

MASTER OF SCIENCE

To my parents

Acknowledgements

I would like to thank Dr. Ted Schaefer for his encouragement, patience, guidance and helpful criticisms during my stay in this lab and over the course of writing this thesis.

I thank Mr. Rudy Sebastian for the many long hours he spent teaching me to use the NMR spectrometer and the large number of computer programs necessary for this work. I also appreciate the advice he has given me on many matters over the past few years.

I also thank Mr. Kirk Marat for his excellence in maintaining the Bruker AM300 spectrometer, which enabled us to obtain many fine high resolution spectra. I thank Jim Mansfield for his preliminary work on benzyl fluorides and for his advice on the synthesis of these compounds.

I would like to thank Dr. Frank Hruska and Dr. Jim Peeling for their insightful comments and criticisms, and for reading this thesis very thoroughly at an unprecedented pace.

I am grateful to my friends and colleagues Guy Bernard, Jeremy Kunkel, Randy Babiuk, Dawn Kardash, Leo Spyracopoulos, Scott Kroeker and Paul Hazendonk for both support and encouragement, as well as many useful and interesting discussions. I thank my friends at the Graduate Students' Association who not only provided many words of encouragement, but a great number of thought provoking discussions.

Finally, I am most in debt to my parents and to my family, who have unfalteringly supported and encouraged me over my six years here at the University of Manitoba. Their tolerance of my bizarre daily schedule is also greatly appreciated.

I would also like to thank the Natural Sciences and Engineering Research Council of Canada and the University of Manitoba for financial support.

Table of Contents

List of Tables

List of Figures

Abstract

^{1}H, ^{13}C and ^{19}F NMR spectra of 2,6-difluorobenzyl fluoride (**2**), 3,5-difluorobenzyl fluoride (**3**) and 4-fluorobenzyl fluoride (**4**) are thoroughly analyzed in acetone-d6 and CS_2. Using a simple hindered-rotor model, the two-fold barrier to rotation about the C_{sp2}-C_{sp3} bond in 3,5-difluorobenzyl fluoride is deduced from ^{6}J(H,CH) and ^{6}J(H,CF). The barrier is 1.9(2) kJ mol^{-1} in acetone-d6 and 3.8(2) kJ mol^{-1} in CS_2. The stable conformer has the benzylic C-F bond in the plane parallel to the phenyl group. The long-range coupling between the *para*-carbon and benzylic fluorine, ^{5}J(C,CF), yields two-fold rotational barriers of 6.4(3) kJ mol^{-1} in acetone-d6 and 5.4(3) kJ mol^{-1} in CS_2 for 2,6-difluorobenzyl fluoride. The conformer of lowest energy is one in which the C-F bond is in the plane perpendicular to the benzene moiety. The orthobenzylic coupling, ^{4}J(H,CH), is used to calculate the internal potentials in 4-fluorobenzyl fluoride. The barriers are 3.6(2) kJ mol^{-1} and 1.9(2) kJ mol^{-1} in acetone-d6 and CS_2, respectively. The minimum energy conformer has the C-F bond perpendicular to the plane of the aromatic ring. The presence of fluorine substituents has profound effects on barrier size and shape in benzyl fluoride systems. Rotational barriers are also strongly dependent on the nature of the surrounding medium.

High-level *ab initio* molecular orbital calculations (Hartree-Fock and second-order Møller-Plesset theory) are used to predict the rotational barriers for **2**, **3**, and **4**, as well as benzyl fluoride (**1**). Molecular orbital

calculations on the free molecules predict the parallel conformer as the most stable for **1**, **3**, and **4**. The perpendicular conformer is the most stable for **2**. Reaction field theory is applied to examine the dielectric solvent effects on these systems at the 6-31G* level. Qualitatively, there is remarkable correspondence between the theoretical calculations and experimental findings.

Coupling constants calculated at the INDO level of approximation are reported for **1** to **4**. Calculated couplings qualitatively agree with experimental findings. Mechanisms of some of the long-range couplings are discussed.

1. Introduction

Introduction

1.1 Internal rotational potentials in molecules

The nature of the hindering barrier to internal rotation in molecules is of great interest to molecular spectroscopists and theorists alike. Internal rotational potentials vary in size and shape. The size of an internal rotational barrier can vary from a few J mol^{-1} (free rotation) to hundreds of kJ mol^{-1} (rigid structure, essentially no rotation). Potential energy curves for internal rotation can be symmetrical or asymmetrical, and may possess several minima and maxima. The method used by an experimentalist to determine the internal rotational potential is dependent upon barrier size, molecular structure, and the approximations made in the physical model applied.

A number of methods have been used for the investigation of barrier sizes and rotational isomerism. These include spectroscopic methods such as infrared, microwave, Raman, nuclear magnetic resonance, and electron spin resonance spectroscopy; diffraction methods such as electron diffraction and neutron scattering; relaxation methods; and classical methods such as dipole moment and thermodynamic studies.[1,2] Purely theoretical studies have been conducted as well, ranging from highly parameterized semi-empirical methods to high-level *ab initio* computations.[3,4,5]

There are only a few experimental methods currently used which consistently allow the accurate determination of small internal rotational

potentials (< 10 kJ mol^{-1}) and minimum energy conformations. High resolution microwave spectroscopy, which is limited to the gas phase, has been used for the determination of rotational barriers in such systems as phenols,[6] methyl-pyrimidines,[7] and anisoles.[8] This technique is restricted to fairly simple systems, since microwave spectra become quite difficult to interpret as the complexity of the molecule increases. Several approximations are made in this approach which may result in unforeseeable errors in the barrier size.[9,13]

Supersonic-jet, mass-resolved, excitation spectroscopy (MRES) has evolved as an important technique for determining the minimum energy conformations in both the ground and excited states of molecules (actual barrier sizes are not determined). Bernstein and Seeman have investigated stable conformers and low frequency modes in alkyl-substituted pyridines,[10] benzylamines,[11] and benzyl alcohols,[12] as well as numerous other substituted aromatic species. This method is successful for a number of reasons. First, the supersonic expansion process causes such low temperatures that most conformational changes occurring rapidly at room temperature or at temperatures lower than those used in DNMR are halted. Second, the low temperature allows for sharply resolved spectral features. Finally, the time scale of optical absorption (required for this technique) is shorter than the time scale of molecular motion.[12] Thus, molecules are observed in a relatively isolated state, at temperatures near 0 K.

1.2 Determination of internal rotational potentials with NMR: The J-method

Chemists are most often interested in the properties of molecules in the liquid phase, since most organic reactions and spectroscopic measurements are performed in this state. The internal rotational potential and minimum energy conformers for many molecules depend on the properties of the surrounding medium; thus, experiments must be conducted which take the nature of the liquid phase into account.

Nuclear magnetic resonance can be easily used to study fairly large, complex systems in solution. Dynamic NMR spectroscopy (DNMR) is a useful technique for the determination of rotational barriers in relatively complex molecules. In this method, the rate of conversion between conformers is determined as a function of temperature. However, the range of barriers studied with DNMR ranges from 15 to 120 kJ mol^{-1}. This excludes molecules with small rotational barriers and rapidly interconverting conformers, which are undetectable on the DNMR time scale (the dephasing process becomes too rapid to measure).

The *J*-method[13] has been used successfully in a number of molecules to determine internal rotational potentials ranging from 0.5 - 12 kJ mol^{-1}.[14] This technique relies on the accurate measurement of long-range nuclear spin-spin couplings in solution by high-resolution NMR spectroscopy. These couplings are believed to depend on a σ-π mechanism[15,16] in which π-electrons polarize the σ-electrons, resulting in the transmission of spin state

information from the π system to a nucleus.[17] There is no π-electron density at the nuclei in the aromatic system, since *p*-orbitals have nodes at the nuclei; the contact contribution to *J* vanishes for *p*-orbitals.

Coupling constants are also transmitted via the σ-mechanism and through-space mechanism. The σ-mechanism involves transmission of spin state information via the σ-bond framework of the molecule. The through-space mechanism involves transmission of coupling information via the overlap of the wave functions of spatially proximate bonds carrying the nuclei.[18,19] For long-range couplings in aromatic systems the σ-π coupling mechanism is dominant; however, σ-electron contributions to four- and five-bond couplings cannot be neglected.[17,20]

For benzylic compounds, couplings over *n* formal bonds are measured between a nucleus at the α-position on the sidechain and nuclei located in the aromatic system (i.e. ring carbons and other aromatic substituents). INDO FPT MO calculations predict a $\sin^2\theta$ dependence for ${}^6J$,[25] where θ is the angle by which the α bond twists out of the plane of the aromatic ring. The observed coupling and the angular dependence are related by (1.1)

$$ {}^6J = {}^6J_0 + {}^6J_{90}\langle\sin^2\theta\rangle \qquad \textbf{(1.1)} $$

${}^6J_0$, the coupling at $\theta = 0°$, is negligible.[21] If ${}^6J_{90}$ is known, the barrier height and the minimum energy conformer can be determined from the ratio ${}^6J/{}^6J_{90}$.

The function describing the internal rotational potential in benzyl and benzal compounds is usually a two-fold, symmetrical function (over a period of 2π). The four possible low energy forms of benzylic compounds are pictured below (for finite barriers)

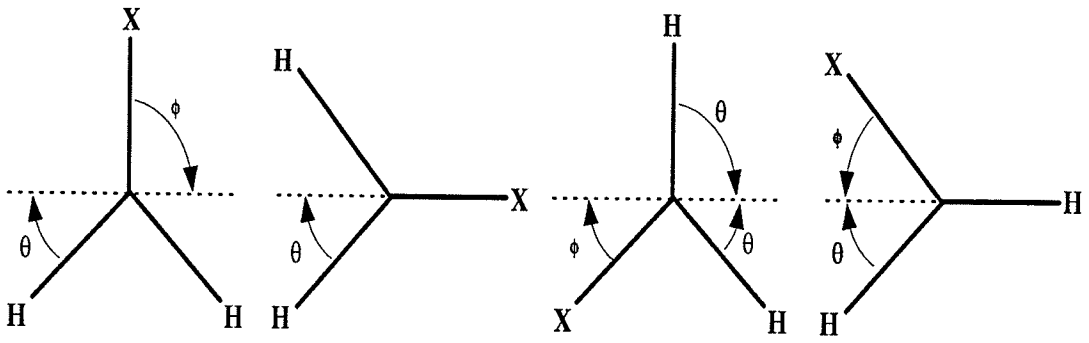

(A)	(B)	(C)	(D)
$\theta = 30°$	$\theta = 60°$	$\theta = 30°, 90°$	$\theta = 0°, 60°$
$\phi = 90°$	$\phi = 0°$	$\phi = 30°$	$\phi = 60°$
$0.5 \geq \sin^2\theta \geq 0.25$	$0.75 \geq \sin^2\theta \geq 0.5$	$0.625 \geq \sin^2\theta \geq 0.5$	$0.5 \geq \sin^2\theta \geq 0.375$

where angles θ and ϕ are related by

$$\langle \sin^2\theta \rangle = 0.75 - 0.5\langle \sin^2\phi \rangle \qquad \textbf{(1.2)}$$

The dashed line represents the plane of the aromatic ring.

For compounds of this nature, a function describing the internal rotational potential can be written in the form of a Fourier series

$$V(\phi) = \sum_{n=0}^{\infty} a_n \sin(n\phi) + \sum_{n=0}^{\infty} b_n \cos(n\phi) \qquad \textbf{(1.3)}$$

Since the potential function is even, the complete potential function can be represented by the cosine term on the right hand side. The function can be

rewritten so that $V(\phi) = 0$ when $\theta = 0°$, to give the familiar equation

$$V(\phi) = \sum_{n=0}^{\infty} \frac{V_n}{2} [1 - \cos(n\phi)] \qquad \textbf{(1.4)}$$

Since symmetrical benzylic systems have two-fold potentials, one can write

$$V(\phi) = \frac{V_2}{2} [1 - \cos(2\phi)] = V_2 [\sin^2\phi] \qquad \textbf{(1.5)}$$

Asymmetric potentials will have other nonzero terms, which are often difficult to ascertain; however, the potential will be better defined if most of the coefficients are determined.

The hindered rotor treatment allows one to write $\langle \sin^2\theta \rangle$ as a function of the potential height, V_2; here, $\langle \sin^2\theta \rangle$ is the quantum statistical average over hindered rotor states for $\sin^2\theta$.

$$\langle \sin^2\theta \rangle = \frac{\sum_{m=1} \exp(-E_m/RT) \langle \psi_m | \sin^2\theta | \psi_m \rangle}{\sum_{m=1} \exp(-E_m/RT)} \qquad \textbf{(1.6)}$$

In a free rotor basis, ψ_m are the hindered rotor states and E_m are the corresponding energies. The quantum mechanical solution to the hindered rotor problem involves solving the eigenvalue problem

$$\left\{ \frac{\hbar^2}{2I} \frac{d^2}{d\theta^2} + \frac{V_0}{2} (1 - \cos 2\theta) \right\} \psi_m = E_m \psi_m \qquad \textbf{(1.7)}$$

where V_0 is the magnitude of a two-fold barrier to rotation, and I is the reduced moment of inertia of the molecule. Solving this equation yields E_m

and ψ_m, which are used to calculate $\langle \sin^2\theta \rangle$ for each state. The ensemble average is then computed from (1.6).[22] The first twenty-one free rotor states provide an adequate basis at ambient temperatures, but can be easily extended. V_2 can be drawn up by computer as functions of T, I, and $\langle \sin^2\theta \rangle$. At constant T and values of V_2 up to 20 kJ mol^{-1}, examination of hindered rotor tables reveals that $\langle \sin^2\theta \rangle$ values are insensitive to values of I (from 0.5 to 4.0 $\times$ 10^{-38} g cm^{-2}).[13]

The J-method commonly uses measured ^6J between α-protons and aromatic *para*-protons. INDO FPT MO calculations predict a $\sin^2\theta$ dependence for a number of other long range couplings. Couplings between a *para*-position nucleus and an α-substituent [such as ^6J(H,CF), ^5J(^{13}C,CF), ^5J(^{13}C,CH), ^6J(F,^{13}C) and ^6J(H,^{13}C)][23] have been used successfully for the determination of rotational barriers. [The convention in this thesis is to list the coupling as ^nJ(aromatic nucleus, benzylic nucleus)]. Also, some angular dependencies are known for couplings from *ortho*- and *meta*-positions to the sidechain. These couplings take on different functional forms which include terms that take σ-contributions into account. In some cases, these couplings can also be used as a monitor of barrier size.[24] (See discussion).

1.3 Previous studies on benzyl fluorides and other benzyl compounds

Determination of the internal rotational potentials and conformation of the sidechain in benzyl compounds present great challenges to both chemists and physicists. Today, the barriers and conformations in even the most simple systems are not known definitely. Numerous studies on benzyl compounds have been undertaken over the past twenty-five years. This brief survey of the literature will focus predominantly on benzyl halides, with an emphasis on internal rotation, electronic structure, substituent effects and coupling mechanisms in benzyl fluoride and its substituted derivatives.

a) Early studies on hindered rotation in benzyl compounds

Hindered rotation in benzyl halides was initially described by Cupas et al. Low temperature DNMR experiments were conducted on 2,4-di-*t*-butyl-6-methylbenzyl halides (X = Cl, Br, and I).[25] This study showed that these benzyl halides have substantial rotational barriers in solution,

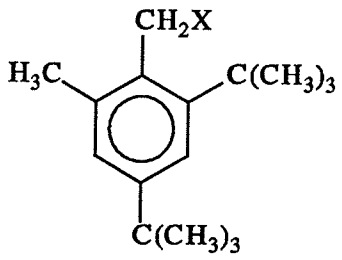

which increase with increasing atomic weight of X. The low energy

conformer was determined to be one in which one of the benzylic protons eclipses the large *t*-butyl group (see conformer (**D**) above). This method was unsuccessful for X=F, OH. A large number of papers followed on many benzyl compounds, including benzyl halides,[26,27] cyanides,[28,29] and neopentylbenzenes.[30]

Schaefer and co-workers conducted one of the earliest conformational studies on a sterically hindered benzyl fluoride derivative, 2,6-dichloro-benzyl fluoride.[31] Signs and magnitudes of long-range coupling constants were related to the conformation of the sidechain. It was assumed by Schaefer that the most stable conformation is one in which the benzylic C-F bond is perpendicular to the nodal plane of the aromatic system (conformer (**A**)), such that steric interactions between the benzylic fluorine and the *ortho*-Cl nuclei were minimized. From the observed $^{6}J_{p}$(H,CH), it was suggested that the benzylic C-H bonds are polarized by the electronegative fluorine atom, thereby decreasing electron density near the proton. In terms of hyperconjugative effects, spin-state information is then less efficiently transferred between the protons and the aromatic π-system. This prompted a study of the angular dependencies of long-range couplings between ring protons and sidechain protons and fluorine atoms in benzal compounds.[32] A study on the conformations of a series of 2,6-dichlorobenzyl compounds was also published at this time.[33]

b) *Internal rotational potentials, preferred conformations and electronic structure in benzyl fluorides*

Schaefer et al. extended their previous work with a study of the conformation of the fluoromethyl group in a number of chlorine-substituted derivatives.[34] 3,5-dichlorobenzyl fluoride was estimated to have a rotational barrier of 1.1 ± 0.2 kJ mol^{-1}, with an energy minimum at $\phi = 0°$ **(B)**. This study included full spectral characterization of the compounds, as well as INDO FPT MO calculations on couplings between the sidechain and ring protons in benzyl fluoride derivatives. It was hypothesized that the barrier is most likely a delicate balance between steric interactions, hyperconjugative effects, and dipole interactions between polarized bonds.

Beguin and co-workers confirmed that **(A)** is the stable conformer of 2,6-dichlorobenzyl fluoride from direct couplings obtained from nematic phase NMR.[35] The internal potential is estimated to lie in the range of 16.7 - 20.9 kJ mol^{-1}. A quadrupolar magnetic resonance study (deuterium relaxation) of substituted benzyl fluorides followed, in which Beguin and Dupeyre suggested that hydrogen bonding solvents and solvation of the benzylic fluorine atom can play a role in determining the preferred conformation of the molecule.[36] Further relaxation measurements on deuterated benzyl fluorides predict activation energies of 11.8 kJ mol^{-1} in neat solution, and 14.7 kJ mol^{-1} in diluted solution.[37]

Beguin and Gout-Mallaret attempted to predict the barrier size and preferential conformation of a number of *para*-substituted benzyl fluorides

(X = OH, OCH_3, CH_3, F, H, CF_3, and NO_2) using CNDO/2 and PCILO calculations.[38] The barriers calculated by this method range from 10.7 - 14.6 kJ mol^{-1}. The stable conformer in all cases was **(B)**. It was observed that the barrier size increases as the energy of the HOMO of X increases. The authors suggested that stabilization of the planar conformer results from increased conjugation between the benzylic fluorine in the plane and the *para*-substituent. The barrier size for benzyl fluoride, 12.3 kJ mol^{-1}, is very different from that estimated by Pople et al. (1.1 kJ mol^{-1}), who estimated the barrier from *ab initio* STO-3G calculations on planar and perpendicular confomers.[39] PCILO calculations on *ortho*-substituted benzyl fluorides predict the perpendicular conformation **(A)** as being the most stable. Barriers range from 16.3 - 18.4 kJ mol^{-1}. From low temperature Raman spectra (77 K), the barrier to rotation in the crystal is calculated to be 36.0 kJ mol^{-1}; the low energy conformer is at $\phi = 90°$. High-resolution NMR of 2,6-dichlorobenzyl fluoride at 250 MHz confirmed the findings of Schaefer et al.,[31] with the perpendicular conformer **(A)** as the most stable.

Shapiro examined the ^{13}C NMR shielding effects for α-substituted toluenes and 3-substituted propenes.[40] Downfield shifts (relative to the unsubstituted compound) were observed for the *para*-carbon for all of the benzyl compounds, suggesting a partial positive charge at this position resulting from loss of charge density. Shapiro suggested that this is the result of a π-inductive effect or conjugative electron withdrawal by the C-X

bond. The participation of no-bond resonance forms (hyperconjugative effect) may be an important factor in determining barrier size and low energy conformers in benzyl compounds.

Infrared and Raman spectra obtained for benzyl fluoride suggest that the molecule has C_1 symmetry, implying that neither **(A)** nor **(B)** exist in rigid forms in solution.[41] A broad, asymmetric band at 404 cm^{-1} indicates nearly free internal rotation about the C-C bond. This agrees with the low barriers for 3,5-dichlorobenzyl fluoride previously determined by Schaefer.[34]

An extensive study of benzyl fluoride by *ab initio* and molecular mechanics calculations, NMR, and electron gas diffraction (ED) was conducted by Abraham et al.[42] STO-3G *ab initio* calculations (no geometry optimization, using the ED geometry) with a relaxed C-C-F angle predict the 0° conformer as the most stable, with an energy barrier of 1.0 kJ mol^{-1}. The molecular mechanics program MODELS 2 predicts a barrier of 1.42 kJ mol^{-1} and a low energy conformer at $\phi = 60°$; however, the potential is extremely flat from 60° to 90°. From ED data, a rigid conformer is suggested to exist at $\phi = 52.3°$. Geminal coupling constants intimate either a preferred nonplanar conformation with a small barrier to rotation, or a single conformer at $\phi = 54°$.

Brownlee and Craik measured ^{19}F chemical shifts in *meta*- and *para*-substituted benzyl fluorides.[43] From plots of temperature against chemical shift, they were able to make some simple conformational interpretations.

When electron donating groups (EDG) are in the *para*-position, a consistent deshielding effect is observed for the benzylic fluorine; the opposite trend is noticed for electron withdrawing groups (EWG). *Ab initio* STO-3G calculations show that the energy difference between planar and perpendicular conformers varies with the *para*-substituent. This is attributed to *para* resonance effects. *Para*-EDG's enhance a hyper-conjugative acceptor interaction with the benzyl group; this interaction is maximized when the C-F bond is perpendicular to the aromatic plane (**E**). *Para*-EWG's favour an alternative hyperconjugative interaction, in which the C-F bond is parallel to the ring plane (**F**). These observations are supported by frontier molecular orbital theory[44] and a similar study on *para*-phenols.[45] These hyperconjugative effects are pictured below.

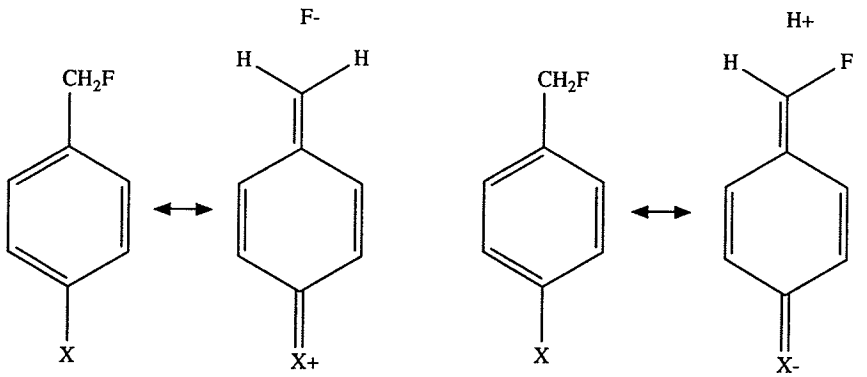

From comparison with substituent chemical shifts and STO-3G data, it is estimated that benzyl fluoride favours the orthogonal conformation (**A**) by approximately 1.7 kJ mol^{-1}. It is also suggested, from the hyperconjugative

arguments above, that *para* EDG's and EWG's stabilize the orthogonal and planar forms, respectively. The greatest contribution to the transmission of substituent effects seems to occur in the π-system. This assumption was reaffirmed by Happer and co-workers, in a study on substituent effects on 3- and 4-XCH_2-substituted fluorobenzenes.[46] Hyperconjugative interactions in benzyl fluoride and other benzyl compounds were also studied by UV photoelectron spectroscopy (UPS) and electron transmission spectroscopy (ETS).[47]

c) *Application of long-range spin-spin couplings to the determination of rotational barriers and low energy conformers in benzyl compounds*

Schaefer and co-workers published a series of studies on benzyl derivatives in the late 1970's. Schaefer's group applied the *J*-method to investigate the internal barriers and coupling mechanisms in *para*-fluorobenzyl compounds (X = CN, Cl, Br).[48] The ^6J(H,CH) and ^6J(F,CH) were used to predict the internal barriers. For *p*-fluorobenzyl cyanide, essentially free rotation was predicted, with a slight preference for the perpendicular conformer. The halides have minimum energy conformers at $\phi = 90°$. The barriers are 1.9 ± 0.8, 8.8 ± 1.7 and > 12.5 kJ mol^{-1} for X = CN, Cl and Br, respectively. ^6J(H,CH) is known to be transmitted through a σ-π mechanism; thus, barriers derived from this coupling are thought to be more reliable. ^6J(F,CH) may have additional σ-components; this coupling is also more sensitive to substituent perturbations. The aromatic C-F bond alters its double bond character in response to substituent (and solvent) perturbations.

This group also studied coupling constants between ring and sidechain fluorine nuclei in benzo, benzal and benzyl derivatives.[49] They determined that the σ-π mechanism is partially operative for $^6J_{90}$(F,CF); however, they concluded that this coupling will not be a useful conformational indicator unless the coupling mechanism can be precisely understood.

The conformational preferences of the benzylic fluorine in *para*-methylbenzyl fluoride and a number of derivatives were also determined by this group.[50] For *ortho*-dihalogen and *ortho*-dimethyl derivatives, barriers of greater than 16 kJ mol^{-1} are predicted, with stable conformers at $\phi = 90°$. For *meta*-disubstituted derivatives, barriers are estimated to be very low (in the order of 0.8 kJ mol^{-1}), with a preferred planar conformation. For unsubstituted *para*-methylbenzyl fluoride, the barrier is estimated to be 3.8 ± 1.3 kJ mol^{-1}, with the perpendicular conformer stable.

Adcock and Abeywickrema used ^5J(C,CF) to examine the conformational preference of the sidechain in benzyl fluoride, through comparison with some rigid model compounds.[51] It was found that ^5J(C,CF) is predominantly a manifestation of hyperconjugation involving the C-F bond (i.e. small σ-component). From the ^{13}C NMR of constrained angle compounds and several benzyl fluoride derivatives, a preferred conformation of $\phi = 49°$ is calculated for benzyl fluoride. The authors suggest essentially free rotation of the fluoromethyl group. Results for *ortho*-substituted compounds predict $\phi = 90°$ as the most stable conformation. These authors have synthesized a number of other rigid model compounds which may be of use in determining constrained angle couplings such as $^5J_{90}$(C,CF) and $^6J_{90}$(F,CF).[52,53]

d) Coupling mechanisms in benzyl fluorides

Long-range proton-fluorine couplings in benzyl fluoride, 4-fluoro-benzyl fluoride and other molecules were investigated theoretically by Contreras et al.[54] Investigations were carried out using partially restricted molecular orbital calculations at the INDO level. The π-components of the ^{n}J(H,CF) were found to have A + B $\sin^2\phi$ dependence. The couplings showed insensitivity to aromatic fluorine substituents.

Fluorine-fluorine couplings are potential conformational monitors in benzyl fluoride derivatives. Interbenzylic fluorine-fluorine couplings were studied theoretically (INDO FPT MO) and experimentally (^{19}F NMR) in bis(fluoromethyl)-arenes.[55] These couplings also exhibit a $\sin^2\phi$ dependence; thus, maximum couplings are found when the benzylic fluorines are perpendicular to the aromatic plane. Orthobenzylic ^{4}J(F,CF) have been studied by Rae et al.[56,57] Their angular dependence was examined through comparison with constrained compounds. In 2,6-difluorobenzyl fluoride, a stable conformer at $\phi = 90°$ is reported from an observed ^{4}J(F,CF) of 2.7 Hz. It is clear that the benzylic fluorine is not close to either of the *ortho*-fluorines, since through-space coupling would substantially increase the value of ^{4}J(F,CF).

e) Recent studies

Schaefer and co-workers studied solvent effects on internal potentials in benzyl fluoride.[58] *Ab initio* calculations at the STO-3G level predicted V_2 (kJ mol^{-1}) = (1.64 ± 0.04) $\sin^2\phi$, with the planar conformer as the low energy form. From ^5J(C,CF), it was determined that the perpendicular conformer is stabilized by 2 kJ mol^{-1} when going from nonpolar to polar solvents. INDO FPT MO calculations were used to investigate the angular dependencies of $^{4,5,6}J$ between aromatic and exocyclic nuclei.

Schaefer and co-workers examined the benzylic anomeric effect[59] in a series of benzyl compounds.[60] They found that the anomeric effect does not exist in benzyl fluoride. *Ab initio* calculations predict that the stable conformation is one in which the C-F bond is in the aromatic plane. From previous experimental data for benzyl fluoride, the authors suggest that the parallel conformation is preferred in CS_2. The perpendicular conformation is stabilized with increasing solvent polarity.

Seeman and Bernstein[12] used MRES to determine the minimum energy conformations of benzyl alcohol. The MRES spectra and rotational constants for benzyl fluoride are very similar to those for benzyl alcohol; Seeman suggested that benzyl fluoride may possess a similar minimum energy conformation at $\phi = 90°$. From hindered rotor calculations, the barrier for the ground state conformation of the benzyl alcohol is calculated to be 1.7 kJ mol^{-1}.

A low resolution microwave study (LRMW) was attempted for benzyl halides (X = F, Cl, Br, and I).[61] The benzyl fluoride spectrum had a vast number of low intensity transitions, and was therefore impossible to assign. A minimum energy conformation of 90° was predicted for the other three benzyl halides.

Celebre and co-workers measured large anisotropic dipolar couplings in benzyl chloride and benzyl fluoride dissolved in liquid crystal solvents of different polarity.[62,63] Barriers in benzyl fluoride are calculated as 0.3 ± 0.02 kJ mol^{-1} in nonpolar I52, and 1.5 ± 0.08 kJ mol^{-1} in polar ZLI1132, agreeing with general trends previously observed by Schaefer.[58] In both cases, the minimum energy conformation is $\phi = 90°$.

This study prompted Schaefer et al. to reexamine NMR data for benzyl fluoride and remeasure ^{n}J(C,CF) in a number of solvents.[23a] Potential sizes ranged from 0.7 - 3.2 kJ mol^{-1} when moving from nonpolar to polar solvents. In all solvents, the minimum energy conformer lies at $\phi = 90°$. From the barriers in solution, extrapolation to the vapour phase using a simple reaction field model gives an internal potential of 1.1(7) kJ mol^{-1}, with the energy minimum at 0°. *Ab initio* calculations using various basis sets predict barriers ranging from 1 - 4 kJ mol^{-1}, all with low energy conformations at 0° (C-F bond in plane).

Finally, the internal rotational potential and its solvent dependence in 3,5-dichlorobenzyl fluoride was reexamined.[64] ^{1}H and ^{19}F NMR spectra

were acquired in six solvents of varying polarity. Barriers range from 0.6 - 3.2 kJ mol^{-1} going from polar to nonpolar solvents. The low energy conformer is at $\phi = 0°$. It is once again suggested that electronegative chlorine substituents may enhance the polarity of the *ortho* C-H bonds. The planar conformer is possibly stabilized by increased electrostatic attraction between the *ortho* $C\text{-}H^{+}$ and benzylic $C\text{-}F^{-}$ dipoles. This effect is noted for 3,5-dichlorobenzyl chloride.[65] The perpendicular conformer is again stabilized in polar solvents.

1.4 Introduction to the problem

Some general observations can be made from previous studies on benzyl halides. The barrier in benzyl fluoride is quite small (of the order of thermal energies). In the gas phase the parallel conformer is the most stable; in the liquid, the perpendicular conformer is likely of lowest energy. For the larger benzyl halides, low energy conformers have the C-X bond perpendicular to the plane in both the gas and liquid phases.

Solvent and substituent effects can drastically effect the size and shape of the internal potential. The perpendicular conformer in benzyl fluoride is stabilized by polar solvents. In *ortho*-disubstituted benzyl compounds, the low energy conformer is invariably at $\phi = 90°$, due to steric effects. Substitution of halogens at the *meta*-positions results in stabilization of the planar conformer; conversely, substitution of electron-donating groups in the *para* position stabilizes the perpendicular conformer.

Clearly, the characteristics of these internal barriers are determined by a cornucopia of delicately balanced electronic, steric and solvent effects; this may account for the diversity in reported barriers and conformational preferences in benzyl compounds.

It is of interest to examine the effects of fluorine substitution in benzyl fluorides. The electronic effects of fluorine substitution in aromatic systems have been investigated extensively.[66] Further, spin-spin coupling constants involving aromatic and sidechain fluorine nuclei have also been of

great interest to NMR spectroscopists.[67] For the most part, detailed study of fluorine-substituted benzyl fluorides has been neglected.

The intent of this work was to determine the internal rotational potentials and minimum energy conformations in three symmetrically fluorinated benzyl fluoride derivatives: 2,6-difluorobenzyl fluoride (**2**), 3,5-difluorobenzyl fluoride (**3**), and 4-fluorobenzyl fluoride (**4**).

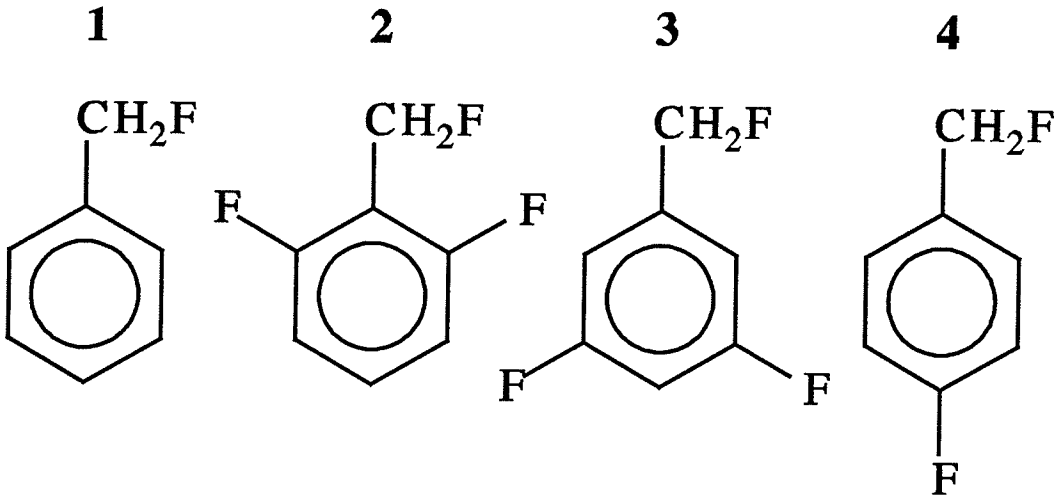

NMR spectral parameters (^{1}H, ^{13}C and ^{19}F) are presented for **2**, **3**, and **4** in two solvents. Rotational barriers are determined experimentally for **2** - **4**. High level *ab initio* molecular orbital calculations are performed on **1** - **4**, including some calculations on the solvated molecules. Coupling constants are calculated at the INDO FPT MO level for all four molecules.

2. Experimental Methods

Experimental Methods

2.1 Preparation of compounds

2,6-difluorobenzyl fluoride (**2**), 3,5-difluorobenzyl fluoride (**3**), and 4-fluoro-benzyl fluoride (**4**) were synthesized from the corresponding benzyl alcohols. The alcohols were fluorinated with morpholinosulfur trifluoride (morpho-DAST), following a generic procedure.[68] All starting compounds were obtained from Aldrich. Synthetic yields are reported below.

The benzyl alcohol (approximately 5.5 mmol) was added to a 30 ml solution of cold CH_2Cl_2. This mixture was added over thirty minutes (while stirring) to a cold solution of morpho-DAST (approximately 13.5 mmol) dissolved in 10 ml of CH_2Cl_2. (N.B.: Due to the highly reactive nature of the morpho-DAST, it was necessary to ensure that a teflon stirring bar was used.) Upon completion of the addition, the solution was stirred for approximately 18 hours. Excess alcohol was removed by washing with three 10 ml portions of 5% $NaHCO_3$. The solution was then washed with 10 ml of water. The layers were separated and the organic layer was stirred and dried over $MgSO_4$ for 8 hours. Solvent was removed by vacuum, leaving a yellowish oil in the bottom of the flask. The yield ranged from 0.3 to 0.6 g. The product weight was determined by measuring the total weight of the oil, and comparing relative amounts of benzyl alcohol and benzyl fluoride by integration on survey ^1H NMR spectra.

Table 2.1.1: Synthetic Yields

Compound	Amount of Product	% Yield
2,6-difluorobenzylfluoride	0.3530 g	44.3
3,5-difluorobenzylfluoride	0.4601 g	57.0
4-fluorobenzylfluoride	0.4913 g	68.8

Figure 2.1.1: Synthesis of 2,6-difluorobenzyl fluoride

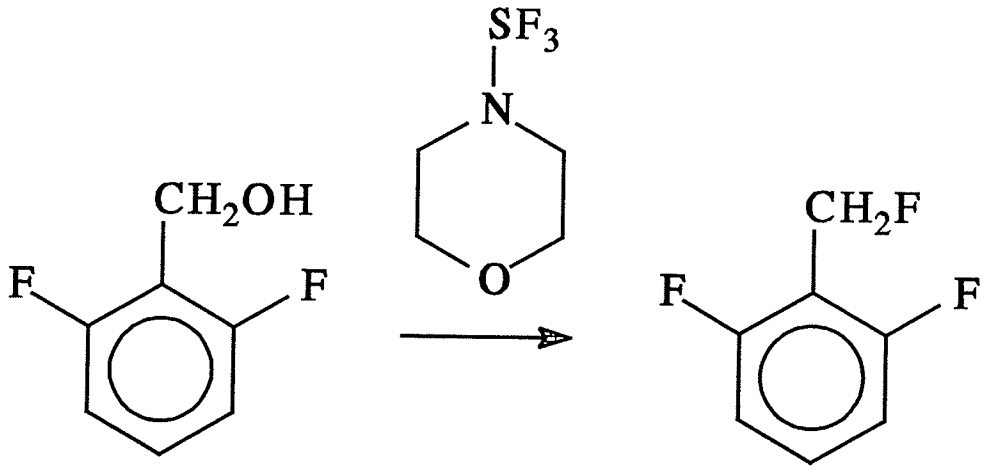

2

Figure 2.1.2: Synthesis of 3,5-difluorobenzyl fluoride

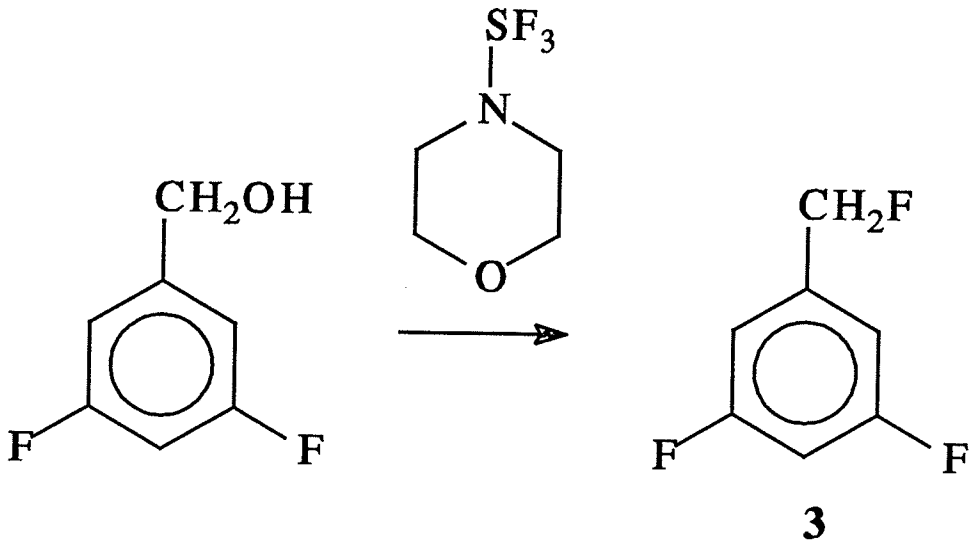

3

Figure 2.1.3: Synthesis of 4-fluorobenzyl fluoride

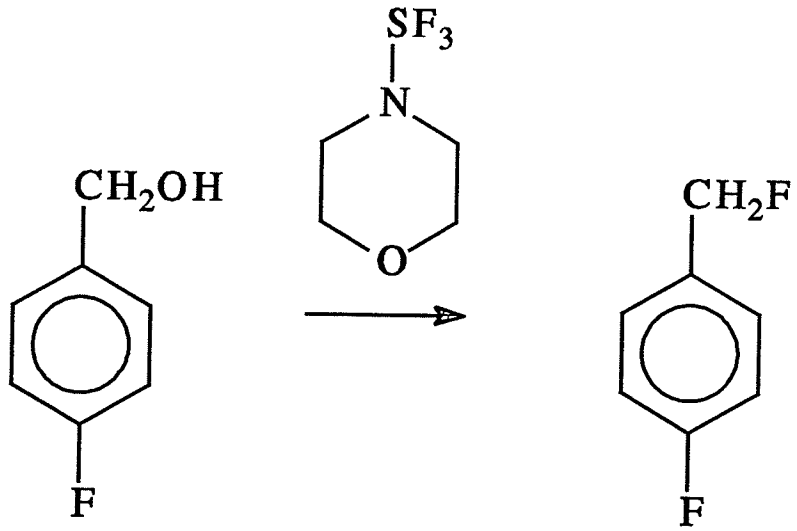

4

2.2 Sample preparation

Compounds **2**, **3**, and **4** were prepared as 5 mol % solutions in CS_2 and acetone-d6. The CS_2 solution was comprised of 85 mol % CS_2, 10 mol % C_6D_{12} (used as the internal lock reference), 0.25 mol % TMS (as the proton reference), and 0.25 mol % C_6F_6 (as the fluorine reference). The acetone-d6 solution was made up of 99.50 mol % acetone-d6, 0.25 mol % C_6F_6, and 0.25 mol % TMS. All samples were filtered through a small piece of cotton wool in a Pasteur pipette into 5 mm od NMR sample tubes. The sample tubes were degassed by six cycles of a freeze-pump-thaw procedure and flame-sealed.

2.3 Spectroscopic method

^{1}H, ^{19}F, and proton-decoupled ^{13}C NMR spectra were acquired on a Bruker AM 300 spectrometer at 300 K. Spectrometer frequencies were 300.135 Hz for protons, 282.38 MHz for fluorine, and 75.48 MHz for carbon-13. Survey spectra were acquired with sweep widths of 6000 Hz (^{1}H), 50000 Hz (^{19}F) and 25000 Hz (^{13}C). Extensive shimming was required before acquiring detailed spectra for each region.[69] For ^{1}H and ^{19}F NMR spectra, the reference peaks (i.e. TMS and C_6F_6, respectively) were examined in detail. The free induction decays (FID's) and line-shapes of these peaks were optimized (by shimming) to ensure a homogeneous field; the precise positions of these peaks were determined in order to accurately reference the compounds. The reference points for ^{13}C NMR spectra (TMS) were taken from survey spectra.

For ^{1}H and ^{19}F NMR spectra, 32 scans were accumulated, with acquisition times of approximately 40 seconds. Proton spectral regions ranged from 70 to 180 Hz; those for fluorine from 80 - 500 Hz. Line widths at half height were as low as 0.025 Hz. Digital resolution was typically 0.004 - 0.006 Hz/point. ^{13}C NMR spectra were run with acquisition times of 10 - 12 seconds, with the number of scans ranging between 200 and 2500, depending on the intensity of the peaks in each region. Digital resolution was typically 0.01 - 0.02 Hz/point.

FID's were zero-filled two or four times prior to Fourier

transformation. All spectra were resolution-enhanced by gaussian multiplication of the FID's. Normally, values of 0.6 for the gaussian multiplication parameter (GB) and -0.1 for the lorentzian parameter (LB) were used.

2.4 Spectral analyses

Spectral analyses were done with the programs ASSIGN[70] and NUMMRIT[71]; the latter has been extensively modified in this laboratory by Rudy Sebastian. Proton and fluorine spectra were analyzed simultaneously for each molecule. The spectra were analyzed as $AA'BM_2RR'X$ (**2** and **3**) and $AA'BB'M_2RX$ (**4**) spin systems. Carbon spectra were analyzed individually for each spectral region. Spectra for the *ortho* and *meta* carbons in **2** and **3** were analyzed as ABMX systems. Other carbon spectra for **2** and **3** were analyzed as AA'MX systems. Carbon spectra for **4** were all analyzed as ABX systems.

2.5 Molecular orbital calculations

Molecular orbital calculations were performed on **1** through **4** with the program GAUSSIAN 92.[72] Hartree-Fock self consistent field (SCF) molecular orbital calculations were performed at the 6-31G*, 6-311G* and 6-31G** levels. Second-order Møller-Plesset perturbation theory calculations were performed with the 6-31G* and 6-31G** bases. The benzylic C-F bond was constrained at 0, 30, 45, 60, 75 and 90° relative to the ring plane. Molecular geometries were fully optimized, except that the benzene moiety was held planar. Dielectric solvent effects were evaluated by geometry-optimized SCF calculations at the 6-31G* level, using SCRFPAC.[73] The majority of calculations were carried out on the IBM RISC System/6000 350 (monmr.chem) and IBM RISC System/6000 590 (regulus.cc) minicomputers at the University of Manitoba.

The SAS nonlinear regression program, NLIN,[74a] was used to fit the potentials to functions of the form

$$V(\phi) = \sum_n V_n \sin^2(\frac{n\phi}{2}) \qquad (2.1)$$

Functions were plotted with the SAS/Graph library's interpolation routine.[74b] Classical expectation values were calculated with a simple routine written for use with the MAPLE V software package.[75]

INDO MO FPT calculations of coupling constants were performed on the optimized MP2/6-31G** (**1** and **2**) and MP2/6-31G* (**3** and **4**)

geometries.[76] Couplings for various geometrical configurations were fit to $\sin^2\phi$ and $\sin^2(\phi/2)$ functions, using the SAS packages mentioned above.

3. Experimental Results

Experimental Results

3.1 Spectral parameters: ^{1}H and ^{19}F NMR spectra

a) 2,6-difluorobenzyl fluoride

Results of analyses of the ^{1}H and ^{19}F NMR spectra of 5.0 mol % solutions of 2,6-difluorobenzyl fluoride in acetone-d6 and CS_2 appear in Tables 3.1.1 and 3.1.2, respectively. Spectra were analyzed as $AA'BM_2RR'X$ systems. Signs of coupling constants were adopted from previous analyses on benzyl fluoride,[58] 2,6-difluorobenzyl fluoride,[57] 2-fluorotoluene[77] and 2-fluorobenzotrifluoride.[78] Figures 3.1.1 to 3.1.5 show the various proton and fluorine regions.

Table 3.1.1: ^{1}H and ^{19}F NMR spectral parameters[a] for a 5.0 mol% solution of 2,6-difluorobenzyl fluoride in acetone-d6/C_6F_6/TMS at 300K

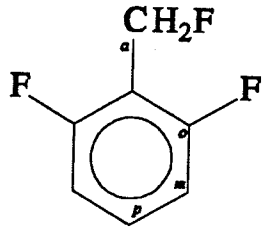

Nuclei	Chemical Shifts (Hz)	Chemical Shifts (ppm)
Ha	1655.777 (1)[b]	5.51677
Hm	2126.826 (1)	7.08623
Hp	2263.533 (1)	7.54172
Fa	-12981.379 (1)	-45.97131
Fo	13458.147 (1)	47.65970

Coupling Constants (Hz)

^{2}J(Ha,Fa)	47.976 (1)	^{5}J(Ha,Hm)	0.357 (1)
^{3}J(Fo,Hm)	9.172 (1)	^{5}J(Fa,Hm)	1.233 (1)
^{3}J(Hm,Hp)	8.485 (1)	^{5}J(Fo,Hm′)	-1.273 (1)
^{4}J(Ha,Fo)	1.395 (1)	^{6}J(Ha,Hp)	-0.207 (1)
^{4}J(Fa,Fo)	2.733 (1)	^{6}J(Fa,Hp)	-2.481 (1)
^{4}J(Fo,Hp)	6.599 (1)		
^{4}J(Fo,Fo′)	5.041 (1)		
^{4}J(Hm,Hm′)	0.995 (1)		

Calculated Transitions	**768**
Assigned Transitions	**581**
Peaks Observed	**338**
Largest Difference	**0.022**
RMS Deviation of Transitions	**0.006**

Parameter Correlation Matrix

^4J(Fo,Fo′), ^5J(Fo,Hm)	0.377

Notes:

a. In hertz, at 300.135 MHz to high frequency of internal TMS (^{1}H NMR), and 282.38 MHz to high frequency of internal C_6F_6 (^{19}F NMR).

b. Numbers in parentheses are standard deviations in the last significant digit, as given by the NUMMRIT analysis.

Figure 3.1.1

A. The *meta* proton region of 2,6-difluorobenzyl fluoride in acetone-d6.

B. Computer simulation of the *meta* region using parameters from Table 3.1.1 assuming a linewidth of 0.03 Hz.

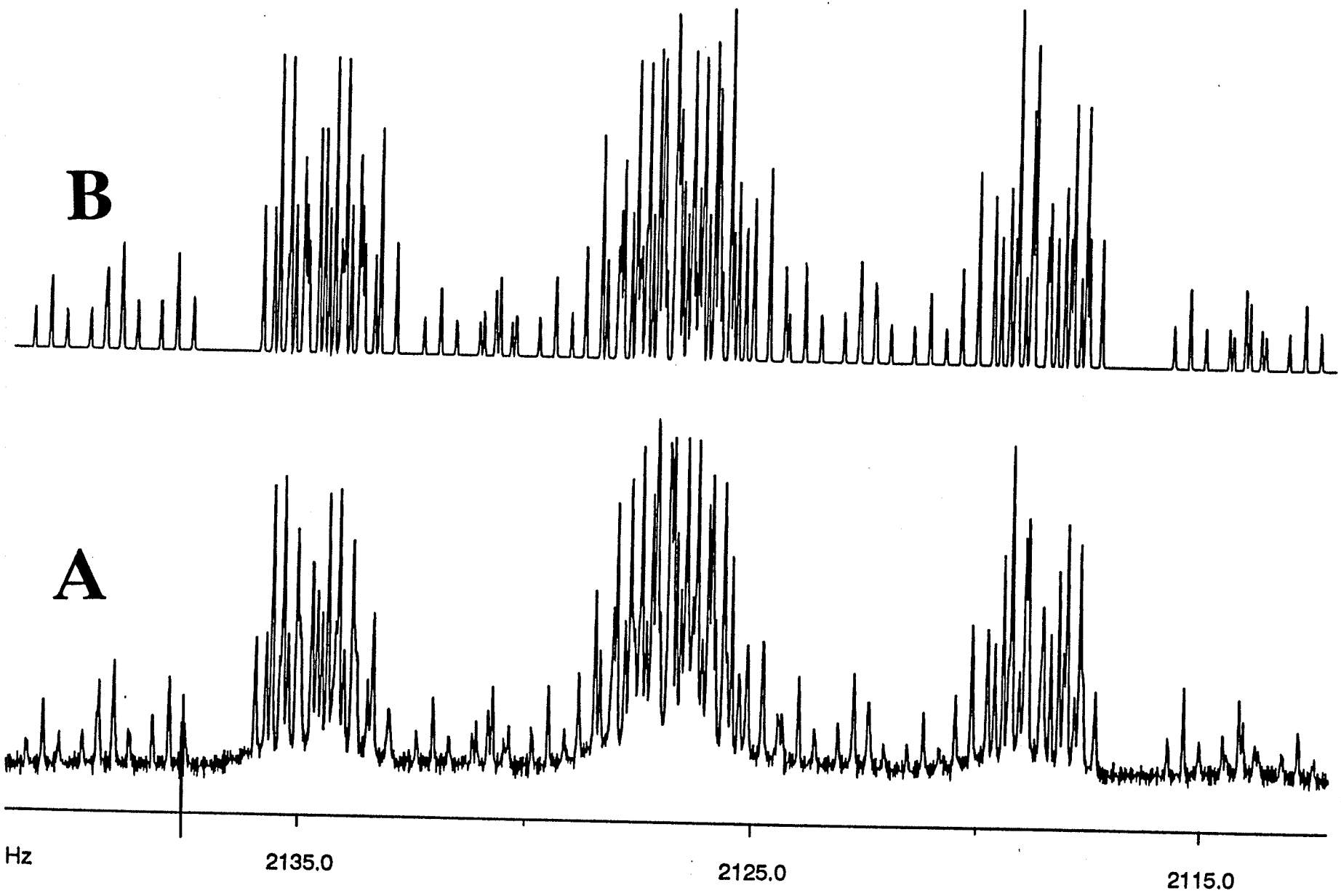
B
A
Hz
2135.0
2125.0
2115.0

Figure 3.1.2

A. The ^{19}F NMR spectrum of the benzyl fluorine of 2,6-difluorobenzyl fluoride in acetone-d6.

B. Computer simulation of the benzyl fluorine using parameters from Table 3.1.1 assuming a linewidth of 0.1 Hz.

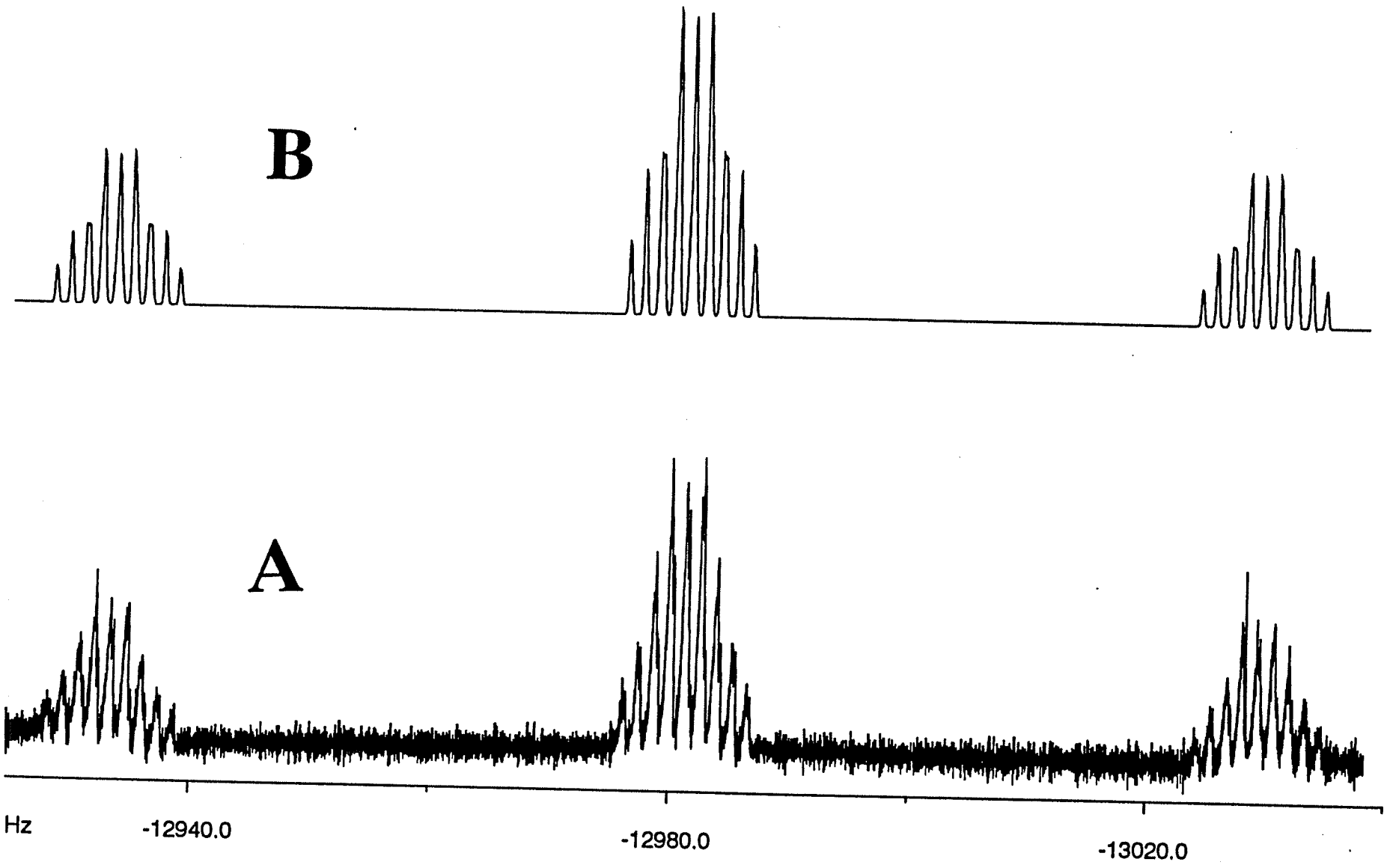
B
A
Hz
-12940.0
-12980.0
-13020.0

Figure 3.1.3

A. The ^{19}F NMR spectrum of the *ortho* fluorine of 2,6-difluorobenzyl fluoride in acetone-d6.

B. Computer simulation of the *ortho* fluorine using parameters from Table 3.1.1 assuming a linewidth of 0.1 Hz.

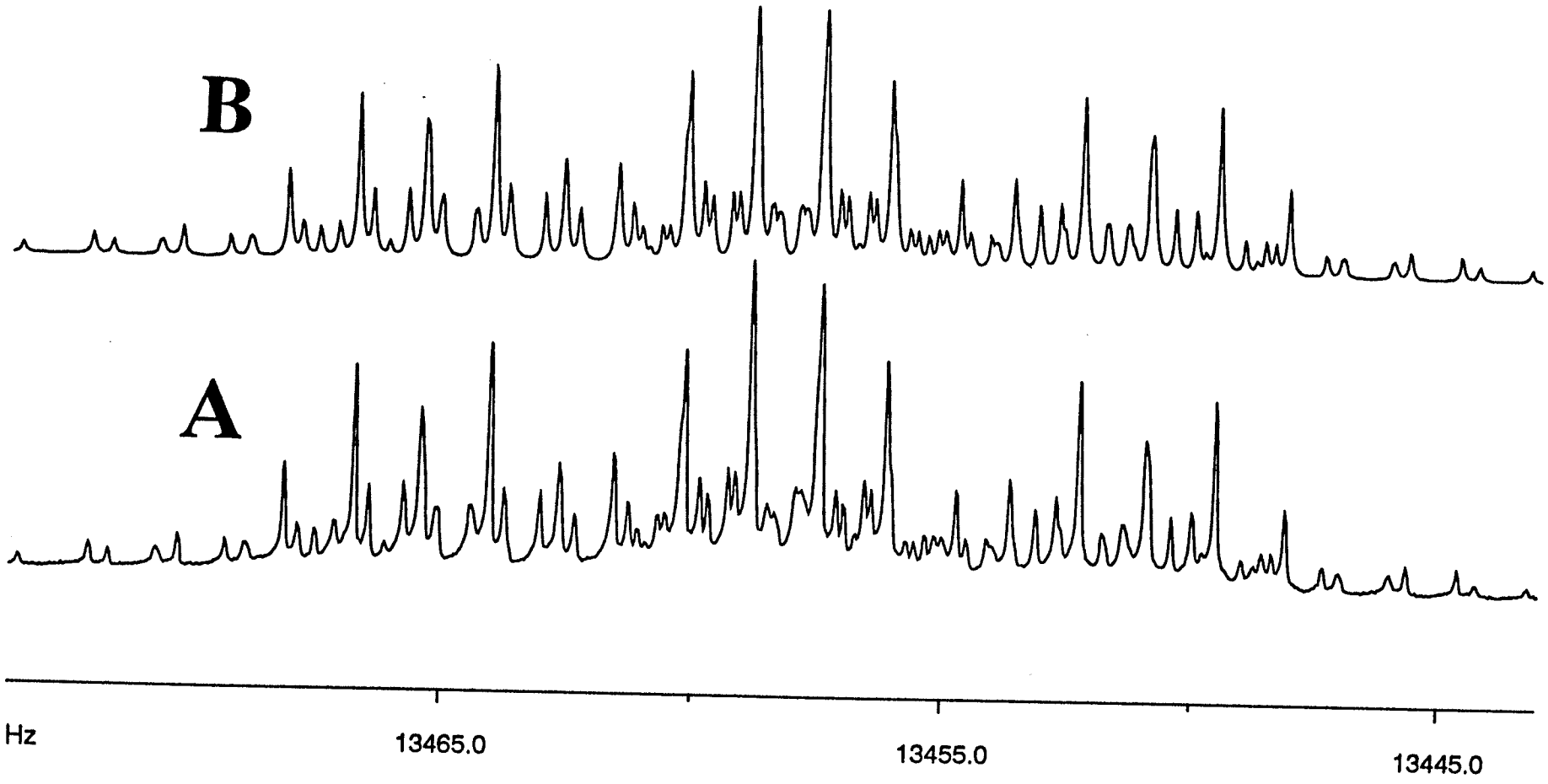
B
A
Hz
13465.0
13455.0
13445.0

Table 3.1.2: ^{1}H and ^{19}F NMR spectral parameters[a] for a 5.0 mol% solution of 2,6-difluorobenzyl fluoride in $CS_2/C_6D_{12}/C_6F_6$/TMS at 300 K.

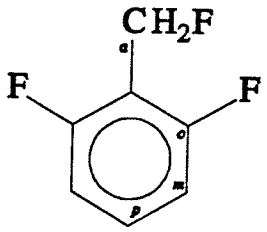

Nuclei	Chemical Shifts (Hz)	Chemical Shifts (ppm)
Ha	1601.910 (1)[b]	5.3373
Hm	2051.442 (1)	6.8351
Hp	2185.754 (1)	7.2826
Fa	-13266.710 (1)	-46.9818
Fo	13580.977 (1)	48.0947

Coupling Constants (Hz)

^{2}J(Ha,Fa)	47.932 (1)	^{5}J(Ha,Hm)	0.355 (1)
^{3}J(Fo,Hm)	8.666 (2)	^{5}J(Fa,Hm)	1.185 (1)
^{3}J(Hm,Hp)	8.429 (1)	^{5}J(Fo,Hm′)	-1.285 (1)
^{4}J(Ha,Fo)	1.415 (1)	^{6}J(Ha,Hp)	-0.211 (1)
^{4}J(Fa,Fo)	2.631 (1)	^{6}J(Fa,Hp)	-2.333 (1)
^{4}J(Fo,Hp)	6.419 (1)		
^{4}J(Fo,Fo′)	5.238 (1)		
^{4}J(Hm,Hm′)	1.033 (1)		

Calculated Transitions	**768**
Assigned Transitions	**586**
Peaks Observed	**428**
Largest Difference	**0.017**
RMS Deviation of Transitions	**0.007**

Parameter Correlation Matrix

$^{5}J(Fo,Hm),^{4}J(Fo,Fo')$	-0.5367

Notes:

a. In hertz, at 300.135 MHz to high frequency of internal TMS (^{1}H NMR), and 282.38 MHz to high frequency of internal C_6F_6 (^{19}F NMR).

b. Numbers in parentheses are standard deviations in the last significant digit, as given by the NUMMRIT analysis.

Figure 3.1.4

A. The *para* proton region of 2,6-difluorobenzyl fluoride in CS_2/C_6D_{12}.

B. Computer simulation of the *para* region using parameters from Table 3.1.2 assuming a linewidth of 0.02 Hz.

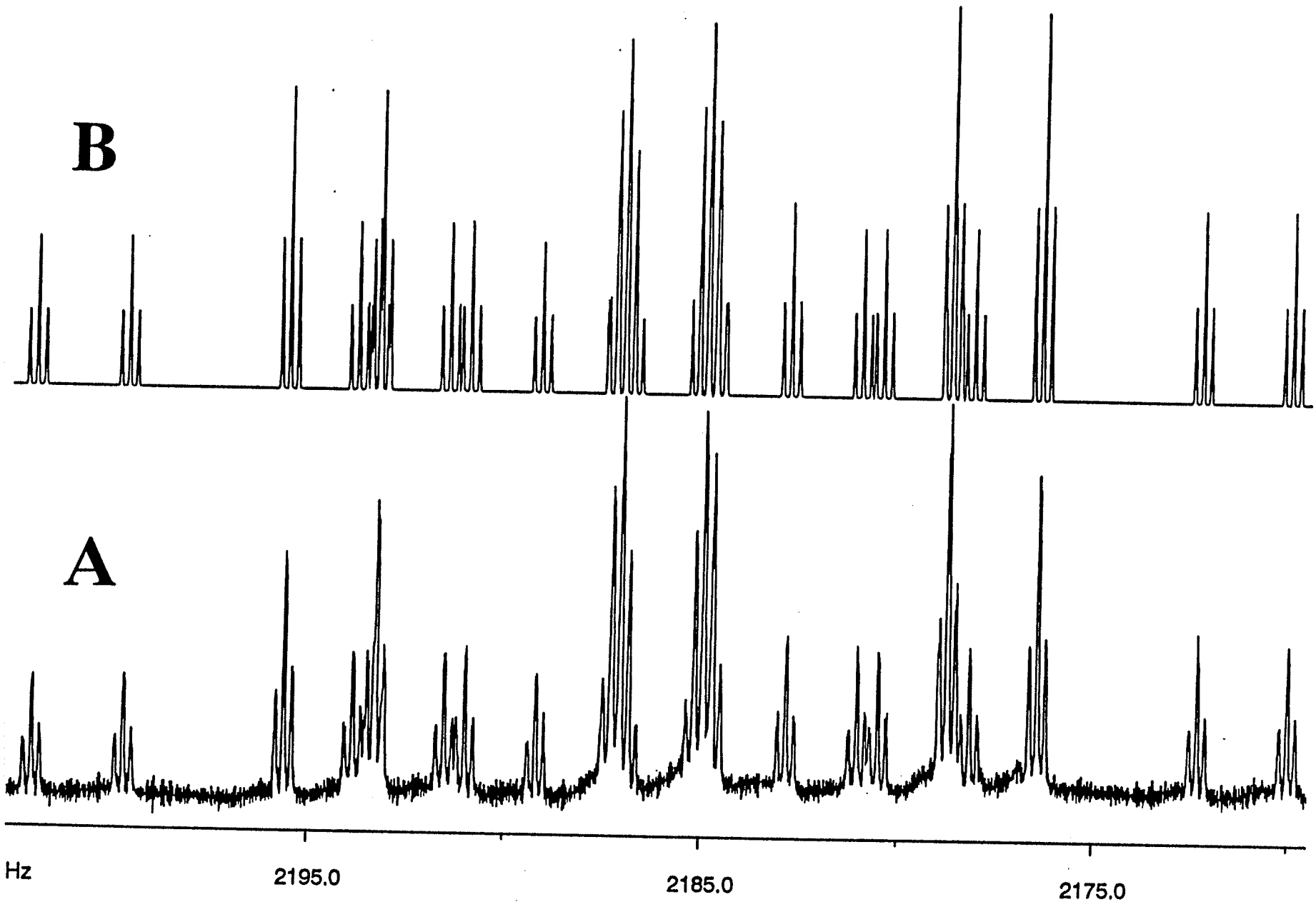
B
A
Hz
2195.0
2185.0
2175.0

Figure 3.1.5

A. The benzyl proton regions of 2,6-difluorobenzyl fluoride in CS_2/C_6D_{12}.

B. Computer simulation of the benzyl proton regions using parameters from Table 3.1.2 assuming a linewidth of 0.06 Hz.

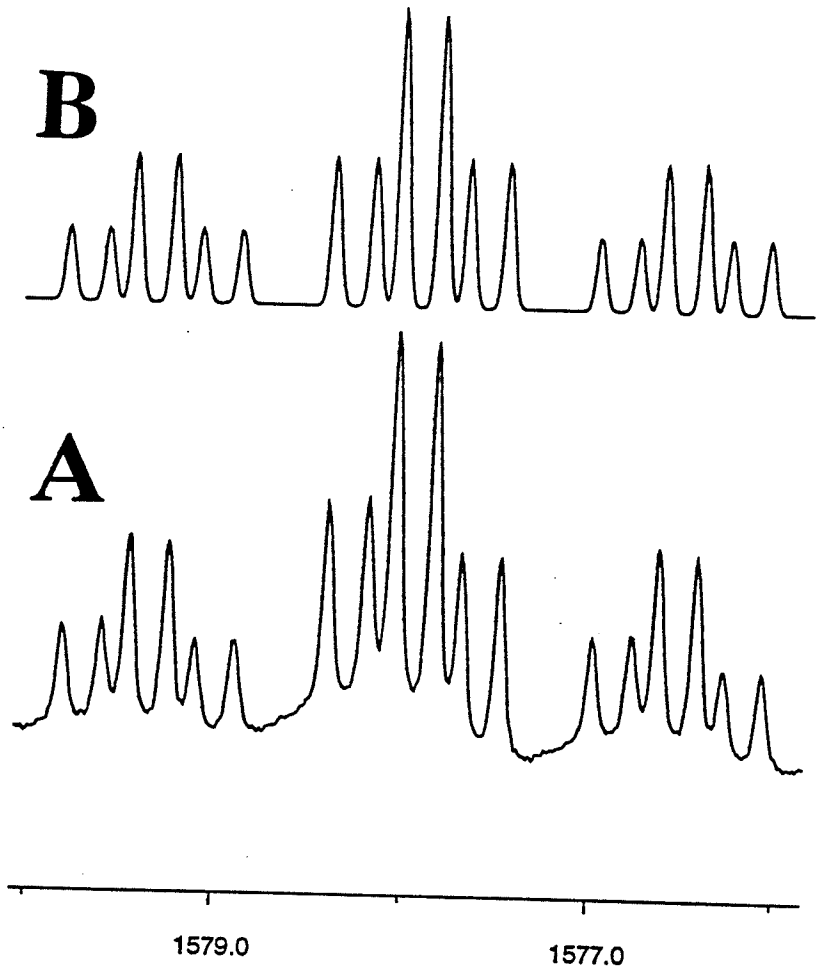
B
A
1579.0
1577.0

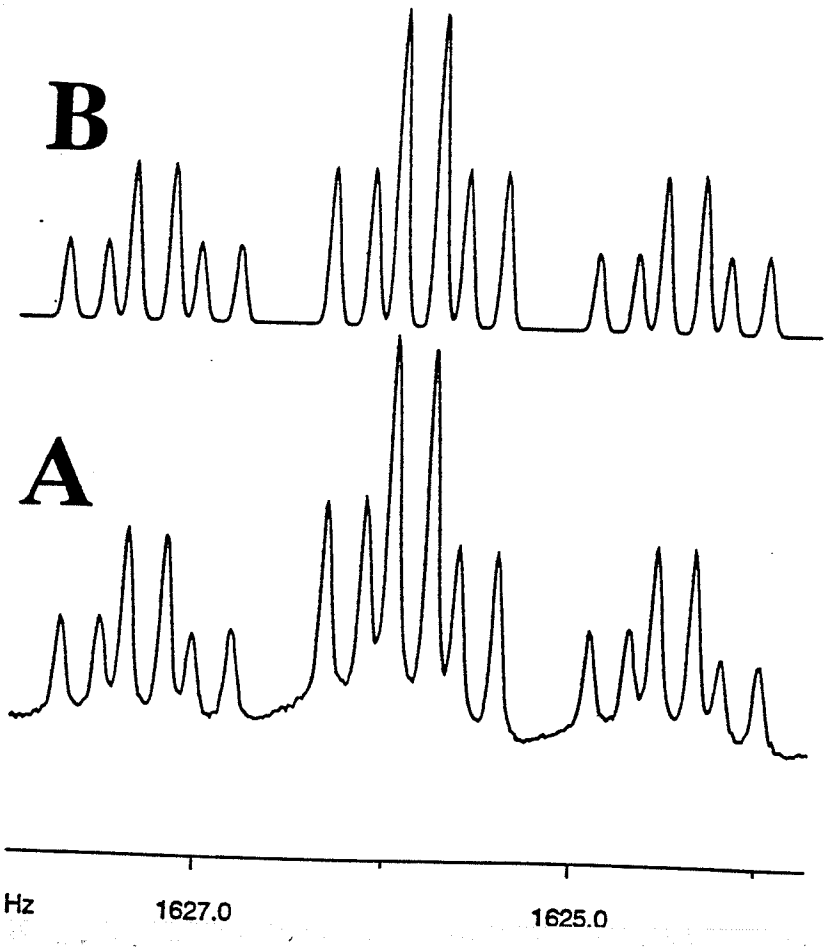
B
A
Hz
1627.0
1625.0

b) 3,5-difluorobenzyl fluoride

Results of analyses of 5.0 mol % solutions of 3,5-difluorobenzyl fluoride in acetone-d6 and CS_2 are shown in Tables 3.1.3 and 3.1.4, respectively. Spectra were analyzed as $AA'BM_2RR'X$ systems. Signs of coupling constants were adopted from previous analyses on benzyl fluoride[58] and 3,5-difluorotoluene.[24] Figures 3.1.6 to 3.1.11 show some of the proton and fluorine spectra and simulations.

Table 3.1.3: ^{1}H and ^{19}F NMR spectral parameters[a] for a 5.0 mol% solution of 3,5-difluorobenzyl fluoride in acetone-d6/C_6F_6/TMS at 300 K.

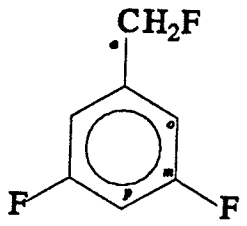

Nuclei	Chemical Shifts (Hz)	Chemical Shifts (ppm)
Ha	1641.446 (1)[b]	5.4690
Ho	2120.665 (1)	7.0657
Hp	2102.956 (1)	7.0067
Fa	-13828.884 (2)	-48.9726
Fm	15167.789 (1)	53.7141

Coupling Constants (Hz)

^{2}J(Ha,Fa)	47.043 (1)	^{5}J(Ha,Fm)	0.155 (1)
^{3}J(Ho,Fm)	9.086 (1)	^{5}J(Fa,Fm)	0.219 (1)
^{3}J(Fm,Hp)	9.240 (1)	^{5}J(Ho,Fm′)	-0.929 (0)
^{4}J(Ha,Ho)	-0.661 (1)	^{6}J(Ha,Hp)	-0.496 (1)
^{4}J(Fa,Ho)	-1.344 (1)	^{6}J(Fa,Hp)	-1.161 (1)
^{4}J(Ho,Hp)	2.372 (1)		
^{4}J(Ho,Ho′)	1.327 (1)		
^{4}J(Fm,Fm′)	6.947 (1)		

Calculated Transitions	**768**
Assigned Transitions	**515**
Peaks Observed	**398**
Largest Difference	**0.016**
RMS Deviation of Transitions	**0.007**

Parameter Correlation Matrix

^4J(Fa,Ho), ν(Ho)	-0.2247
^5J(Ho,Fm′), ^4J(Fm,Fm′)	-0.4741

Notes:

a. In hertz, at 300.137 MHz to high frequency of internal TMS (^{1}H NMR), and 282.38 MHz to high frequency of internal C_6F_6 (^{19}F NMR).

b. Numbers in parentheses are standard deviations in the last significant digit, as given by the NUMMRIT analysis.

Figure 3.1.6

A. The ring proton region of 3,5-difluorobenzyl fluoride in acetone-d6.

B. Computer simulation of the ring proton region using parameters from Table 3.1.3 assuming a linewidth of 0.02 Hz.

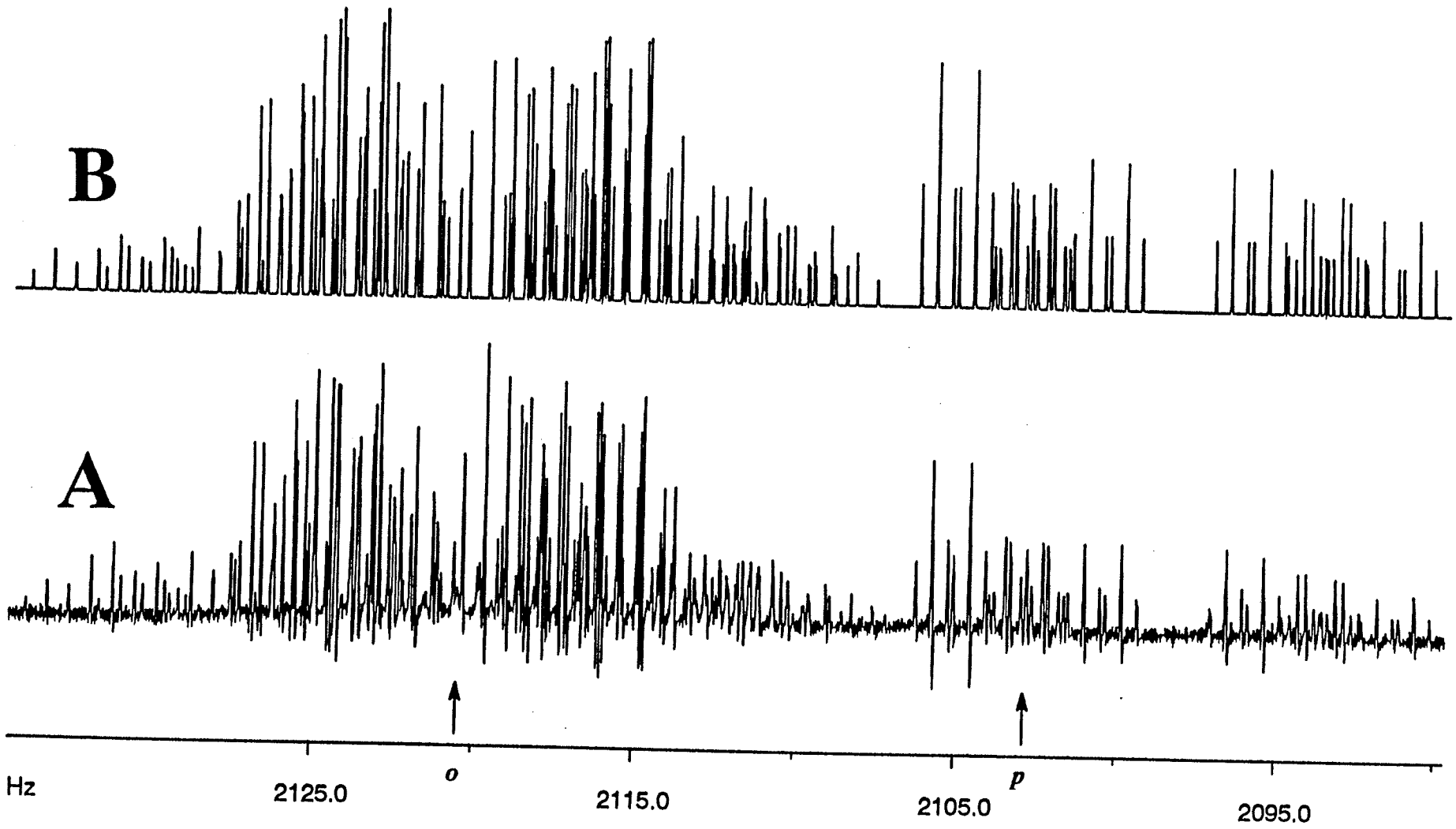
B
A
Hz
2125.0
o
2115.0
2105.0
p
2095.0

Figure 3.1.7

A. The ^{19}F NMR spectrum of the *meta* fluorine region of 3,5-difluorobenzyl fluoride in acetone-d6.

B. Computer simulation of the *meta* fluorine region using parameters from Table 3.1.3 assuming a linewidth of 0.05 Hz.

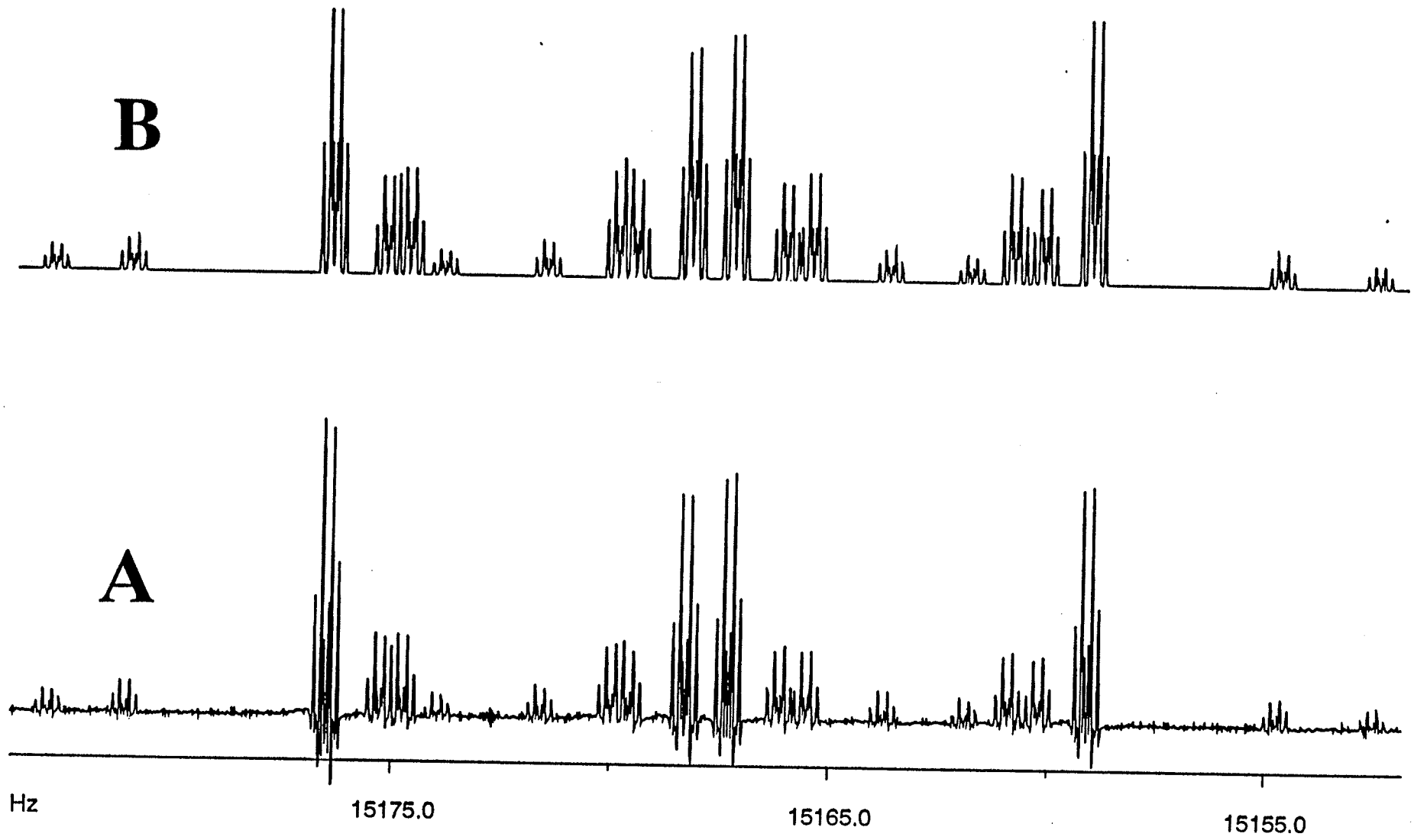
B
A
Hz
15175.0
15165.0
15155.0

Figure 3.1.8

A. Expanded ^{19}F NMR spectrum of the *meta* fluorine region of 3,5-difluorobenzyl fluoride in acetone-d6.

B. Computer simulation of the expanded *meta* fluorine region.

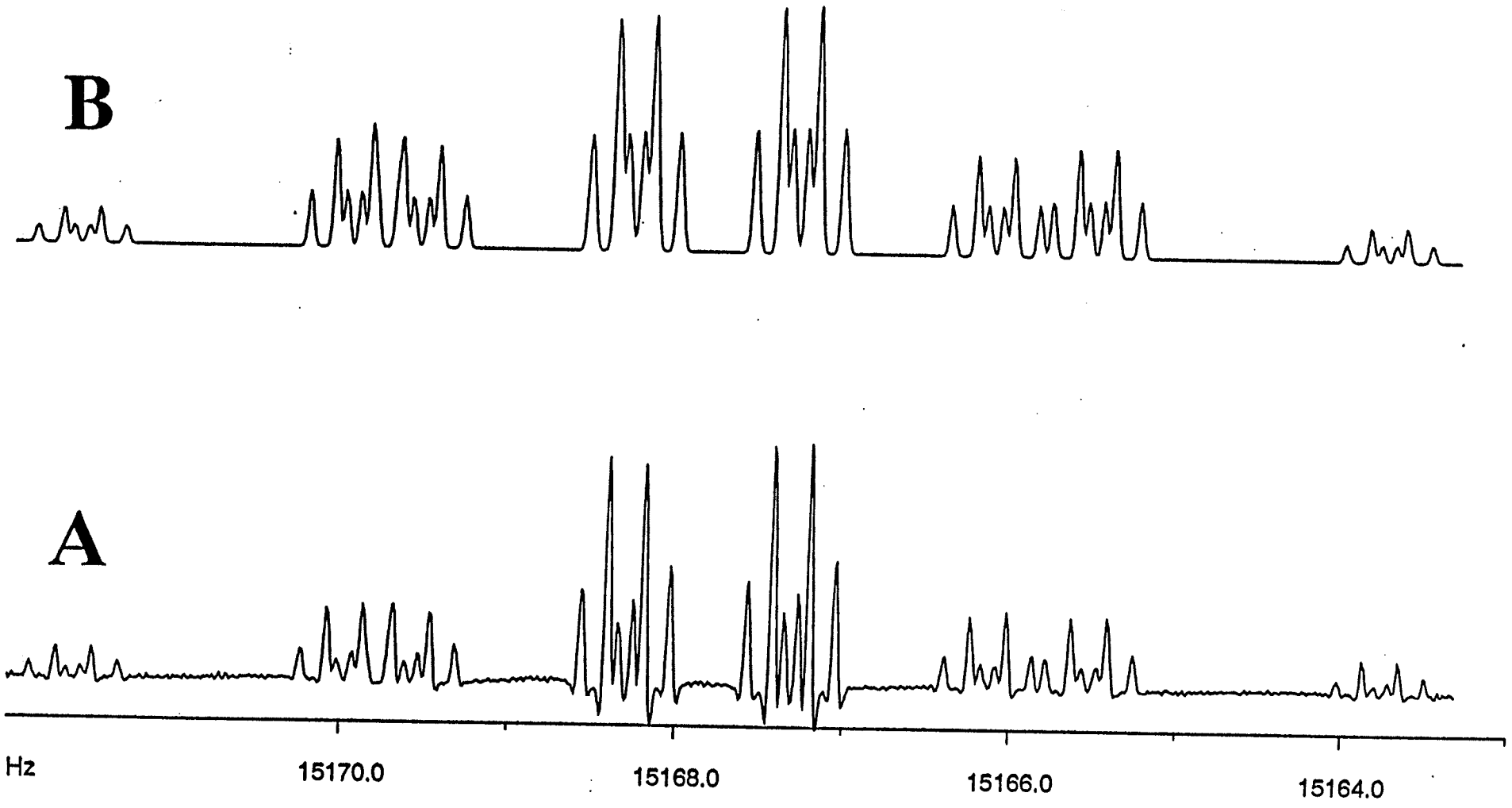
B
A
Hz
15170.0
15168.0
15166.0
15164.0

Table 3.1.4: ^{1}H and ^{19}F NMR spectral parameters[a] for a 5.0 mol% solution of 3,5-difluorobenzyl fluoride in $CS_2/C_6D_{12}/C_6F_6$/TMS at 300 K.

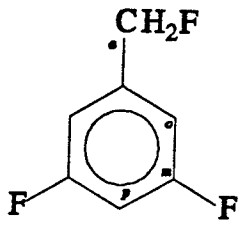

Nuclei	Chemical Shifts (Hz)	Chemical Shifts (ppm)
Ha	1584.813 (1)[b]	5.2803
Ho	2039.128 (1)	6.7940
Hp	2002.425 (1)	6.6717
Fa	-14734.271 (1)	-52.1789
Fm	15010.742 (1)	53.1580

Coupling Constants (Hz)

^{2}J(Ha,Fa)	47.077 (1)	^{5}J(Ha,Fm)	0.240 (1)
^{3}J(Ho,Fm)	8.609 (1)	^{5}J(Fa,Fm)	0.585 (1)
^{3}J(Fm,Hp)	8.760 (1)	^{5}J(Ho,Fm′)	-0.954 (1)
^{4}J(Ha,Ho)	-0.713 (1)	^{6}J(Ha,Hp)	-0.533 (1)
^{4}J(Fa,Ho)	-1.108 (1)	^{6}J(Fa,Hp)	-0.934 (1)
^{4}J(Ho,Hp)	2.350 (1)		
^{4}J(Ho,Ho′)	1.370 (1)		
^{4}J(Fm,Fm′)	7.142 (1)		

Calculated Transitions	**768**
Assigned Transitions	**510**
Peaks Observed	**376**
Largest Difference	**0.014**
RMS Deviation of Transitions	**0.006**

Parameter Correlation Matrix

^{5}J(Ho,Fm′), ^{4}J(Fm,Fm′)	-0.4210

Notes:

a. In hertz, at 300.137 MHz to high frequency of internal TMS (^{1}H NMR), and 282.38 MHz to high frequency of internal C_6F_6 (^{19}F NMR).

b. Numbers in parentheses are standard deviations in the last significant digit, as given by the NUMMRIT analysis.

Figure 3.1.9

A. The ^{19}F NMR spectrum of the *meta* fluorine region of 3,5-difluorobenzyl fluoride in CS_2/C_6D_{12}.

B. Computer simulation of the *meta* fluorine region using parameters from Table 3.1.4 assuming a linewidth of 0.05 Hz.

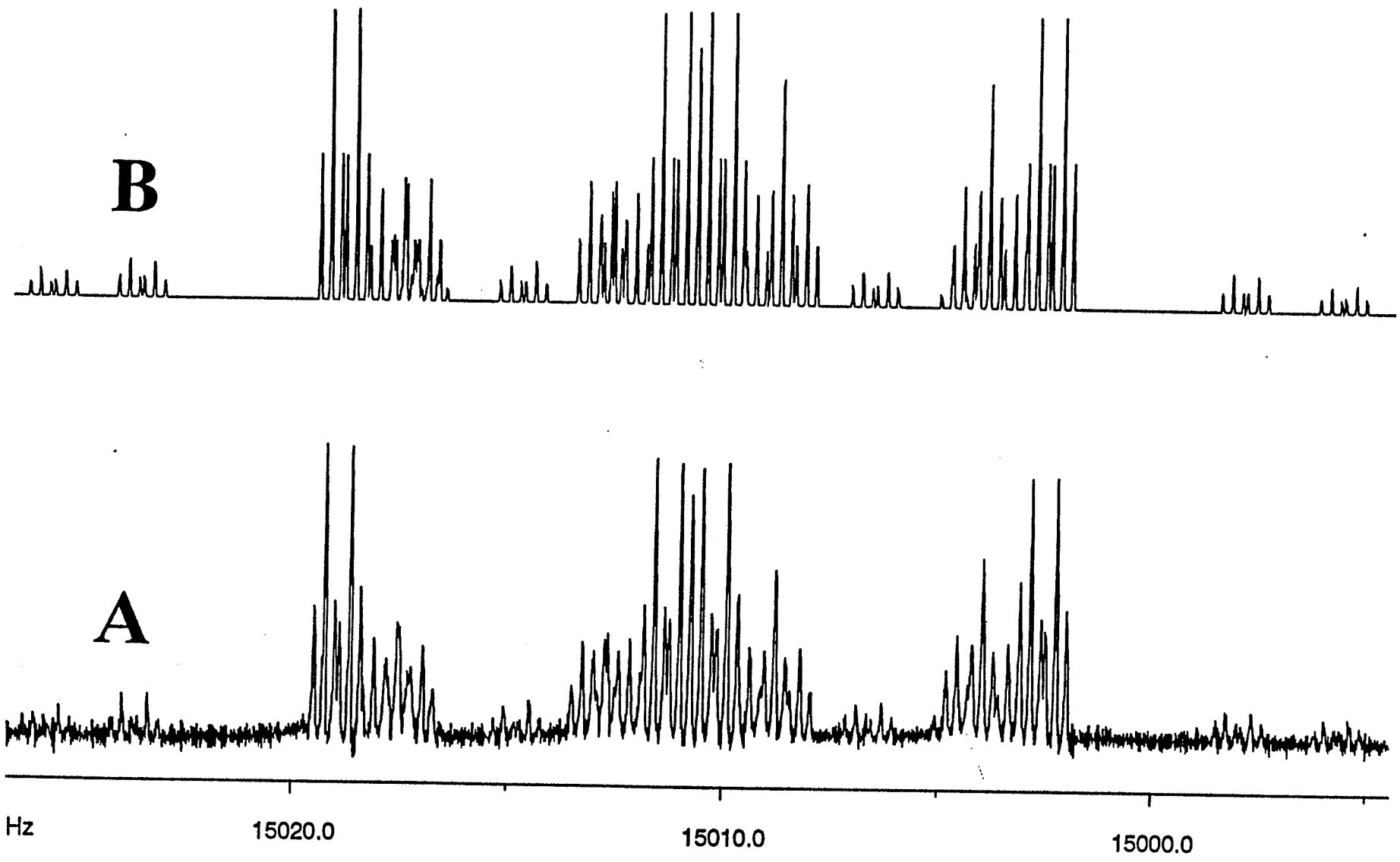
B
A
Hz
15020.0
15010.0
15000.0

Figure 3.1.10

A. The ^{19}F NMR spectrum of the benzyl fluorine region of 3,5-difluorobenzyl fluoride in CS_2/C_6D_{12}.

B. Computer simulation of the benzyl fluorine region using parameters from Table 3.1.4 assuming a linewidth of 0.15 Hz.

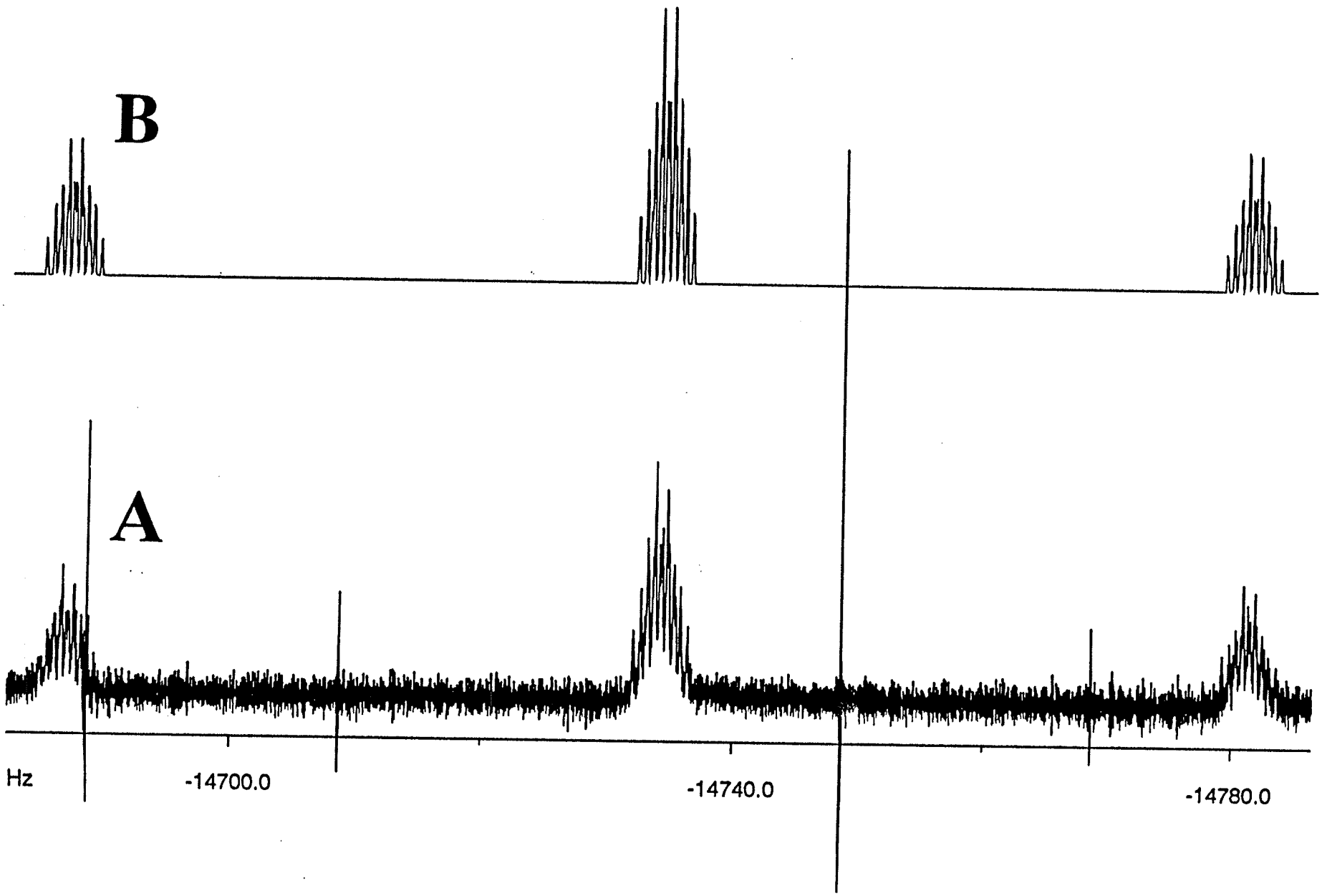
B
A
Hz
-14700.0
-14740.0
-14780.0

Figure 3.1.11

A. Expansion of the high field region of the benzyl proton doublet of 3,5-difluorobenzyl fluoride in CS_2/C_6D_{12}.

B. Computer simulation of the benzyl proton region using parameters from Table 3.1.4 assuming a linewidth of 0.03 Hz.

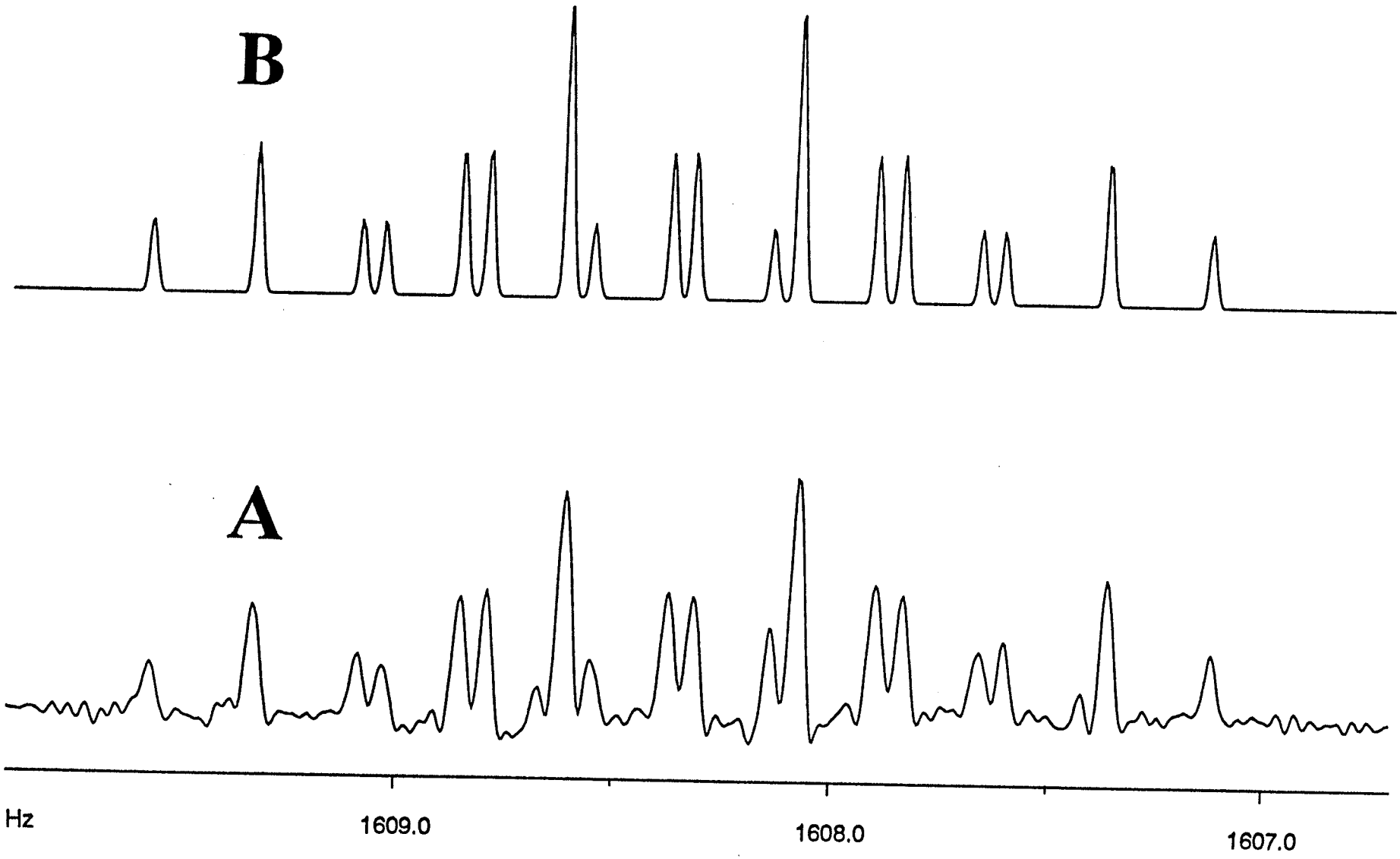
B
A
Hz
1609.0
1608.0
1607.0

c) *4-fluorobenzyl fluoride*

Results of analyses of 5.0 mol % solutions of 4-fluorobenzyl fluoride in acetone-d6 and CS_2 appear in Tables 3.1.5 and 3.1.6, respectively. Spectra were analyzed as $AA'BB'M_2RX$ systems. Signs of coupling constants were adopted from previous analyses on benzyl fluoride,[58] 4-fluorobenzyl fluoride[49] and 4-fluorotoluene.[79] ^1H and ^{19}F NMR spectra and simulations appear in figures 3.1.12 to 3.1.16.

Table 3.1.5: ^{1}H and ^{19}F NMR spectral parameters[a] for a 5.0 mol% solution of 4-fluorobenzyl fluoride in acetone-d6/C_6F_6/TMS at 300 K.

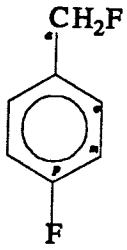

Nuclei	Chemical Shifts (Hz)	Chemical Shifts (ppm)
Ha	1616.338 (1)[b]	5.3853
Ho	2246.545 (1)	7.4851
Hm	2153.131 (1)	7.1738
Fa	-11389.771 (1)	-40.3349
Fp	14035.023 (1)	49.7026

Coupling Constants (Hz)

^{2}J(Ha,Fa)	48.015 (1)	^{5}J(Ha,Hm)	0.288 (1)
^{3}J(Ho,Hm)	8.511 (1)	^{5}J(Fa,Hm)	1.118 (1)
^{3}J(Hm,Fp)	8.955 (1)	^{5}J(Ho,Hm′)	0.410 (0)
^{4}J(Ha,Ho)	-0.532 (1)	^{6}J(Ha,Fp)	0.667 (1)
^{4}J(Fa,Ho)	-2.053 (1)	^{6}J(Fa,Fp)	5.591 (1)
^{4}J(Ho,Fp)	5.407 (1)		
^{4}J(Ho,Ho′)	2.786 (1)		
^{4}J(Hm,Hm′)	2.339 (1)		

Calculated Transitions	**768**
Assigned Transitions	**640**
Peaks Observed	**423**
Largest Difference	**0.026**
RMS Deviation of Transitions	**0.007**

Parameter Correlation Matrix

$^{5}J(Hm,Ho)$, $^{4}J(Hm,Hm)$	-0.2042

Notes:

a. In hertz, at 300.137 MHz to high frequency of internal TMS (^{1}H NMR), and 282.38 MHz to high frequency of internal C_6F_6 (^{19}F NMR).

b. Numbers in parentheses are standard deviations in the last significant digit, as given by the NUMMRIT analysis.

Figure 3.1.12

A. ^{19}F NMR spectrum of the benzyl fluorine region of 4-fluorobenzyl fluoride in acetone-d6.

B. Computer simulation of the benzyl fluorine region using parameters from Table 3.1.5 assuming a linewidth of 0.5 Hz.

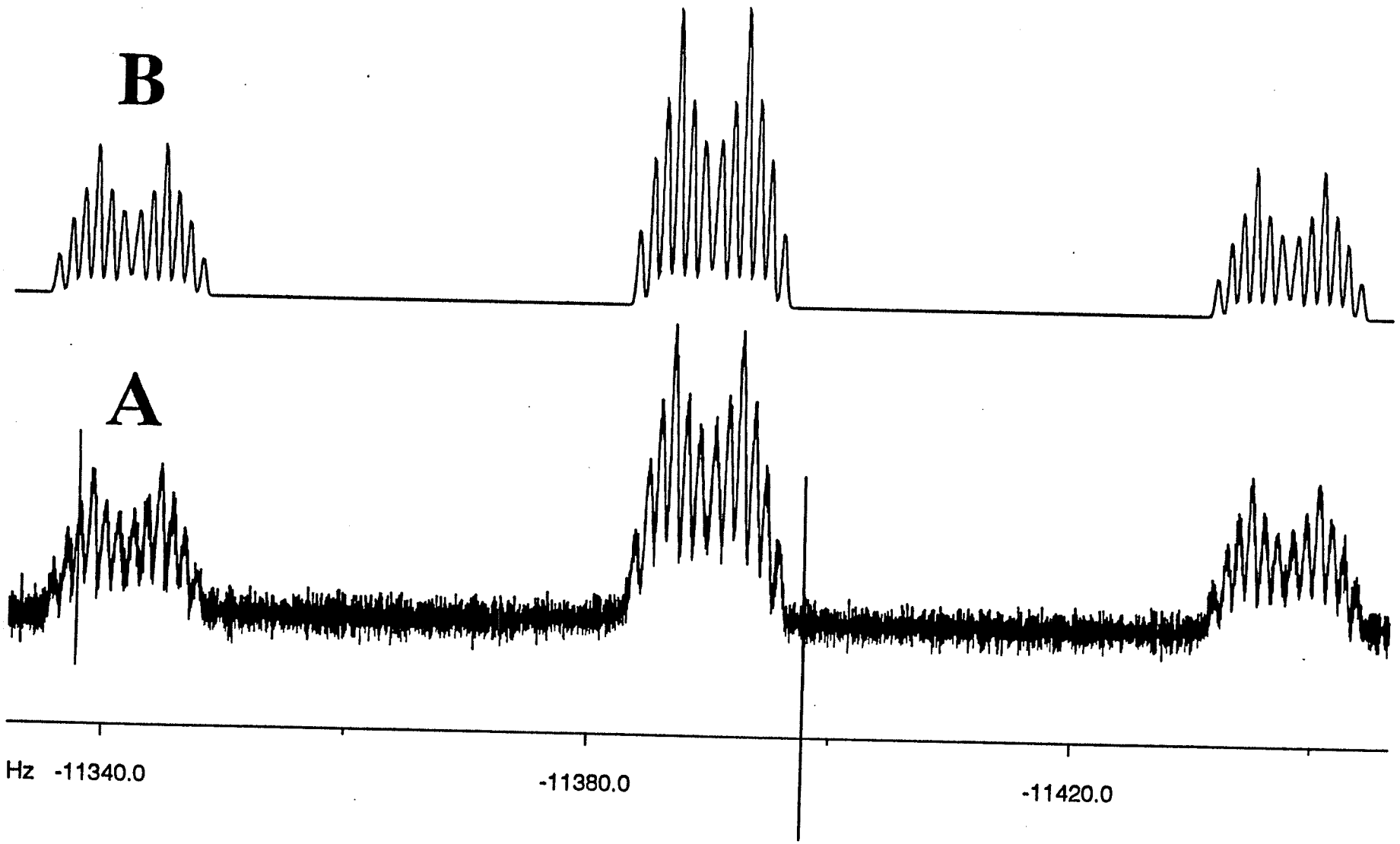
B
A
Hz -11340.0
-11380.0
-11420.0

Figure 3.1.13

A. ^{19}F NMR spectrum of the *para* fluorine region of 4-fluorobenzyl fluoride in acetone-d6.

B. Computer simulation of the *para* fluorine region using parameters from Table 3.1.5 assuming a linewidth of 0.05 Hz.

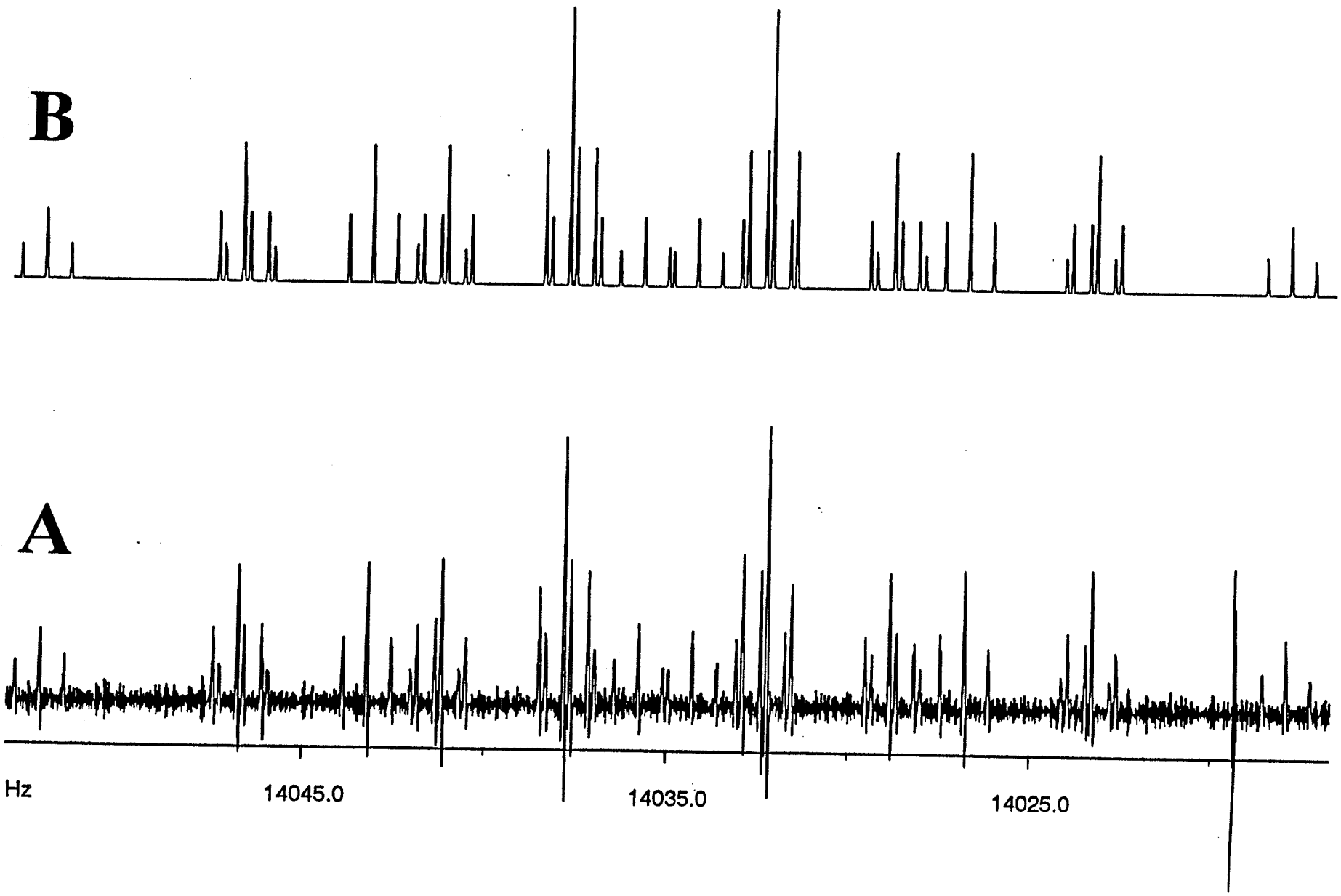
B
A
Hz
14045.0
14035.0
14025.0

Figure 3.1.14

A. Benzyl proton region of 4-fluorobenzyl fluoride in acetone-d6.

B. Computer simulation of the benzyl proton region using parameters from Table 3.1.5 assuming a linewidth of 0.03 Hz.

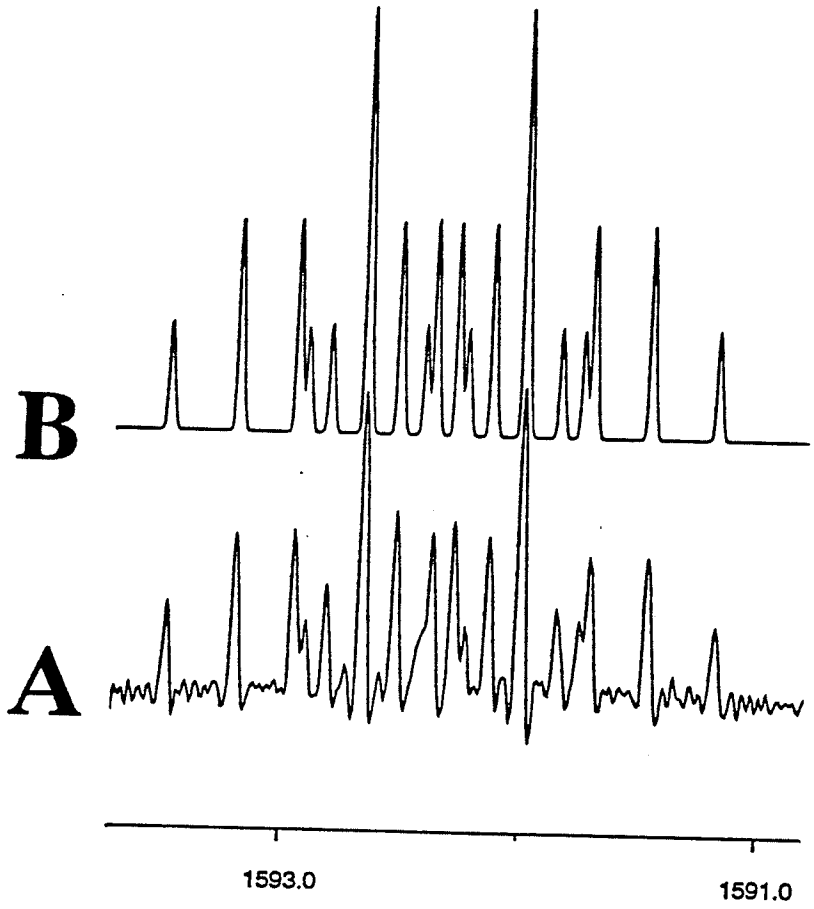
B
A
1593.0
1591.0

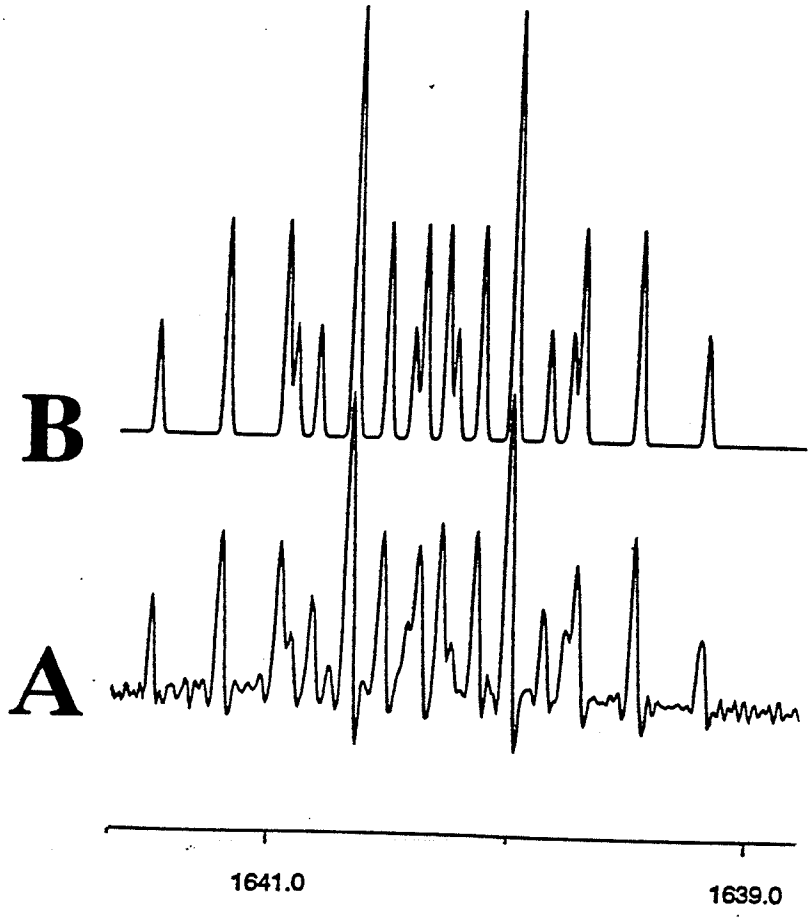
B
A
1641.0
1639.0

Table 3.1.6: ^{1}H and ^{19}F NMR spectral parameters[a] for a 5.0 mol% solution of 4-fluorobenzyl fluoride in $CS_2/C_6D_{12}/C_6F_6$/TMS at 300 K.

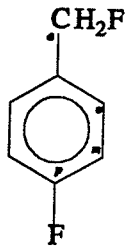

Nuclei	Chemical Shifts (Hz)	Chemical Shifts (ppm)
Ha	1566.022 (1)	5.2177
Ho	2179.956 (1)	7.2632
Hm	2091.491 (1)	6.9685
Fa	-12081.612 (1)	-42.7850
Fp	14069.253 (1)	49.8238

Coupling Constants (Hz)

^{2}J(Ha,Fa)	47.987 (1)	^{5}J(Ha,Hm)	0.296 (1)
^{3}J(Ho,Hm)	8.475 (1)	^{5}J(Fa,Hm)	1.055 (1)
^{3}J(Hm,Fp)	8.439 (1)	^{5}J(Ho,Hm′)	0.405 (0)
^{4}J(Ha,Ho)	-0.580 (1)	^{6}J(Ha,Fp)	0.778 (1)
^{4}J(Fa,Ho)	-1.786 (1)	^{6}J(Fa,Fp)	4.919 (1)
^{4}J(Ho,Fp)	5.253 (1)		
^{4}J(Ho,Ho′)	2.722 (1)		
^{4}J(Hm,Hm′)	2.318 (1)		

Calculated Transitions	**768**
Assigned Transitions	**656**
Peaks Observed	**388**
Largest Difference	**0.017**
RMS Deviation of Transitions	**0.006**

Parameter Correlation Matrix

^{6}J(Fa,Fp), υ(Fa)	-0.2162
^{5}J(Hm,Ho), ^{4}J(Ho,Ho)	-0.2608

Notes:

a. In hertz, at 300.137 MHz to high frequency of internal TMS (^{1}H NMR), and 282.38 MHz to high frequency of internal C_6F_6 (^{19}F NMR).

b. Numbers in parentheses are standard deviations in the last significant digit, as given by the NUMMRIT analysis.

Figure 3.1.15

A. The *ortho* proton region of 4-fluorobenzyl fluoride in CS_2/C_6D_{12}.

B. Computer simulation of the *ortho* proton region using parameters from Table 3.1.6 assuming a linewidth of 0.02 Hz.

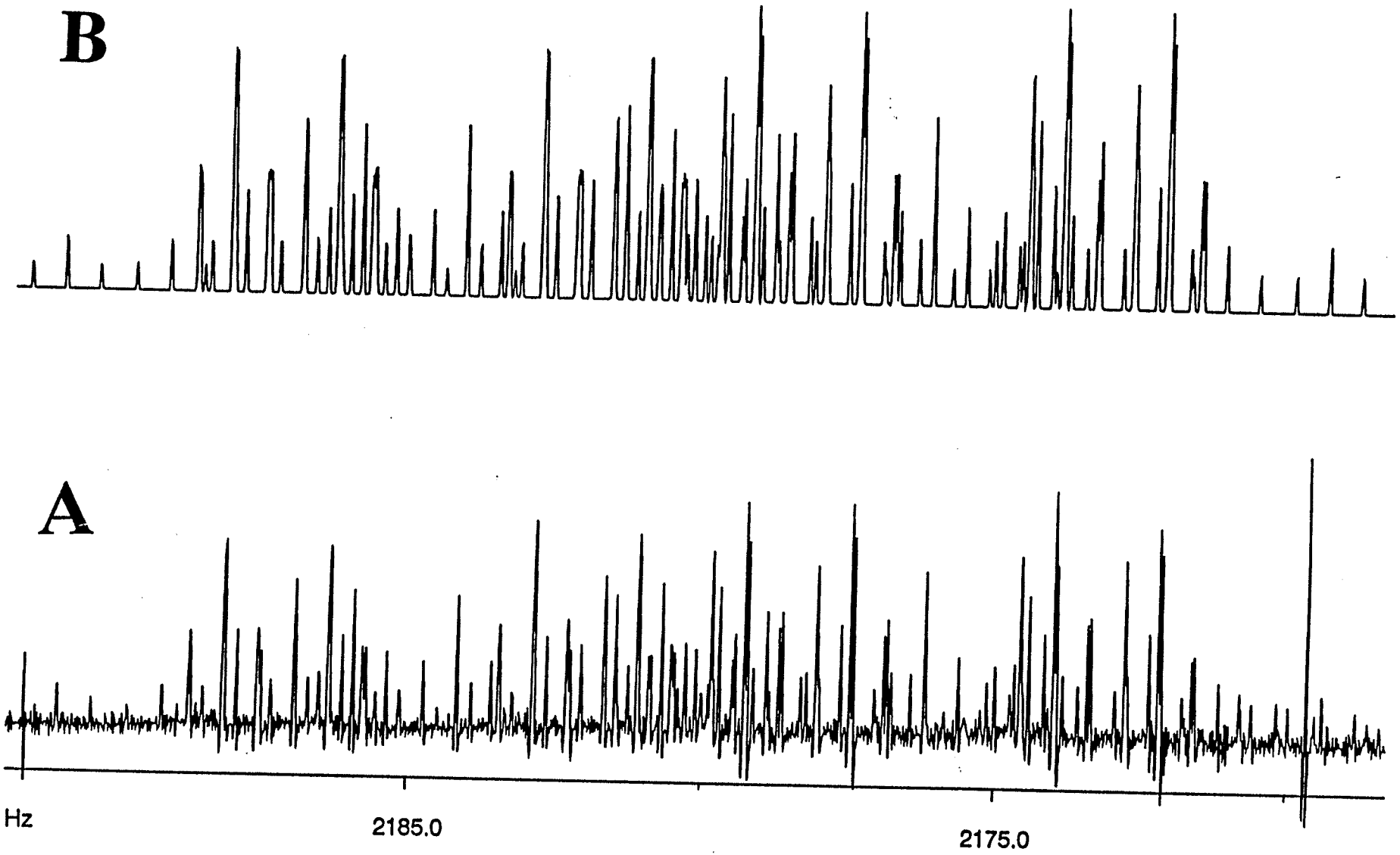
B
A
Hz
2185.0
2175.0

Figure 3.1.16

A. The *meta* proton region of 4-fluorobenzyl fluoride in CS_2/C_6D_{12}.

B. Computer simulation of the *meta* proton region using parameters from Table 3.1.6 assuming a linewidth of 0.02 Hz.

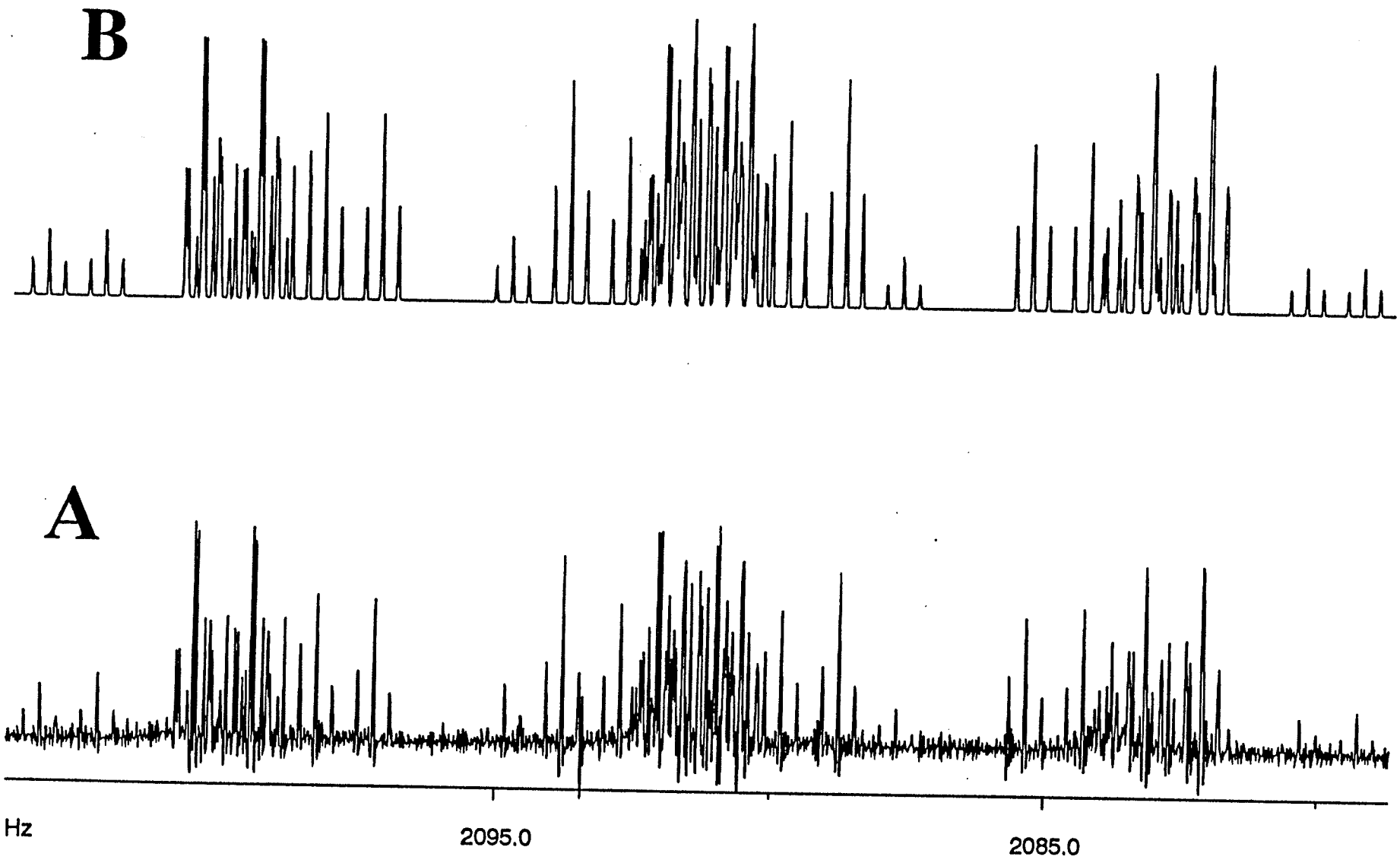
B
A
Hz
2095.0
2085.0

3.2 Spectral parameters: ^{13}C NMR spectra

Results of analyses of proton-decoupled ^{13}C NMR spectra of 5 mol % 2,6-difluorobenzyl fluoride, 3,5-difluorobenzyl fluoride and 4-fluorobenzyl fluoride in acetone-d6 and CS_2 appear in Tables 3.2.1 to 3.2.6. ^{13}C NMR chemical shifts and carbon-fluorine coupling constants are reported. The signs of the coupling constants are adopted from previous works on benzyl fluoride[23a,58] and other fluorine-substituted aromatic compounds.[67c,80]

Each carbon is analyzed individually. In **2** and **3**, the *ortho* and *meta* carbons (Co, Cm) are analyzed as ABMX systems (i.e. *ortho* (**2**) and *meta* (**3**) fluorines are treated as nonequivalent nuclei). All other carbons are analyzed as AA′MX systems. In **4**, all carbons are analyzed as ABX systems.

Table 3.2.1: ^{13}C NMR spectral parameters[a] for a 5.0 mol% solution of 2,6-difluorobenzyl fluoride in acetone-d6/C_6F_6/TMS at 300 K.

Nuclei	Chemical Shifts (Hz)	Chemical Shifts (ppm)
Ca	5454.64 (1)[b]	72.266
Ci	8503.86 (1)	112.664
Co	12263.10 (1)	162.468
Cm	8466.22 (1)	112.165
Cp	10046.52 (1)	133.102
Fo (isotope shift)[c]	+6.163 (7)	
	Coupling Constants (Hz)	
^1J(Fa,Ca)	-163.60 (1)	
^2J(Fa,Ci)	16.81 (1)	
^3J(Fa,Co)	3.47 (1)	
^4J(Fa,Cm)	(-)2.94 (1)	
^5J(Fa,Cp)	3.97 (1)	
^1J(Fo,Co)	-250.33 (1)	
^2J(Fo,Cm)	21.98 (1)	
^2J(Fo,Ci)	19.25 (1)	
^3J(Fo′,Co)	7.30 (1)	
^3J(Fo,Cp)	10.62 (1)	
^3J(Fo,Ca)	5.01 (1)	
^4J(Fo′,Cm)	3.63 (1)	

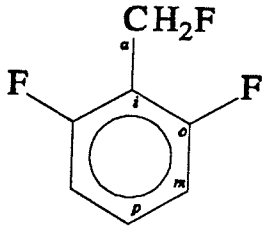

	Ca	Ci	Co	Cm	Cp
Calculated Transitions	24	24	32	36	24
Assigned Transitions	6	8	8	12	8
Peaks Observed	6	6	8	12	6
Largest Difference	0.018	0.013	0.021	0.014	0.014
RMS Deviation of Transitions	0.013	0.008	0.019	0.009	0.015

Notes:

a. In hertz, at 75.48 MHz to high frequency of internal TMS (^{13}C NMR).

b. Numbers in parentheses are standard deviations in the last significant digit, as given by the NUMMRIT analysis.

c. The *ortho* fluorine adjacent to ^{12}Cm is deshielded by +6.163 Hz (isotope shift). See figure 3.2.1 for *meta* carbon region.

Figure 3.2.1

A. The ^{13}C NMR spectrum of the *meta* carbon region of 2,6-difluorobenzyl fluoride in acetone-d6.

B. Computer simulation of the *meta* carbon region using parameters from Table 3.2.1 assuming a linewidth of 0.2 Hz.

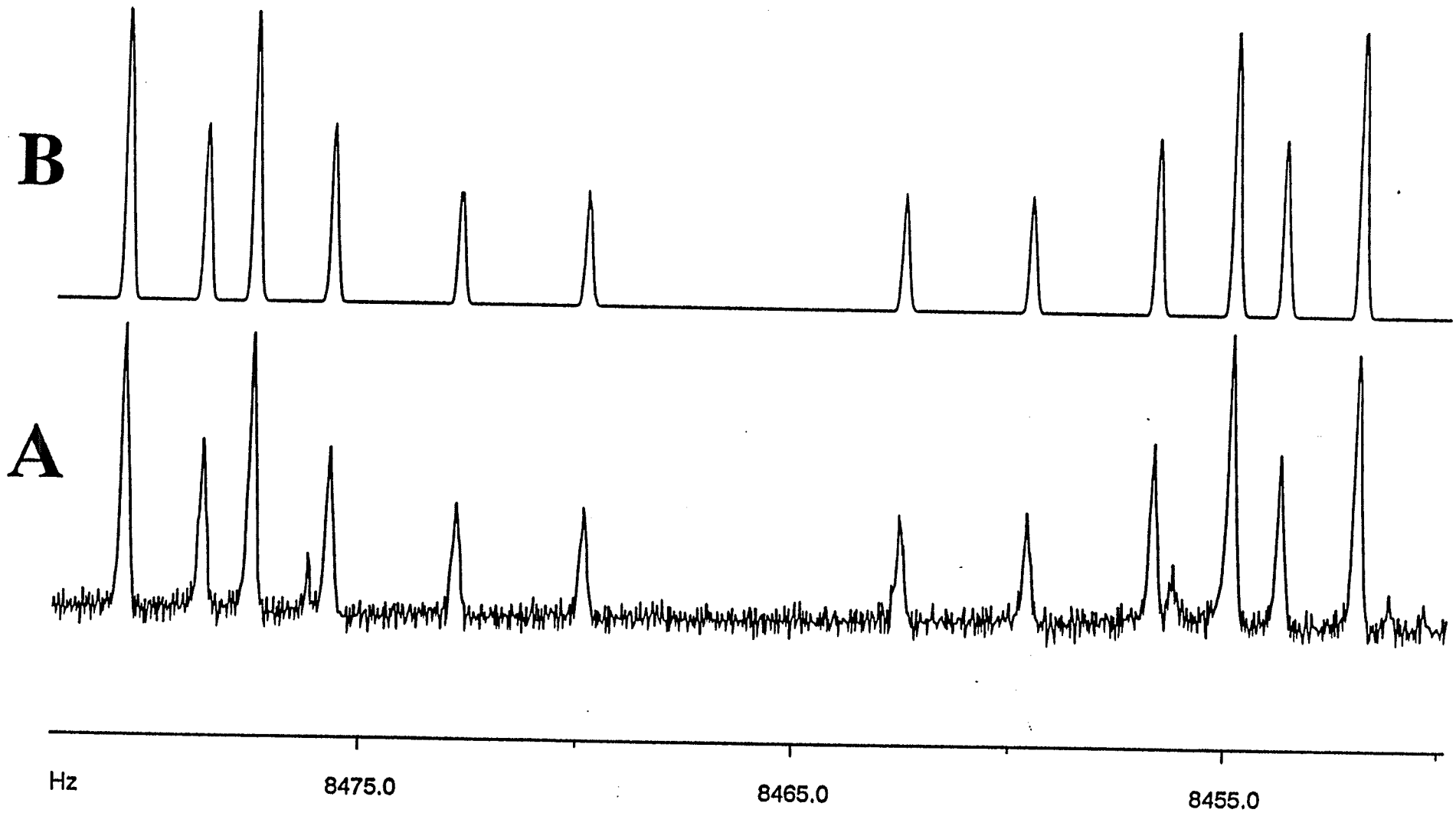
B
A
Hz
8475.0
8465.0
8455.0

Table 3.2.2: ^{13}C NMR spectral parameters[a] for a 5.0 mol% solution of 2,6-difluorobenzyl fluoride in $CS_2/C_6D_{12}/C_6F_6$/TMS at 300 K.

Nuclei	Chemical Shifts (Hz)	Chemical Shifts (ppm)
Ca	5352.05 (1)[b]	70.907
Ci	8478.27 (1)	112.325
Co	12219.23 (1)	161.887
Cm	8393.17 (1)	111.197
Cp	9921.55 (1)	131.446
Fo (isotope shift)[c]	+6.219 (3)	
	Coupling Constants (Hz)	
^1J(Fa,Ca)	-169.2 (1)[d]	
^2J(Fa,Ci)	17.11 (1)	
^3J(Fa,Co)	3.27 (1)	
^4J(Fa,Cm)	(-)2.82 (1)	
^5J(Fa,Cp)	3.82 (1)	
^1J(Fo,Co)	-253.08 (1)	
^2J(Fo,Cm)	21.90 (1)	
^2J(Fo,Ci)	18.94 (1)	
^3J(Fo′,Co)	7.15 (1)	
^3J(Fo,Cp)	10.28 (1)	
^3J(Fo,Ca)	4.6 (1)[d]	
^4J(Fo′,Cm)	3.74 (1)	

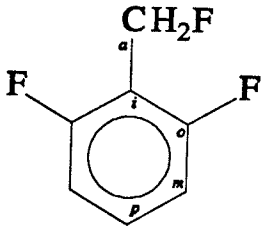

	Ca[d]	Ci	Co	Cm	Cp
Calculated Transitions	24	24	32	36	24
Assigned Transitions	6	8	8	12	8
Peaks Observed	6	6	8	12	6
Largest Difference	0.185	0.011	0.018	0.006	0.017
RMS Deviation of Transitions	0.138	0.009	0.019	0.004	0.019

Notes:

a. In hertz, at 75.48 MHz to high frequency of internal TMS (^{13}C NMR).

b. Numbers in parentheses are standard deviations in the last significant digit, as given by the NUMMRIT analysis.

c. The *ortho* fluorine adjacent to ^{12}Cm is deshielded by +6.219 Hz (isotope shift).

d. A high-resolution spectrum was not done for this region.

Figure 3.2.2

A. The *ortho* carbon region of 2,6-difluorobenzyl fluoride in CS_2/C_6D_{12}. No isotope effect is observed.

B. Computer simulation of the *ortho* carbon region using parameters from Table 3.2.2 assuming a linewidth of 0.1 Hz.

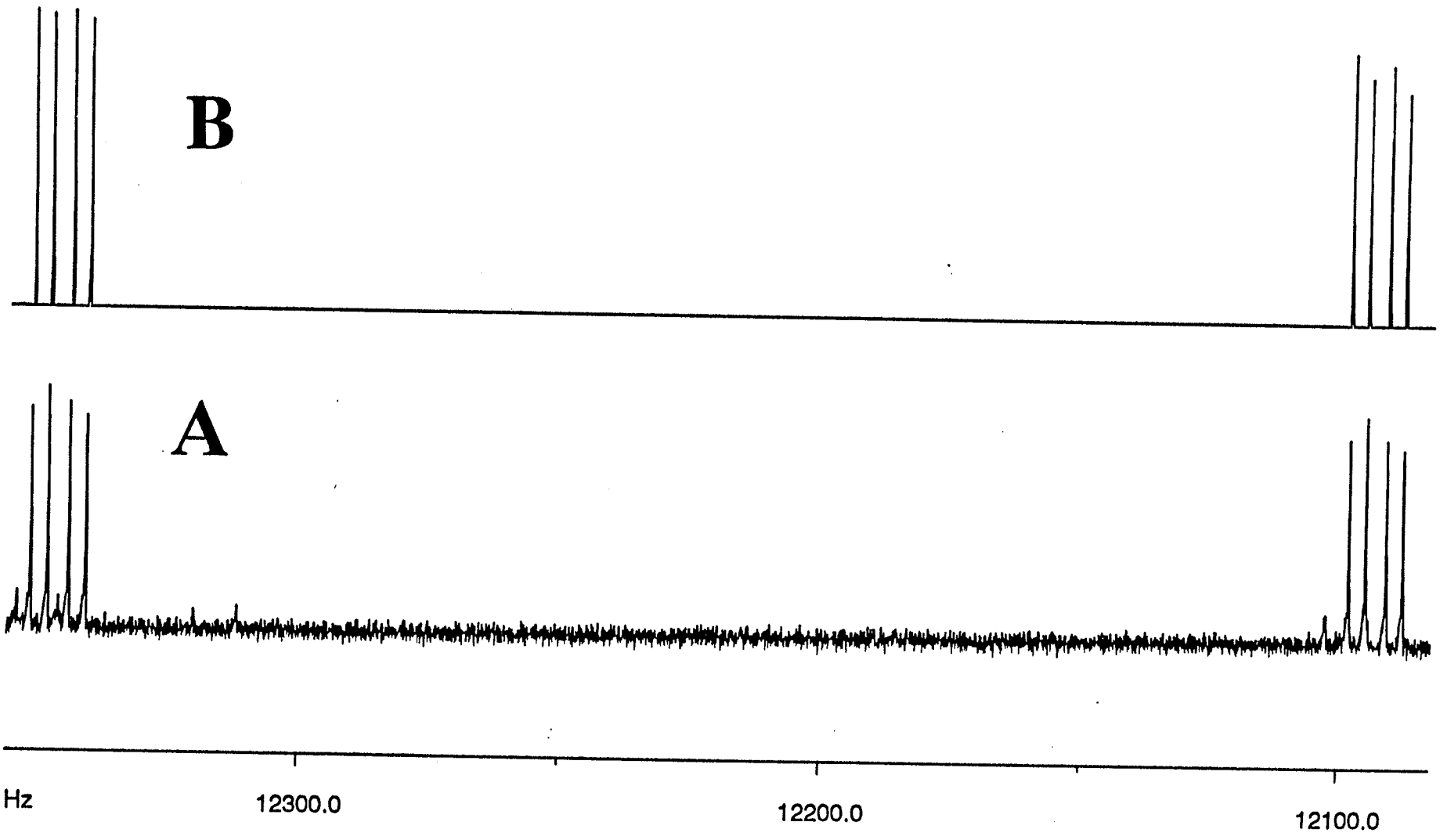
B
A
Hz
12300.0
12200.0
12100.0

Table 3.2.3: ^{13}C NMR spectral parameters[a] for a 5.0 mol% solution of 3,5-difluorobenzyl fluoride in acetone-d6/C_6F_6/TMS at 300 K.

Nuclei	Chemical Shifts (Hz)	Chemical Shifts (ppm)
Ca	6307.08 (1)[b]	83.560
Ci	10720.45 (1)	142.030
Co	8343.62 (1)	110.541
Cm	12373.98 (1)	163.937
Cp	7868.78 (1)	104.250
Fm (isotope shift)[c]	+6.007 (20)	
Coupling Constants (Hz)		
^1J(Fa,Ca)	-166.88 (1)	
^2J(Fa,Ci)	18.18 (1)	
^3J(Fa,Co)	7.01 (1)	
^4J(Fa,Cm)	(-)0.33 (1)	
^5J(Fa,Cp)	2.13 (2)	
^1J(Fm,Cm)	-246.96 (1)	
^2J(Fm,Co)	22.52 (2)	
^2J(Fm,Cp)	25.67 (1)	
^3J(Fm′,Cm)	12.96 (1)	
^3J(Fm,Ci)	9.27 (1)	
^4J(Fm,Ca)	2.26 (1)	
^4J(Fm′,Co)	3.46 (2)	

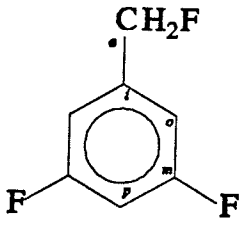

	Ca	Ci	Co	Cm	Cp
Calculated Transitions	24	24	36	32	24
Assigned Transitions	6	8	12	8	8
Peaks Observed	6	6	12	8	6
Largest Difference	0.007	0.018	0.026	0.011	0.025
RMS Deviation of Transitions	0.006	0.012	0.021	0.008	0.027689

Notes:

a. In hertz, at 75.48 MHz to high frequency of internal TMS (^{13}C NMR).

b. Numbers in parentheses are standard deviations in the last significant digit, as given by the NUMMRIT analysis.

c. The *meta* fluorine adjacent to ^{12}Co is deshielded by +6.007 Hz (isotope shift).

Figure 3.2.3

A. Expanded ^{13}C NMR spectrum of the *meta* carbon region of 3,5-difluorobenzyl fluoride in acetone-d6. No isotope effect is observed.

B. Computer simulation of the *meta* carbon region using parameters from Table 3.2.3 assuming a linewidth of 0.1 Hz.

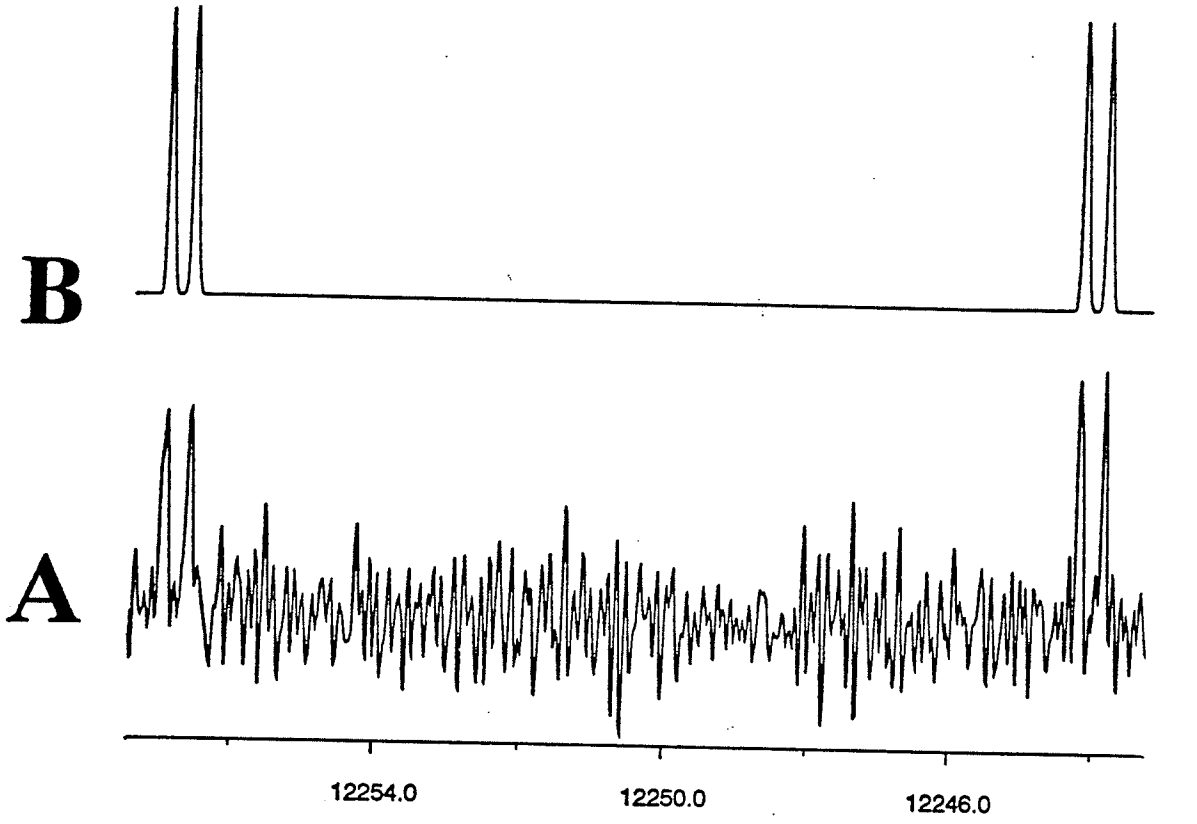
B
A
12254.0
12250.0
12246.0

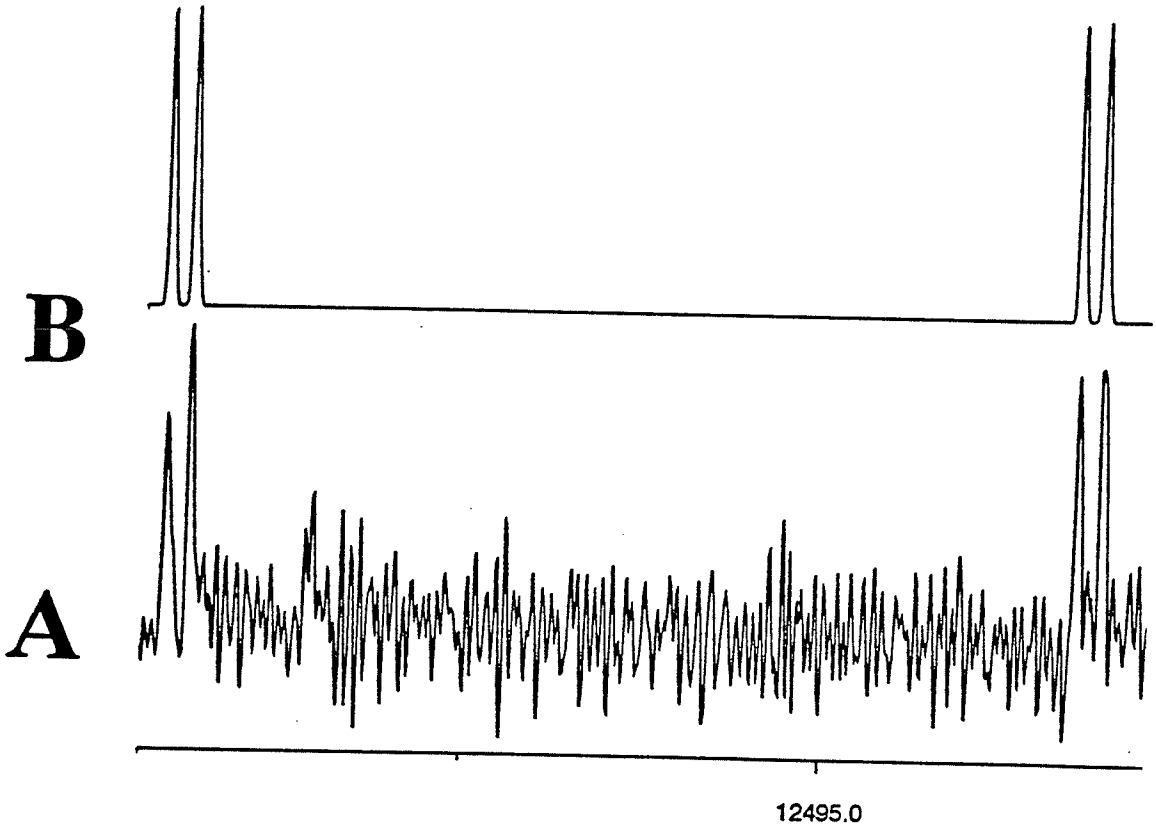
B
A
12495.0

Table 3.2.4: ^{13}C NMR spectral parameters[a] for a 5.0 mol% solution of 3,5-difluorobenzyl fluoride in $CS_2/C_6D_{12}/C_6F_6$/TMS at 300 K.

Nuclei	Chemical Shifts (Hz)	Chemical Shifts (ppm)
Ca	6214.68 (1)[b]	82.335
Ci	10620.05 (1)	140.700
Co	8225.68 (1)	108.978
Cm	12325.36 (1)	163.293
Cp	7808.91 (1)	103.457
Fm (isotope shift)	+5.951 (6)	
	Coupling Constants (Hz)	
^1J(Fa,Ca)	-173.45 (1)	
^2J(Fa,Ci)	18.83 (2)	
^3J(Fa,Co)	7.23 (1)	
^4J(Fa,Cm)	(-)0.21 (2)	
^5J(Fa,Cp)	1.80 (1)	
^1J(Fm,Cm)	-250.13 (2)	
^2J(Fm,Co)	22.60 (1)	
^2J(Fm,Cp)	25.13 (1)	
^3J(Fm′,Cm)	12.51 (2)	
^3J(Fm,Ci)	8.94 (1)	
^4J(Fm,Ca)	2.28 (1)	
^4J(Fm′,Co)	3.29 (1)	

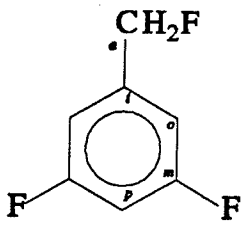

	Ca	Ci	Co	Cm	Cp
Calculated Transitions	24	24	36	32	24
Assigned Transitions	6	8	12	8	8
Peaks Observed	6	6	12	8	6
Largest Difference	0.011	0.033	0.007	0.027	0.010
RMS Deviation of Transitions	0.010	0.026	0.007	0.024	0.007

Notes:

a. In hertz, at 75.48 MHz to high frequency of internal TMS (^{13}C NMR).

b. Numbers in parentheses are standard deviations in the last significant digit, as given by the NUMMRIT analysis.

c. The *meta* fluorine adjacent to ^{12}Co is deshielded by +5.951 Hz (isotope shift).

Figure 3.2.4

A. The ^{13}C NMR spectrum of the *ortho* carbon region of 3,5-difluorobenzyl fluoride in CS_2/C_6D_{12}.

B. Computer simulation of the *ortho* carbon region using parameters from Table 3.2.4 assuming a linewidth of 0.1 Hz.

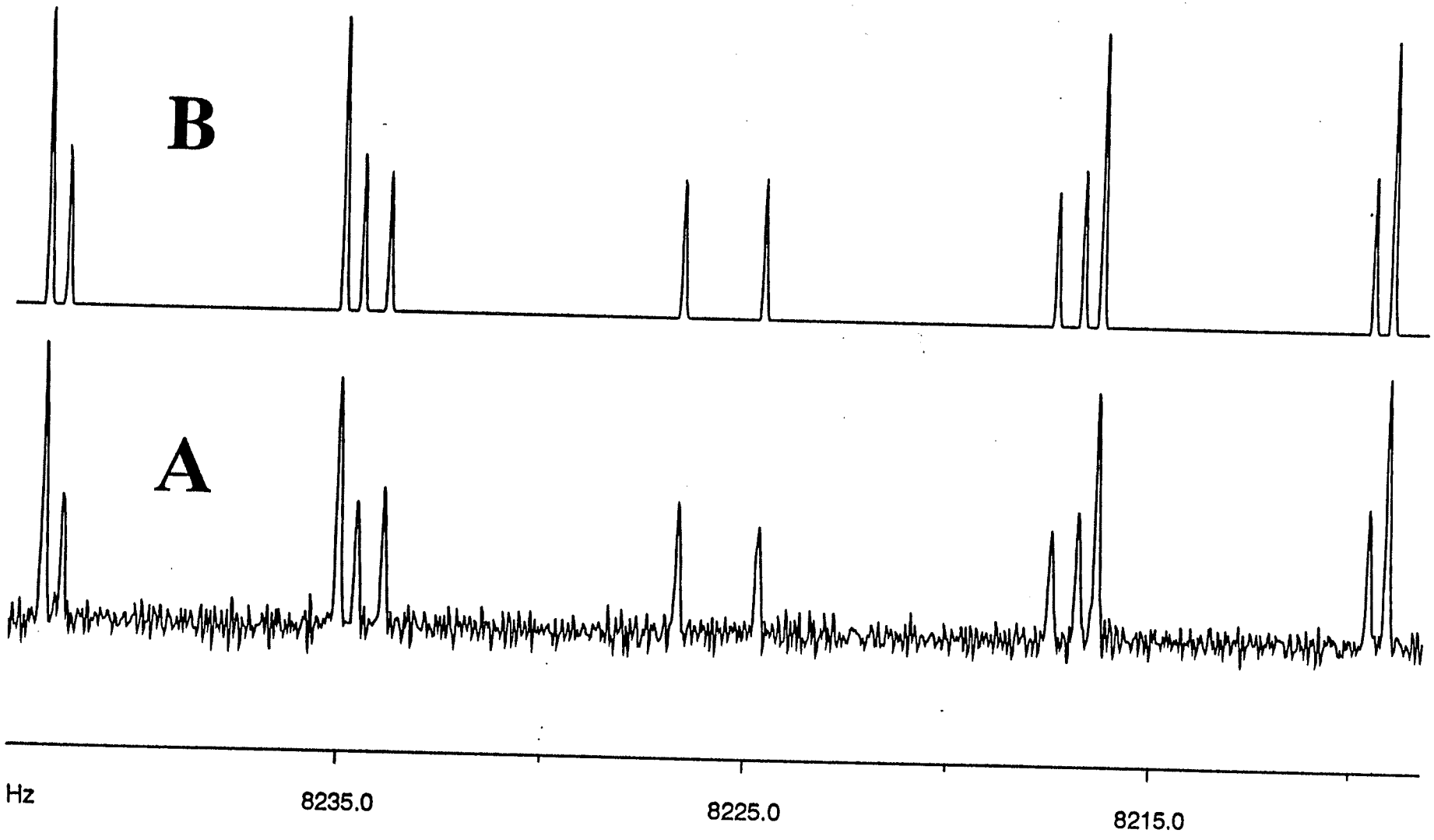
B
A
Hz
8235.0
8225.0
8215.0

Table 3.2.5: ^{13}C NMR spectral parameters[a] for a 5.0 mol% solution of 4-fluorobenzyl fluoride in acetone-d6/C_6F_6/TMS at 300 K.

Nuclei	Chemical Shifts (Hz)	Chemical Shifts (ppm)
Ca	6368.35 (1)[b]	84.371
Ci	10091.20 (1)	133.693
Co	9883.37 (1)	130.940
Cm	8764.18 (1)	116.112
Cp	12359.97 (1)	163.751
	Coupling Constants (Hz)	
^1J(Fa,Ca)	-163.67 (1)	
^2J(Fa,Ci)	17.41 (1)	
^3J(Fa,Co)	5.46 (1)	
^4J(Fa,Cm)	(-)1.71 (1)	
^5J(Fa,Cp)	3.47 (1)	
^1J(Fp,Cp)	-245.14 (1)	
^2J(Fp,Cm)	21.76 (1)	
^3J(Fp,Co)	8.50 (1)	
^4J(Fp,Ci)	3.12 (1)	
^5J(Fp,Ca)	0.89 (1)	

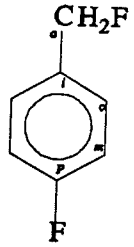

	Ca	Ci	Co	Cm	Cp
Calculated Transitions	12	12	12	12	12
Assigned Transitions	4	4	4	4	4
Peaks Observed	4	4	4	4	4
Largest Difference	0.000	0.007	0.001	0.001	0.002
RMS Deviation of Transitions	0.000	0.013	0.001	0.002	0.003

Notes:

a. In hertz, at 75.48 MHz to high frequency of internal TMS (^{13}C NMR).

b. Numbers in parentheses are standard deviations in the last significant digit, as given by the NUMMRIT analysis.

Table 3.2.6: ^{13}C NMR spectral parameters[a] for a 5.0 mol% solution of 4-fluorobenzyl fluoride in $CS_2/C_6D_{12}/C_6F_6$/TMS at 300 K.

Nuclei	Chemical Shifts (Hz)	Chemical Shifts (ppm)
Ca	6131.95 (1)[b]	81.239
Ci	9854.94 (2)	129.943
Co	9609.72 (1)	127.314
Cm	8569.02 (1)	113.527
Cp	12153.82 (1)	161.020
	Coupling Constants (Hz)	
^1J(Fa,Ca)	-170.04 (1)	
^2J(Fa,Ci)	18.05 (4)	
^3J(Fa,Co)	5.58 (1)	
^4J(Fa,Cm)	(-)1.27 (1)	
^5J(Fa,Cp)	3.10 (1)	
^1J(Fp,Cp)	-248.34 (1)	
^2J(Fp,Cm)	21.56 (1)	
^3J(Fp,Co)	8.16 (1)	
^4J(Fp,Ci)	3.37 (4)	
^5J(Fp,Ca)	0.77 (5)	

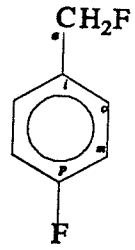

	Ca	Ci	Co	Cm	Cp
Calculated Transitions	12	12	12	12	12
Assigned Transitions	4	4	4	4	4
Peaks Observed	4	4	4	4	4
Largest Difference	0.002	0.020	0.003	0.002	0.005
RMS Deviation of Transitions	0.005	0.040	0.006	0.005	0.010

Notes:

a. In hertz, at 75.48 MHz to high frequency of internal TMS (^{13}C NMR).

b. Numbers in parentheses are standard deviations in the last significant digit, as given by the NUMMRIT analysis.

3.3 Molecular orbital calculations

a) Benzyl fluoride

Tables 3.3.1 to 3.3.5 show the relative energies and dipole moments for benzyl fluoride at 15° intervals of the dihedral angle, ϕ, between the benzylic C-F bond and the ring plane. The minimum energy conformer is at $\phi = 0°$, unless otherwise noted. Potentials fit to functions of the form

$$V(\phi) = \sum_n V_n \sin^2(\frac{n\phi}{2})$$

and classical expectation values are presented in Table 3.3.6. Plots of the potential fits are shown in Figure 3.3.1. The molecular geometry at the MP2/6-31G** level appears in Figure 3.3.2. Bond lengths are reported in angstroms (Å).

Table 3.3.1: Benzyl fluoride at the 6-31G* level

Angle (ϕ)	Total Energy (a.u.)	Relative Energy (kJ mol^{-1})	Dipole Moment (Debye)
0	-368.586377	0.000	1.736
30	-368.586197	0.472	1.814
45	-386.585951	1.117	1.900
60	-386.585580	2.093	1.997
75	-386.585215	3.051	2.072
90	-368.585064	3.446	2.101

Table 3.3.2: Benzyl fluoride at the 6-311G* level

Angle (ϕ)	Total Energy (a.u.)	Relative Energy (kJ mol^{-1})	Dipole Moment (Debye)
0	-368.662713	0.000	1.813
30	-368.662444	0.707	1.879
45	-368.662212	1.316	1.960
60	-368.661946	2.015	2.053
75	-368.661690	2.687	2.126
90	-368.661576	2.986	2.155

Table 3.3.3: Benzyl fluoride at the 6-31G level**

Angle (ϕ)	Total Energy (a.u.)	Relative Energy (kJ mol^{-1})	Dipole Moment (Debye)
0	-368.598780	0.000	1.727
30	-368.598532	0.652	1.804
45	-368.598242	1.415	1.891
60	-368.597857	2.426	1.986
75	-368.597347	3.373	2.059
90	-368.598780	3.763	2.086

Table 3.3.4: Benzyl fluoride at the MP2/6-31G* level

Angle (ϕ)	Total Energy (a.u.)	Relative Energy (kJ mol^{-1})	Dipole Moment (Debye)
0	-369.639849	0.000	1.848
15	-369.639864	-0.041	1.873
18.70§	-369.639866	-0.046	1.886
30	-369.639830	0.048	1.933
45	-369.639614	0.617	2.027
60	-369.639216	1.660	2.131
75	-369.638849	2.625	2.217
90	-369.638712	2.986	2.249

§ Lowest energy conformation

Table 3.3.5: Benzyl fluoride at the MP2/6-31G level**

Angle (ϕ)	Total Energy (a.u.)	Relative Energy (kJ mol^{-1})	Dipole Moment (Debye)
0	-369.695569	0.000	1.836
13.49§	-369.695574	-0.014	1.854
15	-369.695574	-0.012	1.858
30	-369.695511	0.151	1.920
45	-369.695268	0.790	2.014
60	-369.694879	1.812	2.116
75	-369.694537	2.710	2.197
90	-369.694411	3.041	2.228

§ Lowest energy conformation

Table 3.3.6: Least squares fits and classical expectation values at 300 K for benzyl fluoride

Basis	V_2	V_4	V_6	V_8	$\langle\sin^2\phi\rangle$
6-31G*	3.379	-0.607	0.068	0.020	0.349
6-311G*	2.861	-0.176	0.124	---	0.364
6-31G**	3.692	-0.468	0.072	0.011	0.334
MP2/6-31G*	3.068	-0.878	-0.080	0.026	0.365
MP2/6-31G**	3.137	-0.733	-0.094	0.014	0.360

Figure 3.3.1

Potential energy functions for the internal rotation of the benzylic C-F bond in benzyl fluoride. Relative energies were calculated at the

A. 6-31G*, 6-311G* and 6-31G** levels.

B. MP2/6-31G* and MP2/6-31G** levels.

Benzyl fluoride M.O. Calculations

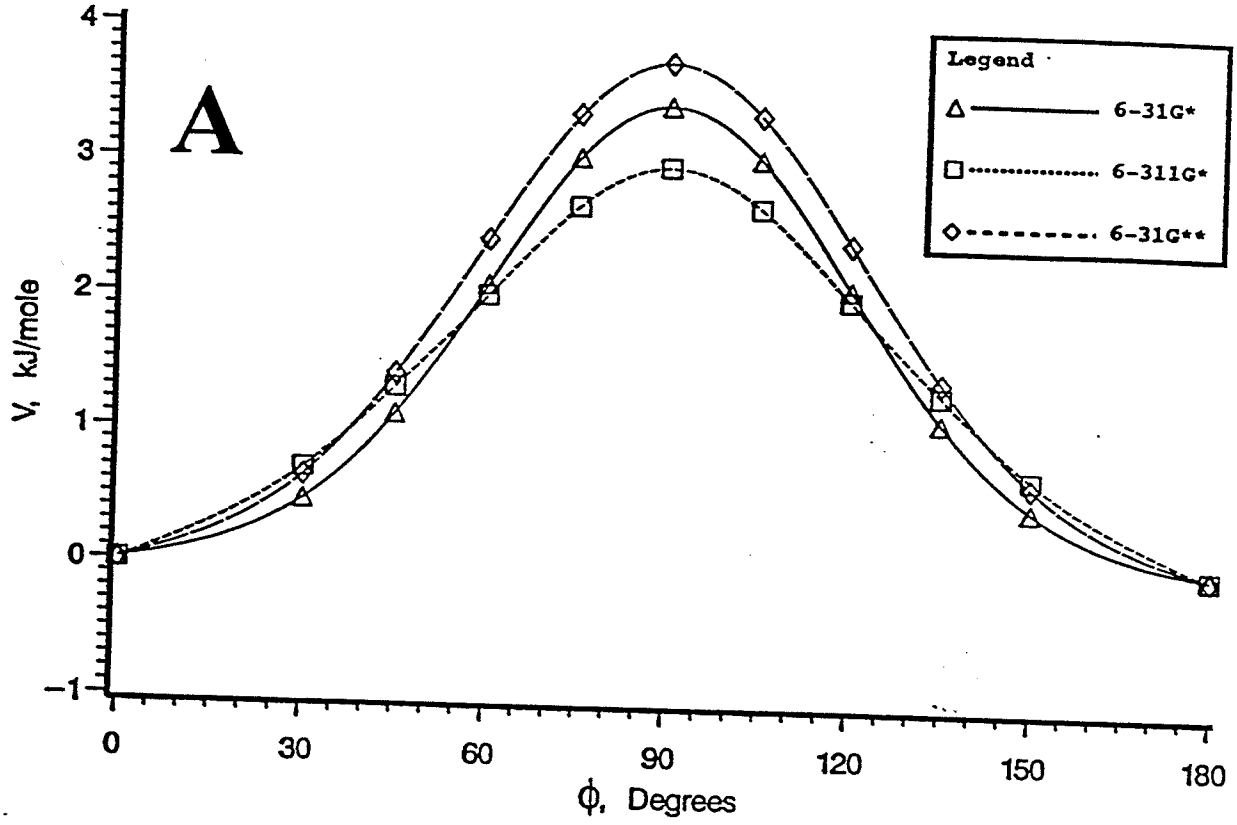

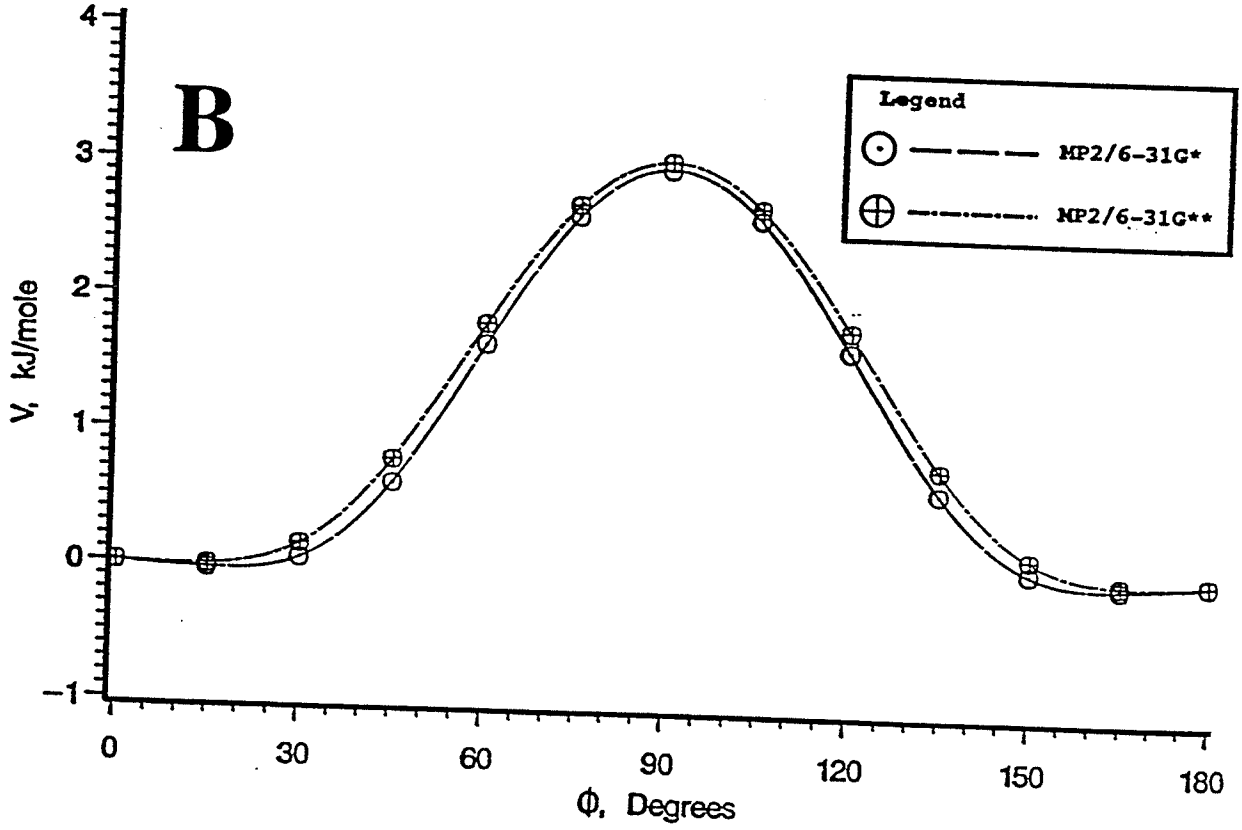

Figure 3.3.2

The molecular geometries of benzyl fluoride calculated at the MP2/6-31G** level.

A. Parallel conformer.

B. Perpendicular conformer.

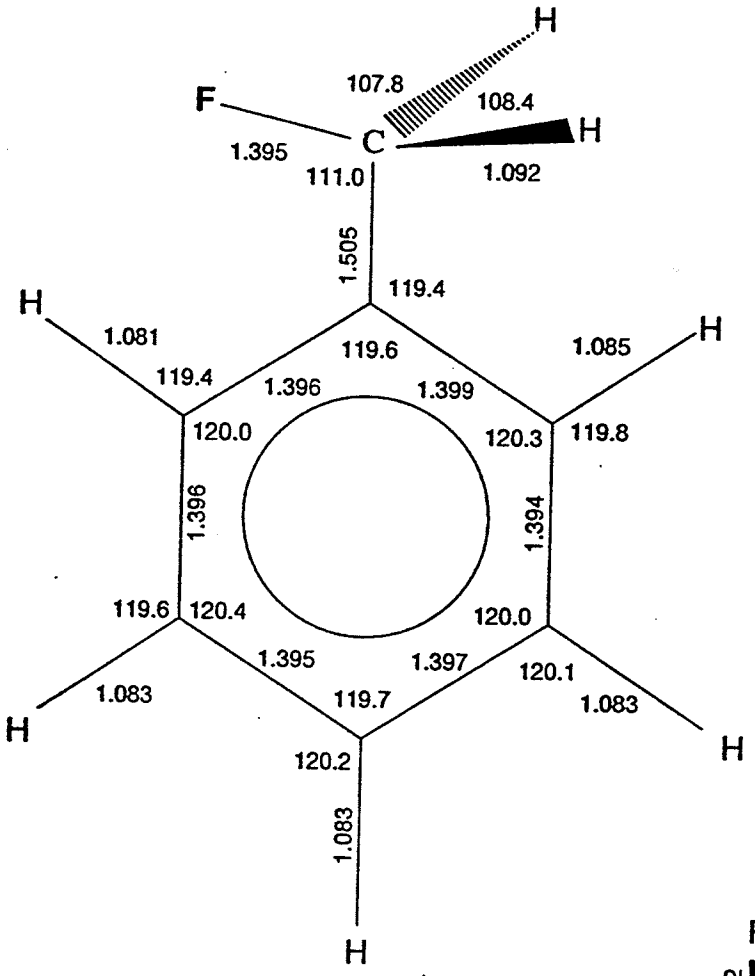
H
F
107.8
108.4
H
C
1.395
1.092
111.0
1.505
119.4
H
1.081
119.6
1.085
H
119.4
1.396
1.399
120.0
120.3
119.8
1.396
1.394
119.6
120.4
120.0
1.395
1.397
120.1
1.083
119.7
1.083
H
H
120.2
1.083
H

A

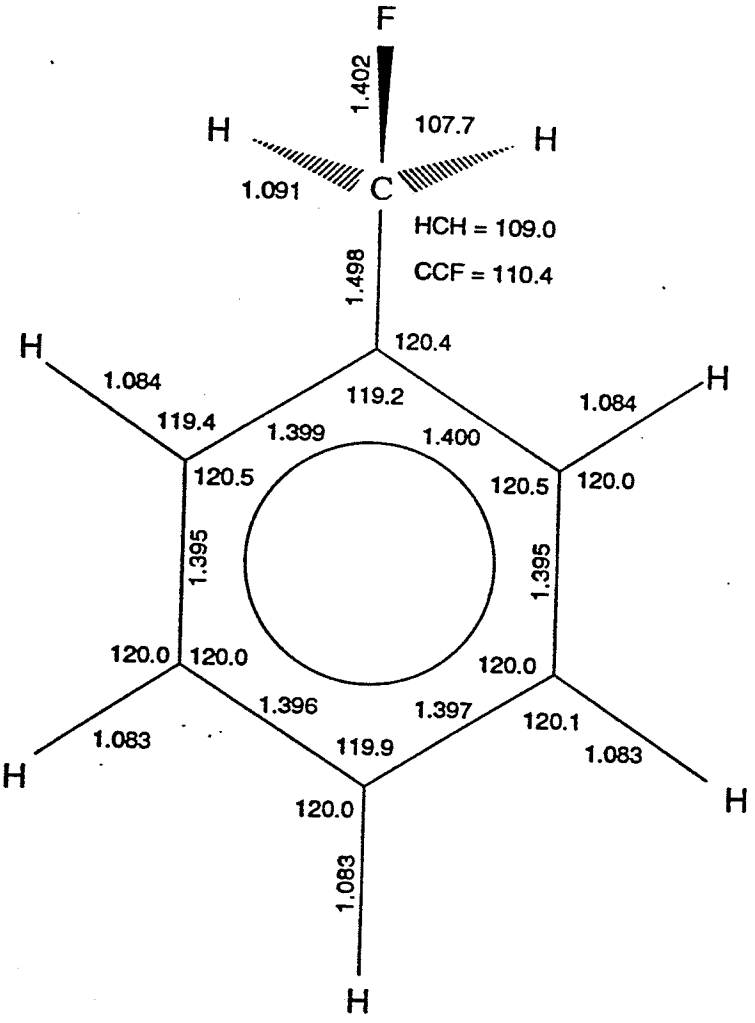
F
1.402
H
107.7
H
1.091
C
HCH = 109.0
CCF = 110.4
1.498
120.4
H
1.084
119.2
1.084
H
119.4
1.399
1.400
120.5
120.5
120.0
1.395
1.395
120.0
120.0
120.0
1.396
1.397
120.1
1.083
119.9
1.083
H
H
120.0
1.083
H

B

b) 2,6-difluorobenzyl fluoride

Tables 3.3.7 to 3.3.11 show the relative energies and dipole moments for 2,6-difluorobenzyl fluoride at 15° intervals of the dihedral angle, ϕ, between the benzylic C-F bond and the ring plane. The minimum energy conformer is at ϕ = 90° in all cases. Potentials fits and classical expectation values are presented in Table 3.3.12. Plots of the potential fits are shown in Figure 3.3.3. The molecular geometry of 2,6-difluorobenzyl fluoride calculated at the MP2/6-31G** level appears in Figure 3.3.4. Bond lengths are reported in angstroms (Å).

Table 3.3.7: 2,6-difluorobenzyl fluoride at the 6-31G* level

Angle (ϕ)	Total Energy (a.u.)	Relative Energy (kJ mol^{-1})	Dipole Moment (Debye)
0	-566.282315	0.000	2.803
30	-566.283651	-3.508	2.812
45	-566.285107	-7.331	2.863
60	-566.286147	-10.062	2.961
75	-566.286452	-10.863	3.063
90	-566.286487	-10.954	3.106

Table 3.3.8: 2,6-difluorobenzyl fluoride at the 6-311G* level

Angle (ϕ)	Total Energy (a.u.)	Relative Energy (kJ mol^{-1})	Dipole Moment (Debye)
0	-566.415130	0.000	2.893
30	-566.416555	-3.741	2.903
45	-566.418157	-7.946	2.959
60	-566.419452	-11.348	3.054
75	-566.419972	-12.713	3.152
90	-566.420070	-12.970	3.195

Table 3.3.9: 2,6-difluorobenzyl fluoride at the 6-31G level**

Angle (ϕ)	Total Energy (a.u.)	Relative Energy (kJ mol^{-1})	Dipole Moment (Debye)
0	-566.291183	0.000	2.793
30	-566.292539	-3.561	2.803
45	-566.293975	-7.332	2.857
60	-566.294993	-10.005	2.954
75	-566.295300	-10.811	3.054
90	-566.295341	-10.919	3.096

Table 3.3.10: 2,6-difluorobenzyl fluoride at the MP2/6-31G* level

Angle (ϕ)	Total Energy (a.u.)	Relative Energy (kJ mol^{-1})	Dipole Moment (Debye)
0	-567.671796	0.000	3.084
30	-567.673116	-3.466	3.081
45	-567.674570	-7.282	3.127
60	-567.675617	-10.032	3.226
75	-567.675891	-10.751	3.338
90	-567.675906	-10.791	3.384

Table 3.3.11: 2,6-difluorobenzyl fluoride at the MP2/6-31G level**

Angle (ϕ)	Total Energy (a.u.)	Relative Energy (kJ mol^{-1})	Dipole Moment (Debye)
0	-567.711130	0.000	3.067
30	-567.712471	-3.521	3.069
45	-567.713879	-7.218	3.116
60	-567.714880	-9.845	3.214
75	-567.715161	-10.581	3.324
90	-567.715190	-10.658	3.370

Table 3.3.12: Least squares fits and classical expectation values at 300 K for 2,6-difluorobenzyl fluoride

Basis	V_2	V_4	V_6	V_8	$\langle\sin^2\phi\rangle$
6-31G*	-11.65	-1.875	0.718	0.130	0.832
6-311G*	-13.70	-1.478	0.748	0.065	0.863
6-31G**	-11.55	-1.892	0.656	0.127	0.830
MP2/6-31G*	-11.54	-1.914	0.780	0.108	0.829
MP2/6-31G**	-11.29	-1.913	0.663	0.108	0.826

Figure 3.3.3

Potential energy functions for the internal rotation of the benzylic C-F bond in 2,6-difluorobenzyl fluoride. Relative energies were calculated at the

A. 6-31G*, 6-311G* and 6-31G** levels.

B. MP2/6-31G* and MP2/6-31G** levels.

2,6-difluorobenzyl fluoride M.O. Calculations

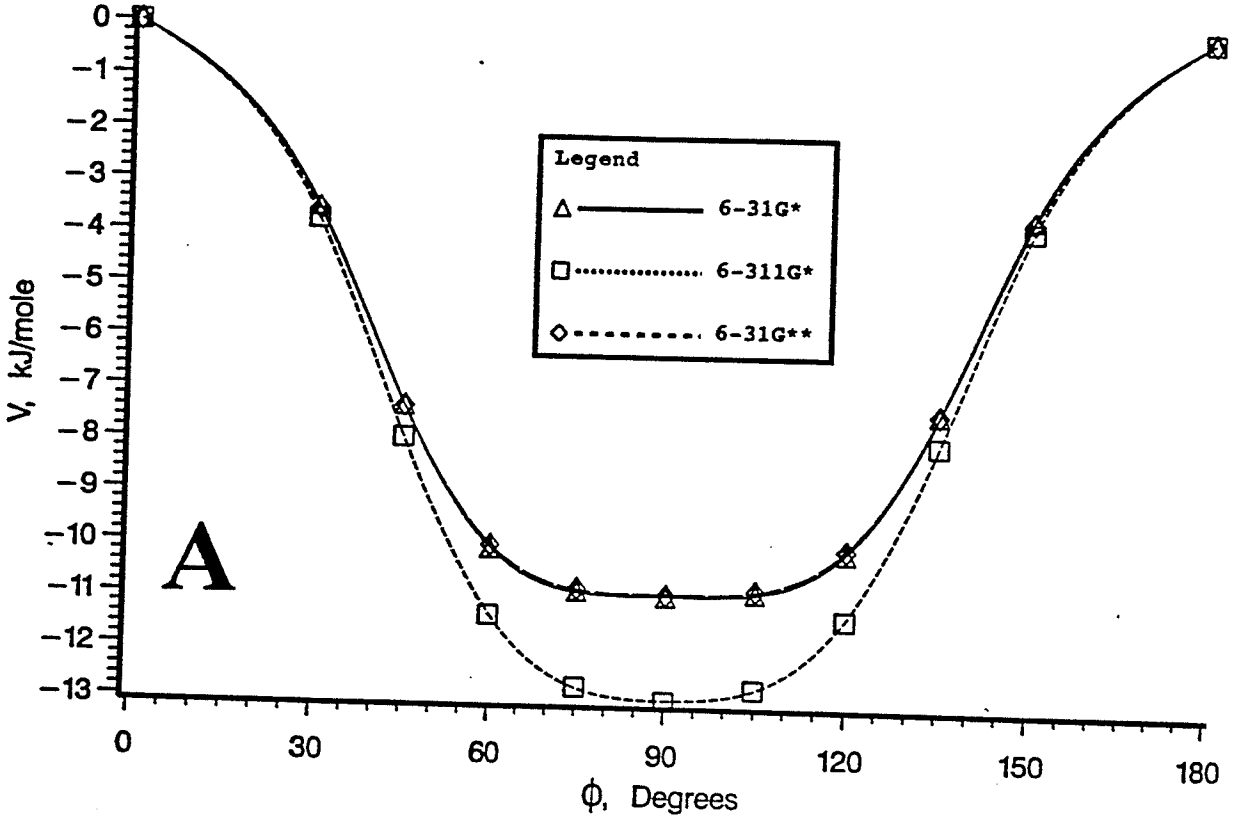

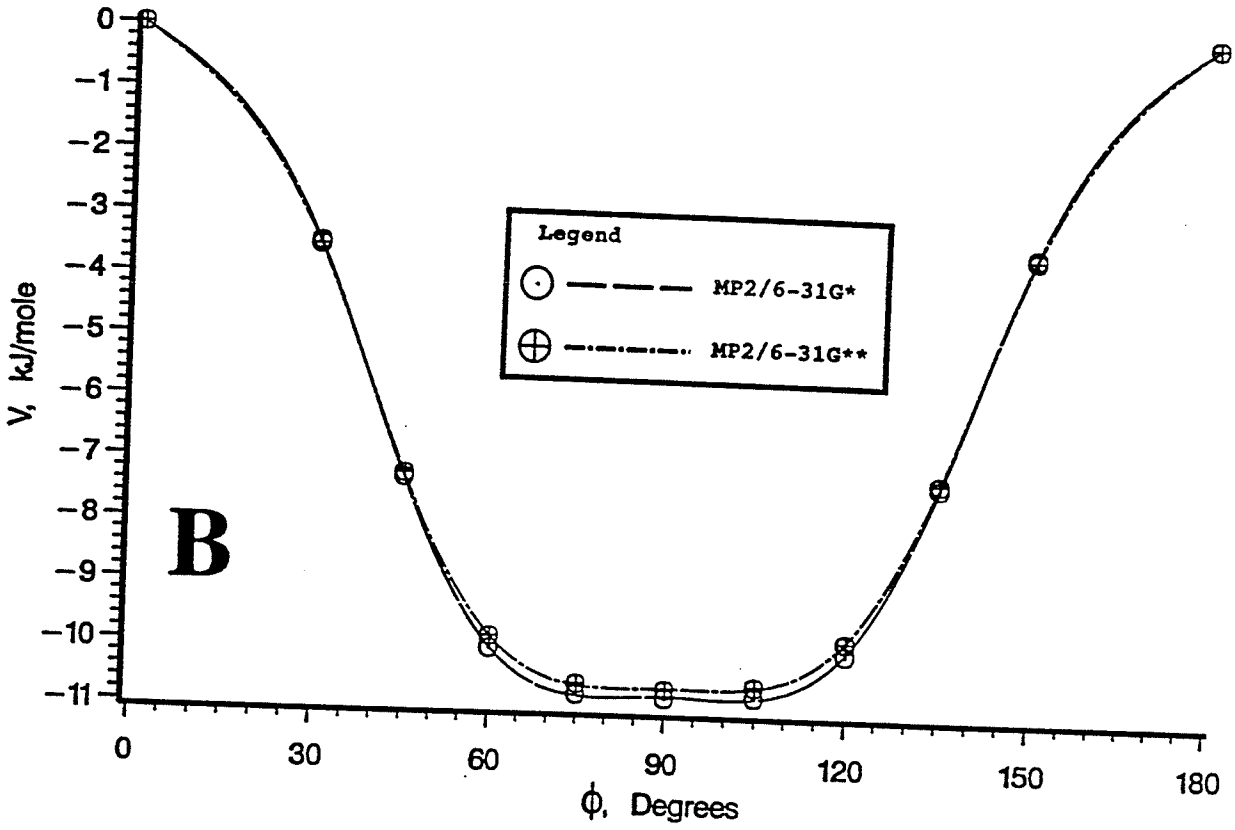

Figure 3.3.4

The molecular geometries of 2,6-difluorobenzyl fluoride calculated at the MP2/6-31G** level.

A. Parallel conformer.

B. Perpendicular conformer.

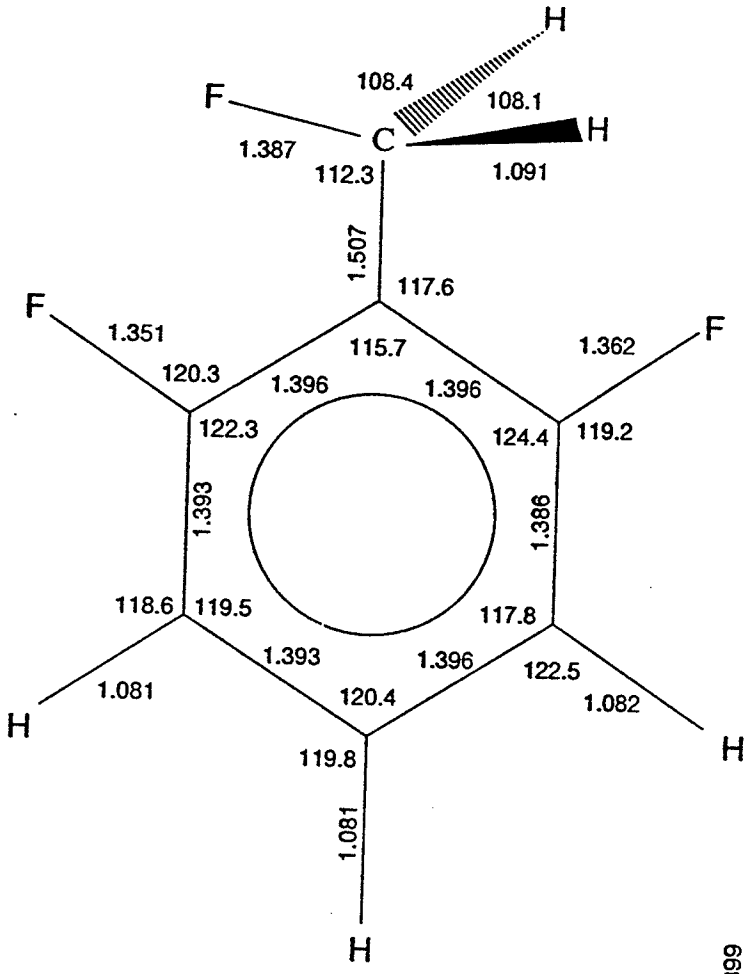
H
108.4
F
108.1
C
H
1.387
1.091
112.3
1.507
117.6
F
1.351
115.7
1.362
F
120.3
1.396
1.396
122.3
124.4
119.2
1.393
1.386
118.6
119.5
117.8
1.393
1.396
122.5
1.081
120.4
1.082
H
H
119.8
1.081
H

A

B

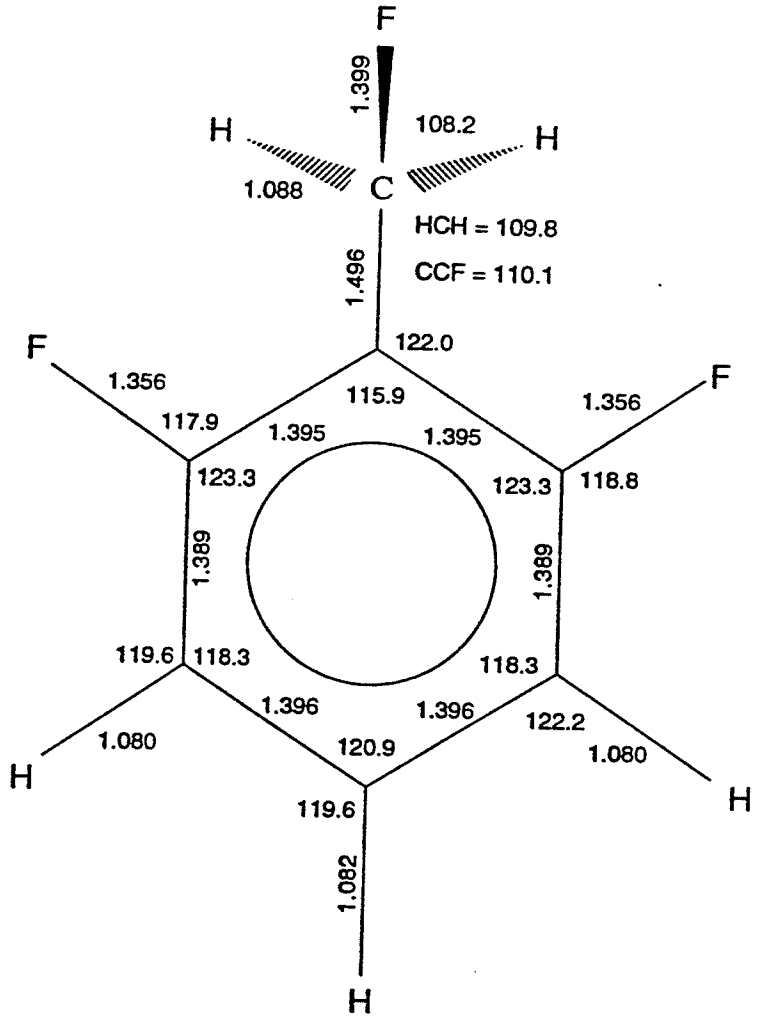
F
1.399
H
108.2
H
1.088
C
HCH = 109.8
CCF = 110.1
1.496
122.0
F
1.356
115.9
1.356
F
117.9
1.395
1.395
123.3
123.3
118.8
1.389
1.389
119.6
118.3
118.3
1.396
1.396
122.2
1.080
120.9
1.080
H
H
119.6
1.082
H

c) 3,5-difluorobenzyl fluoride

Tables 3.3.13 to 3.3.17 show the relative energies and dipole moments for 3,5-difluorobenzyl fluoride at 15° intervals of the dihedral angle, ϕ, between the benzylic C-F bond and the ring plane. The minimum energy conformer is at $\phi = 0°$ in all cases. Potentials fits and classical expectation values are presented in Table 3.3.18. Plots of the potential fits are shown in Figure 3.3.5. The molecular geometry of 3,5-difluorobenzyl fluoride calculated at the MP2/6-31G** level appears in Figure 3.3.6. Bond lengths are reported in angstroms (Å).

Table 3.3.13: 3,5-difluorobenzyl fluoride at the 6-31G* level

Angle (ϕ)	Total Energy (a.u.)	Relative Energy (kJ mol^{-1})	Dipole Moment (Debye)
0	-566.288524	0.000	1.839
30	-566.288001	1.373	1.859
45	-566.287422	2.892	1.867
60	-566.286729	4.712	1.862
75	-566.286129	6.286	1.851
90	-566.285891	6.913	1.846

Table 3.3.14: 3,5-difluorobenzyl fluoride at the 6-311G* level

Angle (ϕ)	Total Energy (a.u.)	Relative Energy (kJ mol^{-1})	Dipole Moment (Debye)
0	-566.422230	0.000	1.922
30	-566.421615	1.616	1.934
45	-566.421057	3.080	1.934
60	-566.420481	4.592	1.927
75	-566.420001	5.853	1.917
90	-566.419805	6.368	1.911

Table 3.3.15: 3,5-difluorobenzyl fluoride at the 6-31G level**

Angle (ϕ)	Total Energy (a.u.)	Relative Energy (kJ mol^{-1})	Dipole Moment (Debye)
0	-566.297511	0.000	1.850
30	-566.296917	1.557	1.867
45	-566.296294	3.193	1.873
60	-566.295588	5.048	1.867
75	-566.294990	6.618	1.854
90	-566.294752	7.242	1.848

Table 3.3.16: 3,5-difluorobenzyl fluoride at the MP2/6-31G* level

Angle (ϕ)	Total Energy (a.u.)	Relative Energy (kJ mol^{-1})	Dipole Moment (Debye)
0	-567.677043	0.000	2.102
30	-567.676802	0.635	2.032
45	-567.676347	1.828	2.040
60	-567.675706	3.510	2.028
75	-567.675160	4.945	2.007
90	-567.674957	5.478	2.000

Table 3.3.17: 3,5-difluorobenzyl fluoride at the MP2/6-31G level**

Angle (ϕ)	Total Energy (a.u.)	Relative Energy (kJ mol^{-1})	Dipole Moment (Debye)
0	-567.716015	0.000	2.022
30	-567.715749	0.698	2.038
45	-567.715289	1.906	2.040
60	-567.714676	3.515	2.026
75	-567.714166	4.855	2.005
90	-567.713977	5.350	1.994

Table 3.3.18: Least squares fits and classical expectation values at 300 K for 3,5-difluorobenzyl fluoride

Basis	V_2	V_4	V_6	V_8	$\langle \sin^2\phi \rangle$
6-31G*	6.836	-0.565	0.078	0.013	0.230
6-311G*	6.229	-0.104	0.139	-0.003	0.237
6-31G**	7.157	-0.430	0.087	0.005	0.218
MP2/6-31G*	5.571	-0.914	-0.091	0.025	0.275
MP2/6-31G**	5.448	-0.7713	-0.0950	0.0133	0.276

Figure 3.3.5

Potential energy functions for the internal rotation of the benzylic C-F bond in 3,5-difluorobenzyl fluoride. Relative energies were calculated at the

A. 6-31G*, 6-311G* and 6-31G** levels.

B. MP2/6-31G* and MP2/6-31G** levels.

3,5-difluorobenzyl fluoride M.O. Calculations

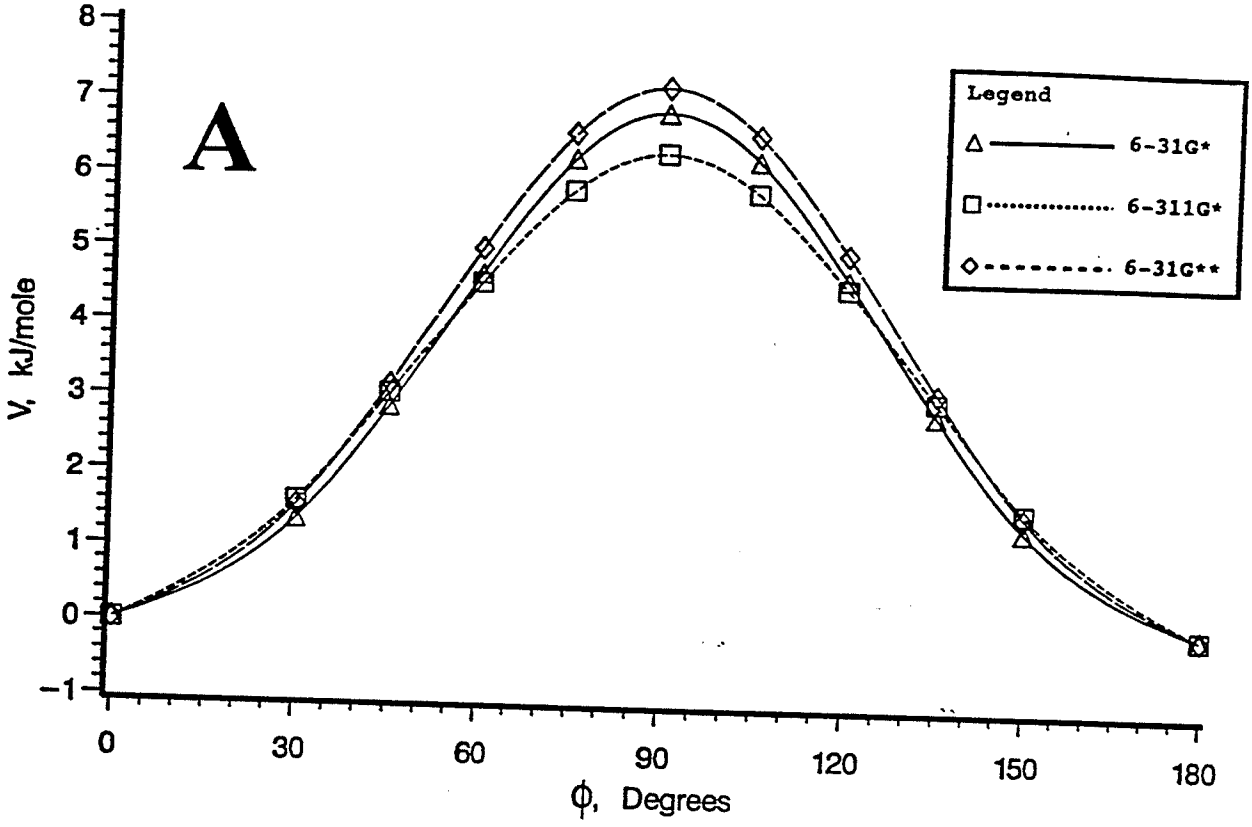

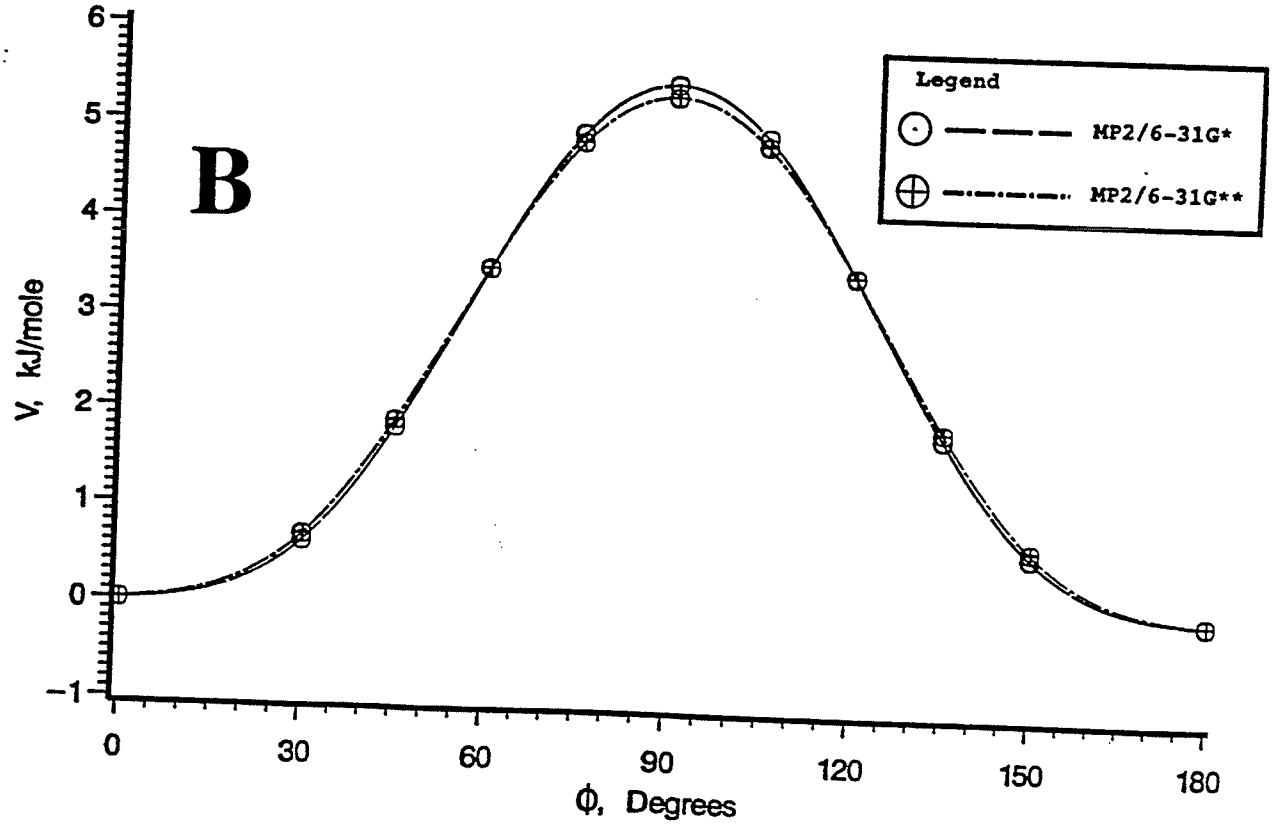

Figure 3.3.6

The molecular geometries of 3,5-difluorobenzyl fluoride calculated at the MP2/6-31G** level.

A. Parallel conformer.

B. Perpendicular conformer.

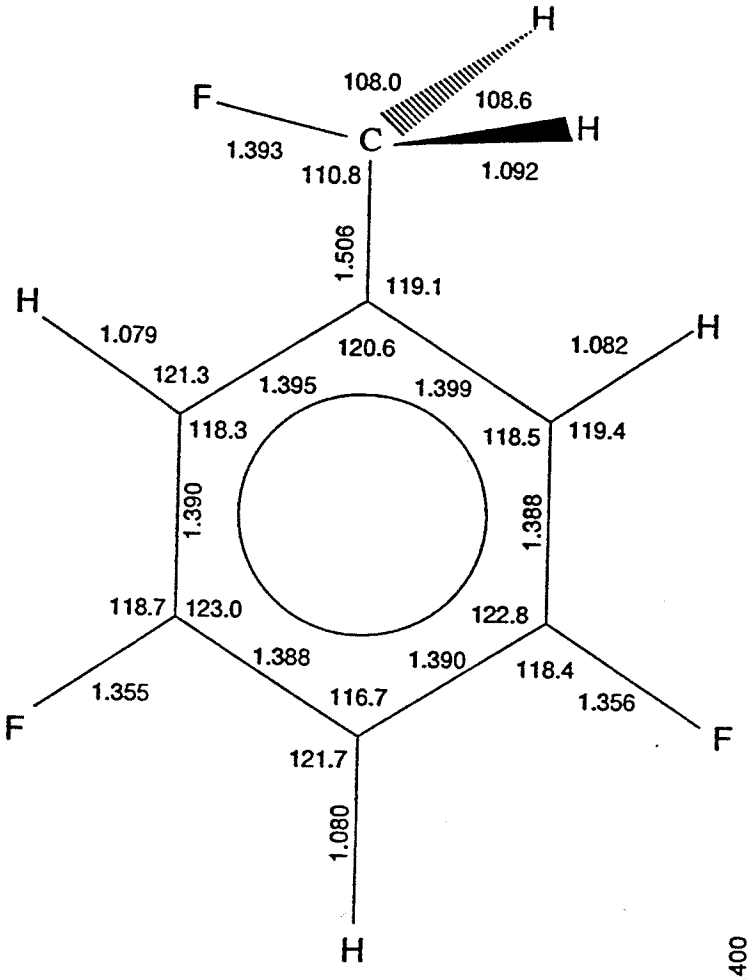
H
108.0
F
108.6
C
H
1.393
1.092
110.8
1.506
119.1
H
1.079
120.6
1.082
H
121.3
1.395
1.399
118.3
118.5
119.4
1.390
1.388
118.7
123.0
122.8
1.388
1.390
118.4
1.355
116.7
1.356
F
F
121.7
1.080
H

A

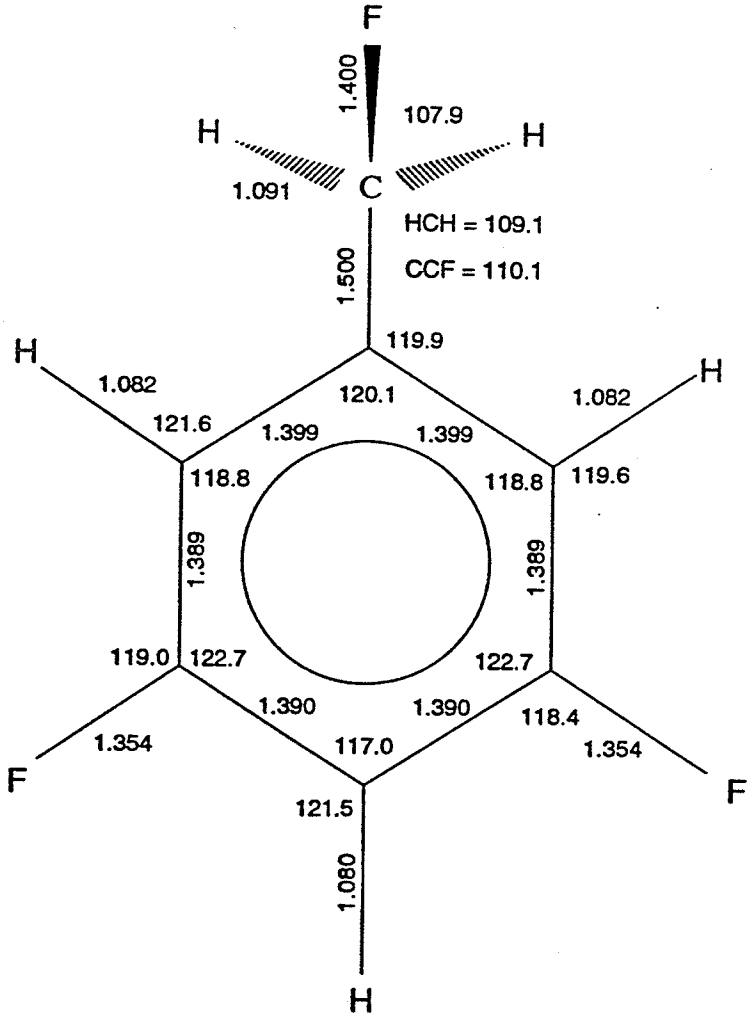
F
1.400
107.9
H
H
1.091
C
HCH = 109.1
CCF = 110.1
1.500
119.9
H
1.082
120.1
1.082
H
121.6
1.399
1.399
118.8
118.8
119.6
1.389
1.389
119.0
122.7
122.7
1.390
1.390
118.4
1.354
117.0
1.354
F
F
121.5
1.080
H

B

d) 4-fluorobenzyl fluoride

Tables 3.3.19 to 3.3.23 show the relative energies and dipole moments for 4-fluorobenzyl fluoride at 15° intervals of the dihedral angle, ϕ, between the benzylic C-F bond and the ring plane. The minimum energy conformer is at ϕ = 0°, except where noted otherwises. Potentials fits and classical expectation values are presented in Table 3.3.24. Plots of the potential fits are shown in Figure 3.3.7. The molecular geometry of 4-fluorobenzyl fluoride calculated at the MP2/6-31G** level appears in Figure 3.3.8. Bond lengths are reported in angstroms (Å).

Table 3.3.19: 4-fluorobenzyl fluoride at the 6-31G* level

Angle (ϕ)	Total Energy (a.u.)	Relative Energy (kJ mol^{-1})	Dipole Moment (Debye)
0	-467.437253	0.000	1.813
30	-467.437189	0.169	1.816
45	-467.437036	0.570	1.818
60	-467.436742	1.341	1.818
75	-467.436431	2.158	1.817
90	-467.436301	2.500	1.816

Table 3.3.20: 4-fluorobenzyl fluoride at the 6-311G* level

Angle (ϕ)	Total Energy (a.u.)	Relative Energy (kJ mol^{-1})	Dipole Moment (Debye)
0	-467.542287	0.000	1.902
30	-467.542134	0.402	1.894
45	-467.542002	0.748	1.887
60	-467.541823	1.218	1.882
75	-467.541625	1.739	1.881
90	-467.541532	1.982	1.880

Table 3.3.21: 4-fluorobenzyl fluoride at the 6-31G level**

Angle (ϕ)	Total Energy (a.u.)	Relative Energy (kJ mol^{-1})	Dipole Moment (Debye)
0	-467.447907	0.000	1.824
30	-467.447776	0.342	1.824
45	-467.447581	0.855	1.822
60	-467.447277	1.654	1.820
75	-467.446971	2.457	1.817
90	-467.446843	2.792	1.816

Table 3.3.22: 4-fluorobenzyl fluoride at the MP2/6-31G* level

Angle (ϕ)	Total Energy (a.u.)	Relative Energy (kJ mol^{-1})	Dipole Moment (Debye)
0	-468.658545	0.000	1.955
15	-468.658579	-0.089	1.959
24.69§	-468.658599	-0.142	1.937
30	-468.658589	-0.115	1.967
45	-468.658417	0.337	1.975
60	-468.658054	1.290	1.973
75	-468.657711	2.189	1.967
90	-468.657584	2.523	1.965

§ Lowest energy conformation

Table 3.3.23: 4-fluorobenzyl fluoride at the MP2/6-31G level**

Angle (ϕ)	Total Energy (a.u.)	Relative Energy (kJ mol^{-1})	Dipole Moment (Debye)
0	-468.705874	0.000	1.963
15	-468.705899	-0.064	1.966
21.10§	-468.705906	-0.083	1.968
30	-468.705881	-0.017	1.970
45	-468.705684	0.501	1.973
60	-468.705331	1.426	1.970
75	-468.705016	2.254	1.961
90	-468.704900	2.558	1.956

§ Lowest energy conformation

Table 3.3.24: Least squares fits and classical expectation values at 300 K for 4-fluorobenzyl fluoride

Basis	V_2	V_4	V_6	V_8	$\langle\sin^2\phi\rangle$
6-31G*	2.450	-0.682	0.052	0.022	0.389
6-311G*	1.865	-0.243	0.117	0.001	0.410
6-31G**	2.737	-0.543	0.056	0.012	0.375
MP2/6-31G*	2.622	-0.927	-0.096	0.028	0.384
MP2/6-31G**	2.671	-0.780	-0.110	0.013	0.380

Figure 3.3.7

Potential energy functions for the internal rotation of the benzylic C-F bond in 4-fluorobenzyl fluoride. Relative energies were calculated at the

A. 6-31G*, 6-311G* and 6-31G** levels.

B. MP2/6-31G* and MP2/6-31G** levels.

4–fluorobenzyl fluoride M.O. Calculations

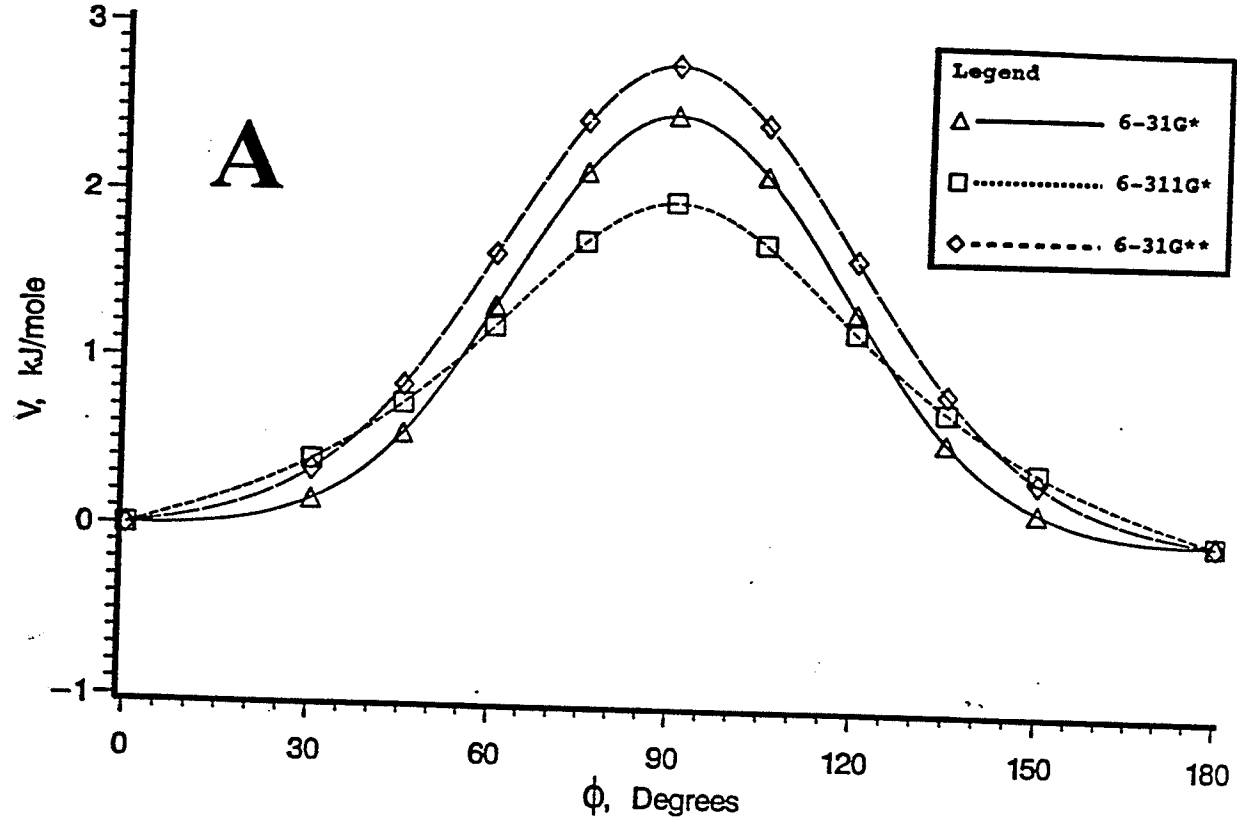

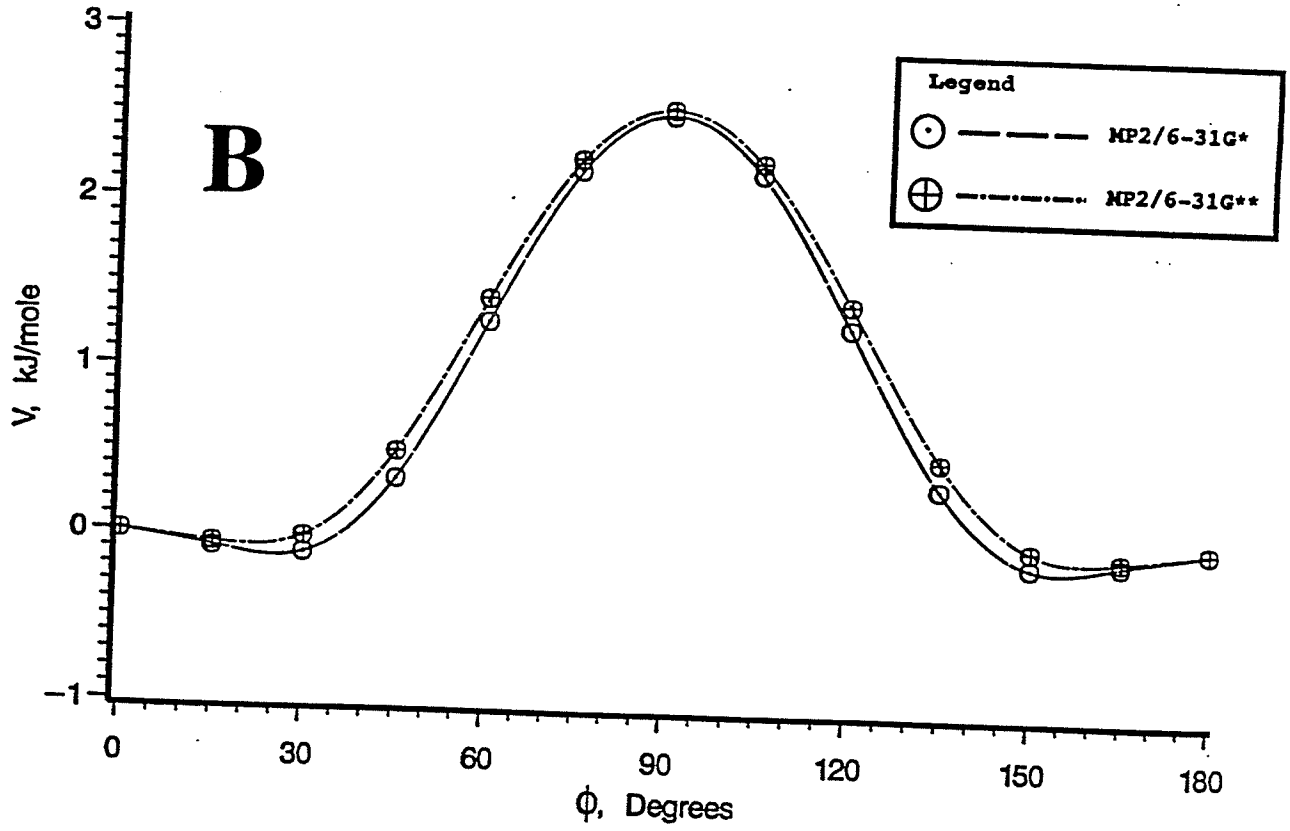

Figure 3.3.8

The molecular geometries of 4-fluorobenzyl fluoride calculated at the MP2/6-31G** level.

A. Parallel conformer.

B. Perpendicular conformer.

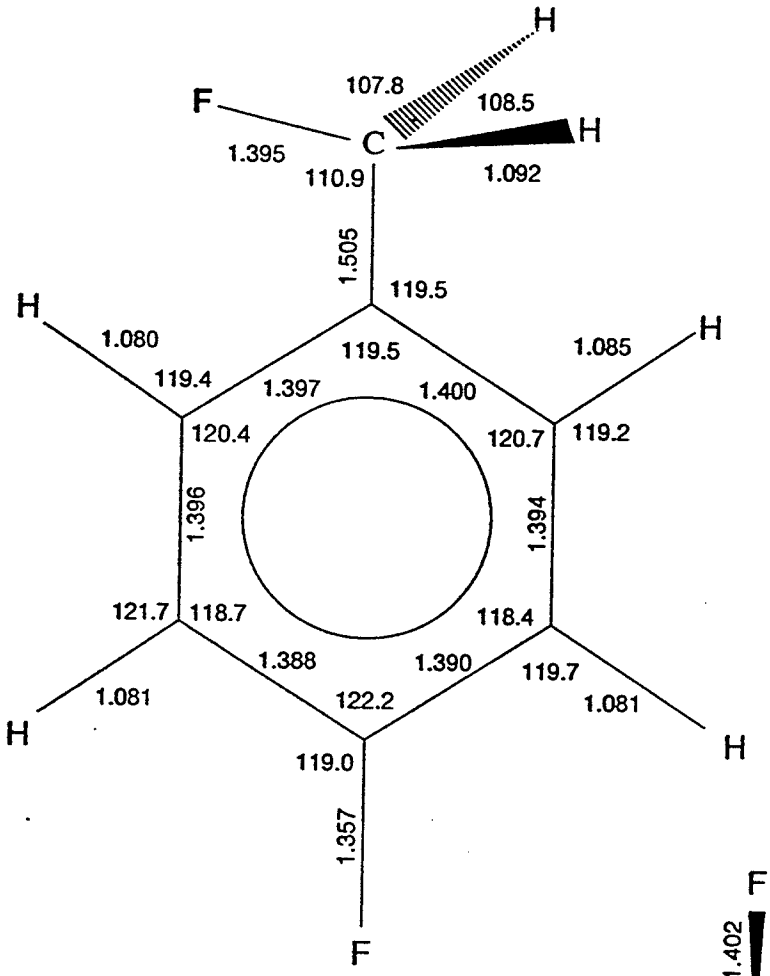
H
107.8
F
108.5
H
C
1.395
1.092
110.9
1.505
119.5
H
1.080
119.5
1.085
H
119.4
1.397
1.400
120.4
120.7
119.2
1.396
1.394
121.7
118.7
118.4
1.388
1.390
119.7
1.081
122.2
1.081
H
H
119.0
1.357
F

A

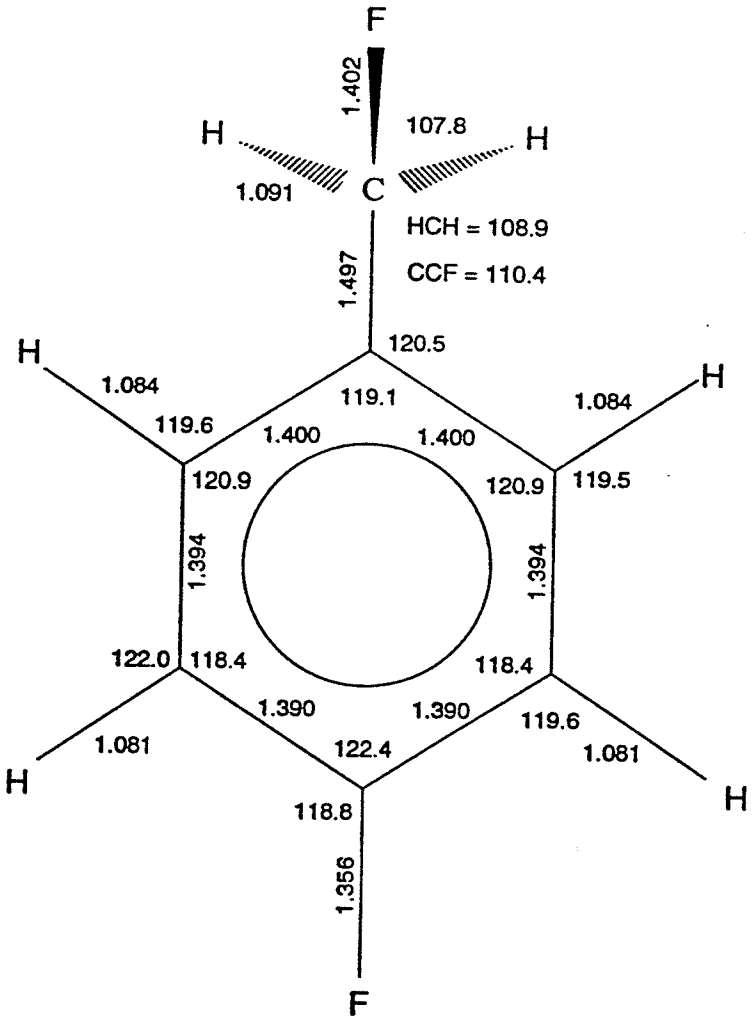
F
1.402
H
107.8
H
1.091
C
HCH = 108.9
CCF = 110.4
1.497
120.5
H
1.084
119.1
1.084
H
119.6
1.400
1.400
120.9
120.9
119.5
1.394
1.394
122.0
118.4
118.4
1.390
1.390
119.6
1.081
122.4
1.081
H
H
118.8
1.356
F

B

e) Solvent Effect Calculations

Dielectric solvent effects on the size and shape of internal rotational potentials are evaluated by geometry-optimized SCF calculations at the 6-31G* level using SCRFPAC. The ellipsoidal cavity is made up of van der Waals spheres to allow for geometry optimization. Continuum dielectric permittivity constants for acetone and CS_2 are 20.3 and 2.62, respectively. Relative energies and dipole moments for **1** to **4** in both acetone and CS_2 appear in Tables 3.3.25-3.3.32. Potential fits and classical expectation values appear in Table 3.3.33. Plots of the potential functions appear in Figures 3.3.9 and 3.3.10.

Table 3.3.25: Dielectric solvent effects on benzyl fluoride in acetone

Angle (ϕ)	Total Energy (a.u.)	Relative Energy (kJ mol^{-1})	Dipole Moment (Debye)
0	-368.590842	0.000	2.077
15	-368.590979	-0.360	2.091
30	-368.591268	-1.118	2.174
45	-368.591571	-1.914	2.340
60	-368.591813	-2.549	2.477
75	-368.592020	-3.094	2.548
90	-368.592201	-3.570	2.622

Table 3.3.26: Dielectric solvent effects on benzyl fluoride in CS_2

Angle (ϕ)	Total Energy (a.u.)	Relative Energy (kJ mol^{-1})	Dipole Moment (Debye)
0	-368.588653	0.000	1.908
15	-368.588702	-0.130	1.939
30	-368.588772	-0.313	2.004
45	-368.588739	-0.227	2.115
60	-368.588596	0.150	2.213
75	-368.588476	0.465	2.292
90	-368.588462	0.500	2.334

Table 3.3.27: Dielectric solvent effects on 2,6-difluorobenzyl fluoride in acetone

Angle (ϕ)	Total Energy (a.u.)	Relative Energy (kJ mol^{-1})	Dipole Moment (Debye)
0	-566.286829	0.000	3.233
30	-566.288706	-4.928	3.324
45	-566.290657	-10.050	3.416
60	-566.292183	-14.057	3.568
75	-566.292865	-15.846	3.757
90	-566.293179	-16.671	3.875

Table 3.3.28: Dielectric solvent effects on 2,6-difluorobenzyl fluoride in CS_2

Angle (ϕ)	Total Energy (a.u.)	Relative Energy (kJ mol^{-1})	Dipole Moment (Debye)
0	-566.284703	0.000	3.064
30	-566.286252	-4.069	3.092
45	-566.287895	-8.383	3.170
60	-566.289141	-11.652	3.283
75	-566.289591	-12.836	3.418
90	-566.289713	-13.154	3.494

Table 3.3.29: Dielectric solvent effects on 3,5-difluorobenzyl fluoride in acetone

Angle (ϕ)	Total Energy (a.u.)	Relative Energy (kJ mol^{-1})	Dipole Moment (Debye)
0	-566.293090	0.000	2.488
30	-566.293239	-0.391	2.485
45	-566.293311	-0.580	2.467
60	-566.293279	-0.498	2.467
75	-566.293261	-0.451	2.463
90	-566.293279	-0.498	2.467

Table 3.3.30: Dielectric solvent effects on 3,5-difluorobenzyl fluoride in CS_2

Angle (ϕ)	Total Energy (a.u.)	Relative Energy (kJ mol^{-1})	Dipole Moment (Debye)
0	-566.290886	0.000	2.125
30	-566.290610	0.725	2.154
45	-566.290279	1.594	2.153
60	-566.289854	2.711	2.140
75	-566.289474	3.708	2.117
90	-566.289326	4.097	2.113

Table 3.3.31: Dielectric solvent effects on 4-fluorobenzyl fluoride in acetone

Angle (ϕ)	Total Energy (a.u.)	Relative Energy (kJ mol^{-1})	Dipole Moment (Debye)
0	-467.441787	0.000	2.295
30	-467.442329	-1.422	2.327
45	-467.442755	-2.541	2.323
60	-467.443182	-3.663	2.305
75	-467.443449	-4.362	2.331
90	-467.443586	-4.724	2.334

Table 3.3.32: Dielectric solvent effects on 4-fluorobenzyl fluoride in CS_2

Angle (ϕ)	Total Energy (a.u.)	Relative Energy (kJ mol^{-1})	Dipole Moment (Debye)
0	-467.439589	0.000	2.058
30	-467.439769	-0.472	2.060
45	-467.439869	-0.735	2.047
60	-467.439857	-0.702	2.048
75	-467.439788	-0.521	2.040
90	-467.439755	-0.435	2.044

Table 3.3.33: Least squares fits and classical expectation values at 300 K (errors appear in parentheses)

Molec.	Solvent	V_2	V_4	V_6	V_8	$\langle \sin^2\phi \rangle$
1	acetone	-3.26(3)	-0.17(3)	-0.25(3)	0.08(3)	0.653
1	CS_2	0.67(2)	-0.48(2)	-0.14(2)	--	0.468
2	acetone	-17.09(8)	-1.81(7)	0.53(7)	0.27(8)	0.891
2	CS_2	-13.78(4)	-1.85(3)	0.67(3)	0.14(4)	0.859
3	acetone	-0.40(1)	-0.33(1)	-0.09(1)	0.07(1)	0.519
3	CS_2	4.06(1)	-0.46(1)	0.04(1)	0.02(1)	0.319
4	acetone	-4.61(3)	-0.23(3)	-0.08(3)	--	0.706
4	CS_2	-0.44(1)	-0.52(1)	0.01(1)	0.02(1)	0.521

Figure 3.3.9

Potential energy functions for the internal rotation of the benzylic C-F bond in

A. benzyl fluoride

B. 2,6-difluorobenzyl fluoride

Dielectric solvent effects, calculated at the 6-31G* level.

Benzyl fluoride M.O. Calculations (6–31G*)
Dielectric Solvent Effects

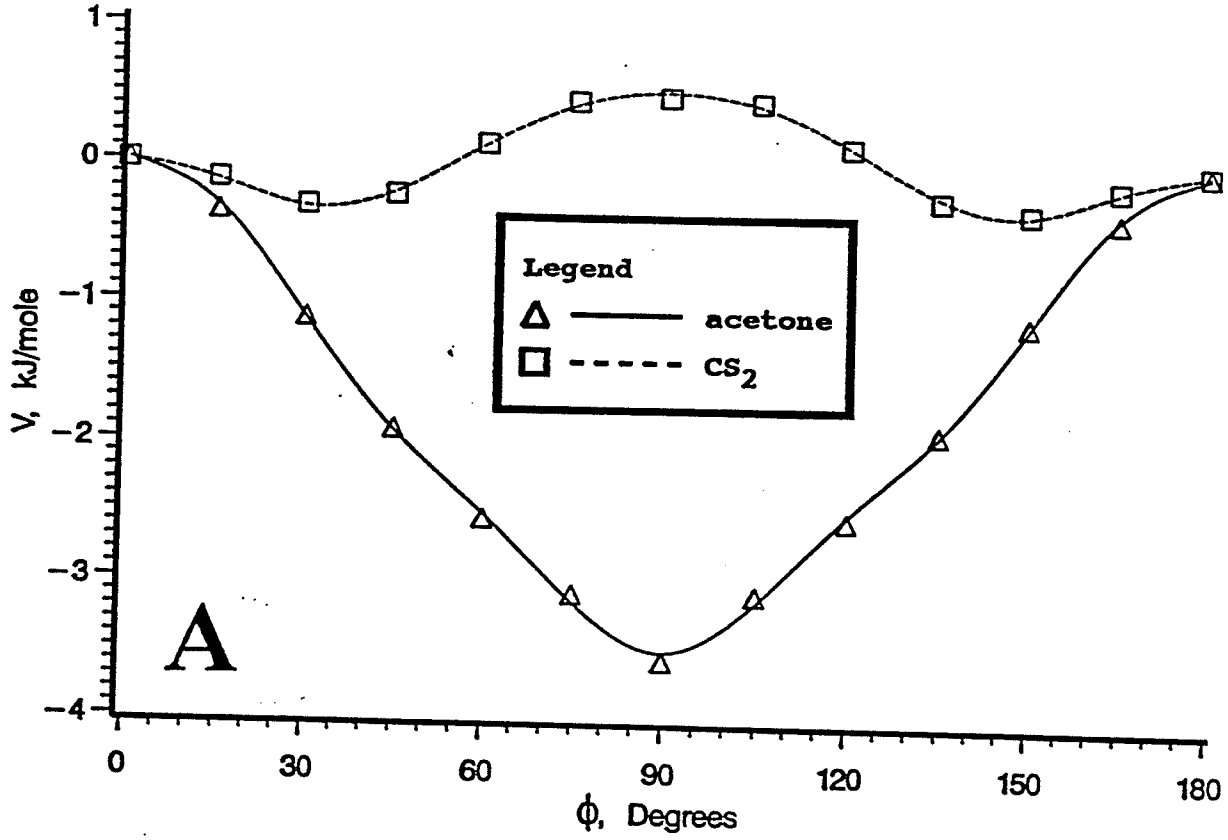

2,6–difluorobenzylfluoride M.O. Calculations (6–31G*)
Dielectric Solvent Effects

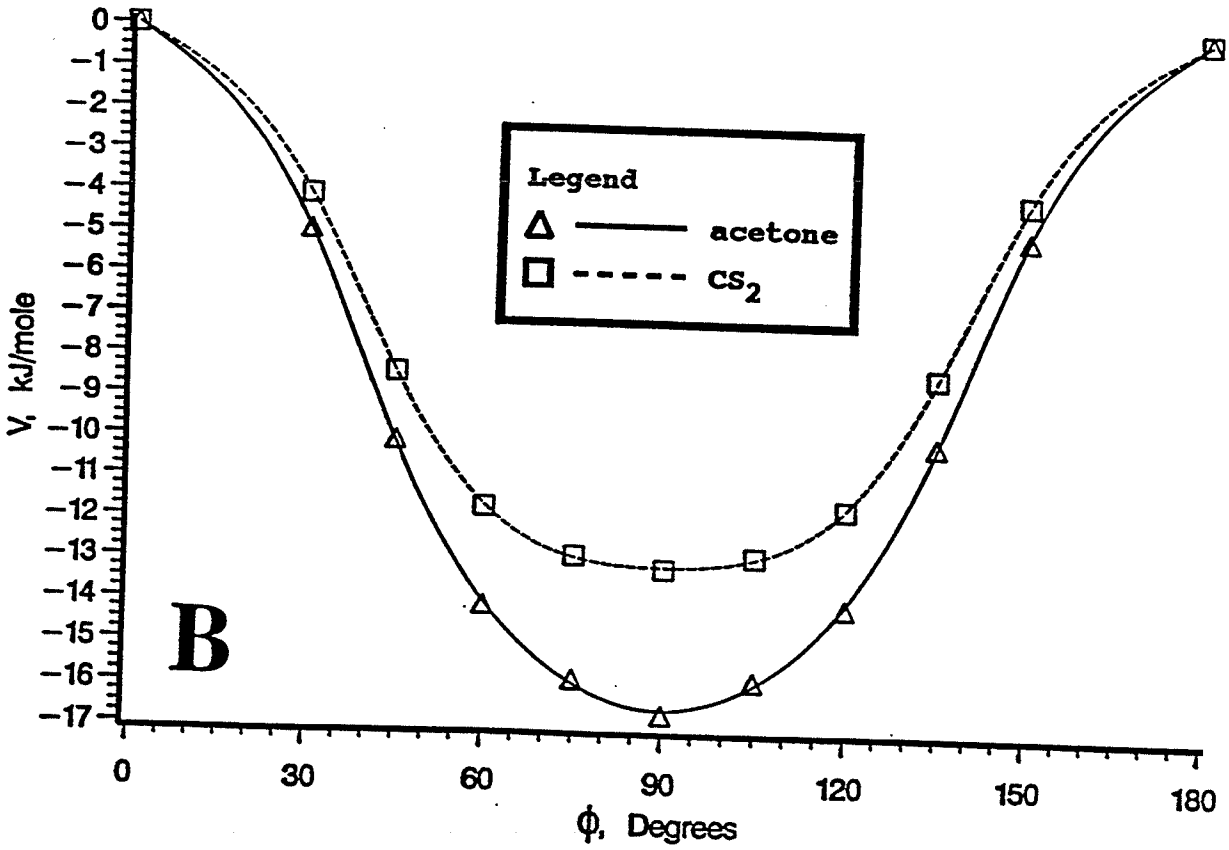

Figure 3.3.10

Potential energy functions for the internal rotation of the benzylic C-F bond in

A. 3,5-difluorobenzyl fluoride

B. 4-fluorobenzyl fluoride

Dielectric solvent effects, calculated at the 6-31G* level.

3,5–difluorobenzylfluoride M.O. Calculations (6–31G*)
Dielectric Solvent Effects

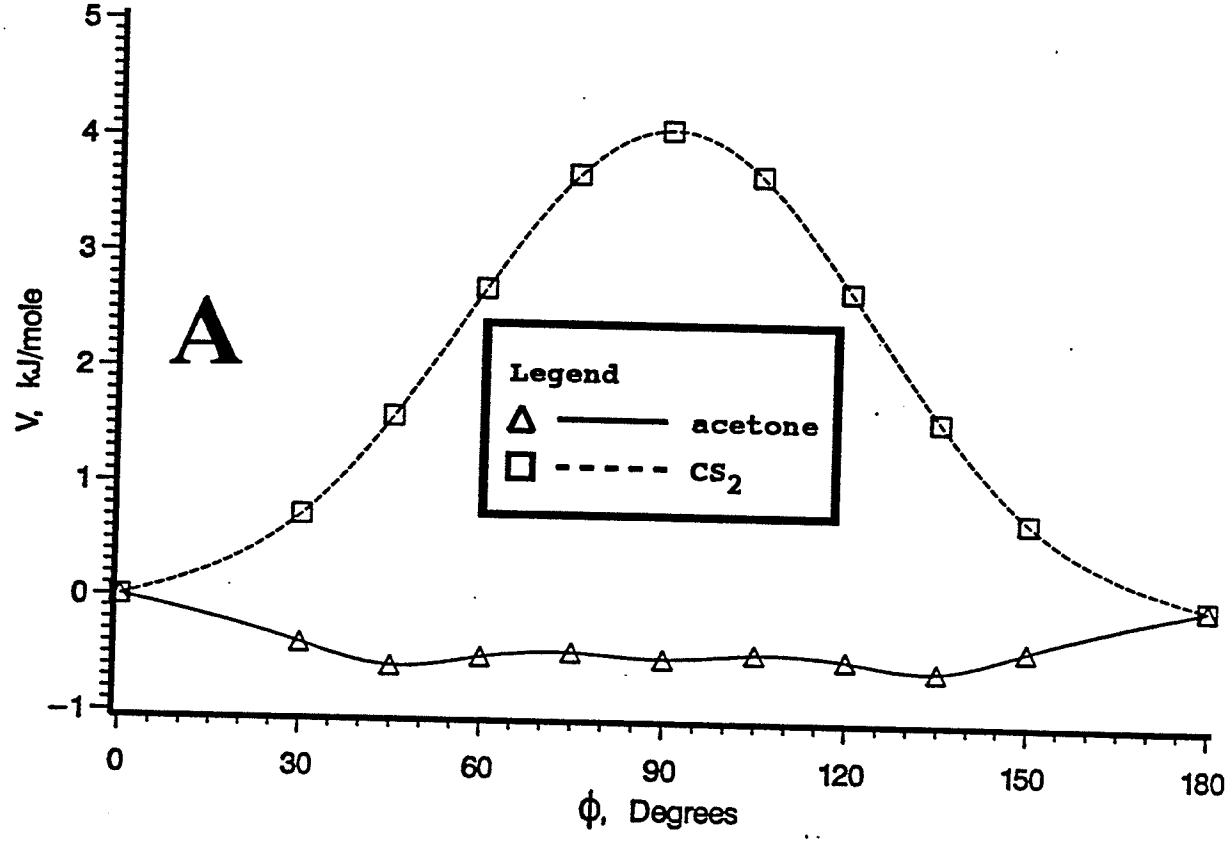

4–fluorobenzylfluoride M.O. Calculations (6–31G*)
Dielectric Solvent Effects

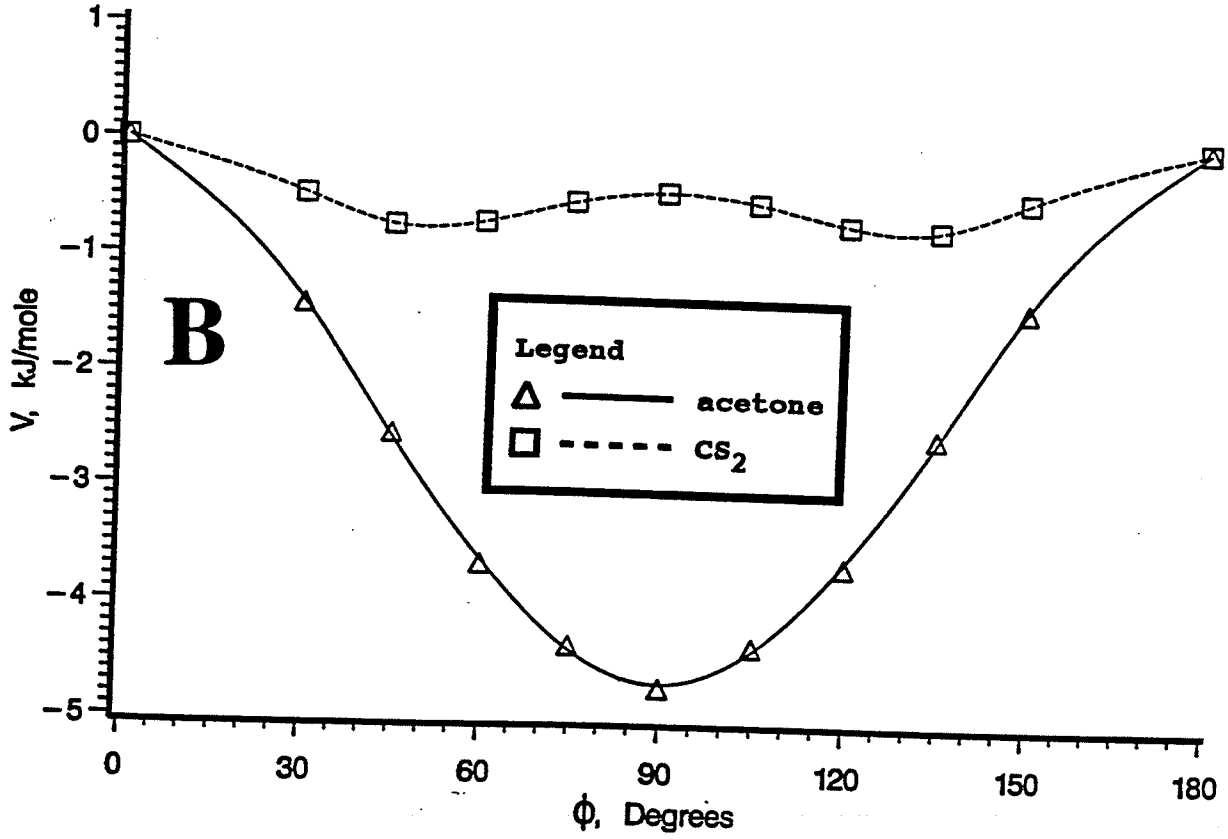

3.4 INDO FPT MO Calculation of Coupling Constants

Long-range coupling constants between the benzylic fluorine and aromatic nuclei were calculated at 15° intervals of the dihedral angle, ϕ, between the benzylic C-F bond and the ring plane by INDO FPT MO methods. Couplings are tabulated in Tables 3.4.1 to 3.4.4 . Plots of least squares fits appear in Figures 3.4.1 to 3.4.4.

Table 3.4.1: INDO FPT MO coupling constants for benzyl fluoride (MP2/6-31G geometries)**

Angle(ϕ)	^4J(H,CF)	^5J(H,CF)	^6J(H,CF)	^5J(C,CF)	^4J(C,CF)
0.0	-3.327	0.606	-0.072	0.354	0.897
30.0	-2.893	1.048	-0.840	2.840	-1.693
45.0	-2.759	1.442	-1.631	5.419	-4.310
60.0	-2.935	1.796	-2.423	8.035	-6.787
75.0	-3.234	2.077	-2.978	9.889	-8.355
90.0	-3.447	2.307	-3.171	10.537	-8.750
105.0	-3.444	2.485	-2.978	9.889	-8.022
120.0	-3.150	2.564	-2.423	8.035	-6.289
135.0	-2.620	2.535	-1.631	5.419	-3.917
150.0	-2.053	2.464	-0.840	2.840	-1.544
180.0	-1.494	2.407	-0.0720	0.354	0.834

Least Sqaures Fits (errors in parentheses)

^4J(H,CF) = -3.35(25) $\sin^2\phi$ - 2.28(27) $\cos^2\phi$

^5J(H,CF) = 0.70(04) + 0.82(05) $\sin^2\phi$ + 1.67(05) $\sin^2(\phi/2)$

^6J(H,CF) = -0.07(01) - 3.12(01) $\sin^2\phi$

^5J(C,CF) = 0.32(02) + 10.24(03) $\sin^2\phi$

^4J(C,CF) = 0.67(12) - 9.68(15) $\sin^2\phi$ + 0.26(15) $\sin^2(\phi/2)$

Figure 3.4.1

Least squares fits of INDO FPT MO coupling constants for benzyl fluoride. See Table 3.4.1 for functions.

INDO couplings in benzylfluoride

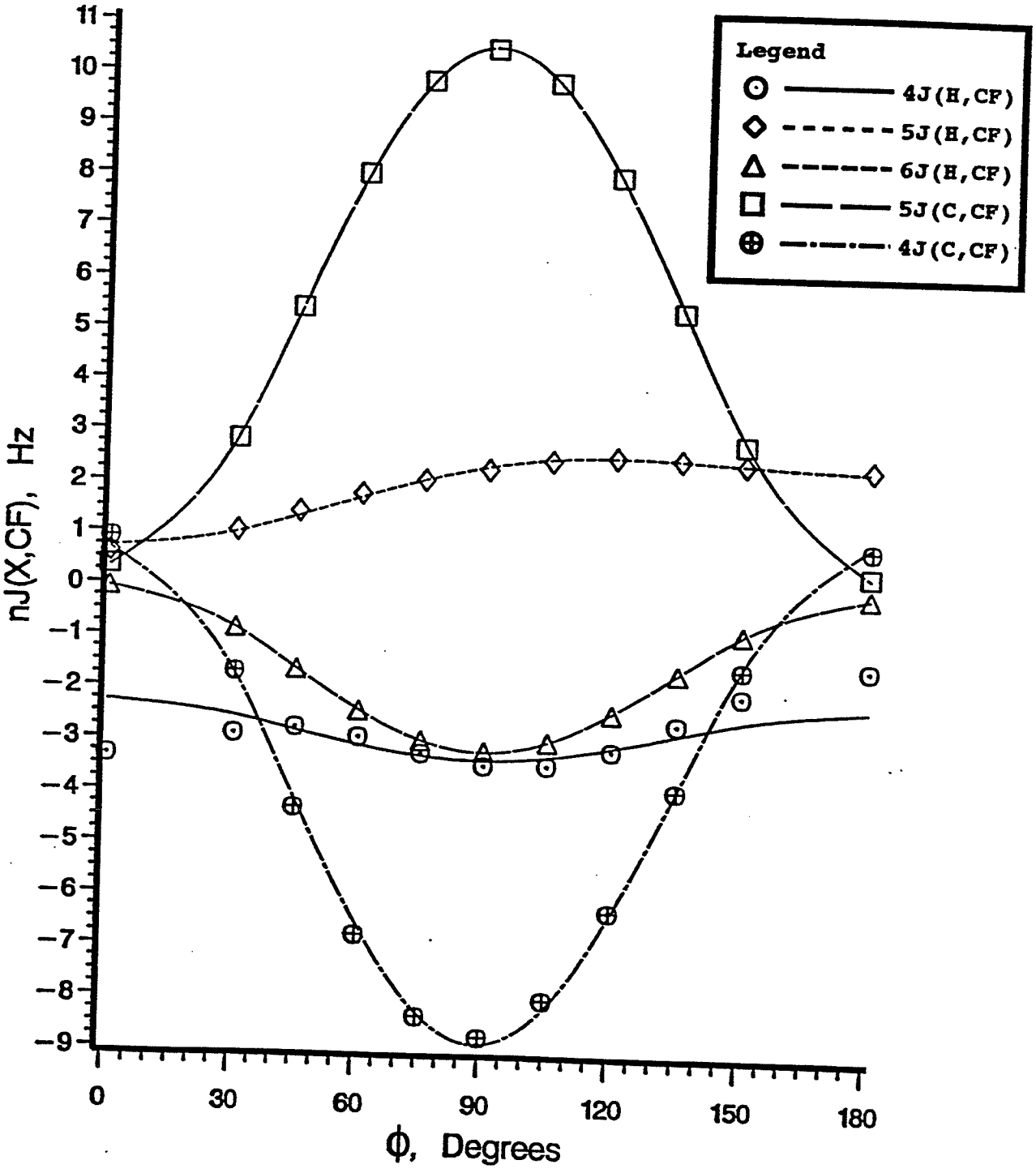

Table 3.4.2: INDO FPT MO coupling constants for 2,6-difluorobenzyl fluoride (MP2/6-31G geometries)**

Angle(ϕ)	^4J(F,CF)	^5J(H,CF)	^6J(H,CF)	^5J(C,CF)	^4J(C,CF)
0.0	-5.327	0.799	-0.025	0.153	-0.168
30.0	-2.773	1.141	-0.699	2.285	-1.976
45.0	-0.495	1.434	-1.427	4.594	-3.961
60.0	1.634	1.677	-2.183	6.987	-6.028
75.0	3.952	1.874	-2.716	8.674	-7.446
90.0	5.228	2.060	-2.897	9.245	-7.846
105.0	4.725	2.215	-2.716	8.674	-7.242
120.0	2.772	2.285	-2.183	6.987	-5.682
135.0	-0.006	2.304	-1.427	4.594	-3.506
150.0	-2.741	2.371	-0.699	2.285	-1.368
180.0	-4.960	2.542	-0.025	0.153	0.679

Least Sqaures Fits (errors in parentheses)

^4J(F,CF) = -5.27(21) + 10.22(33) $\sin^2\phi$

^5J(H,CF) = 0.92(06) + 0.41(08) $\sin^2\phi$ + 1.49(08) $\sin^2(\phi/2)$

^6J(H,CF) = 0.00(01) - 2.90(02) $\sin^2\phi$

^5J(C,CF) = 0.07(04) + 9.18(06) $\sin^2\phi$

^4J(C,CF) = -0.06(04) - 8.17(05) $\sin^2\phi$ + 0.74(05) $\sin^2(\phi/2)$

Figure 3.4.2

Least squares fits of INDO FPT MO coupling constants for 2,6-difluorobenzyl fluoride. See Table 3.4.2 for functions.

INDO couplings in 2,6–difluorobenzylfluoride

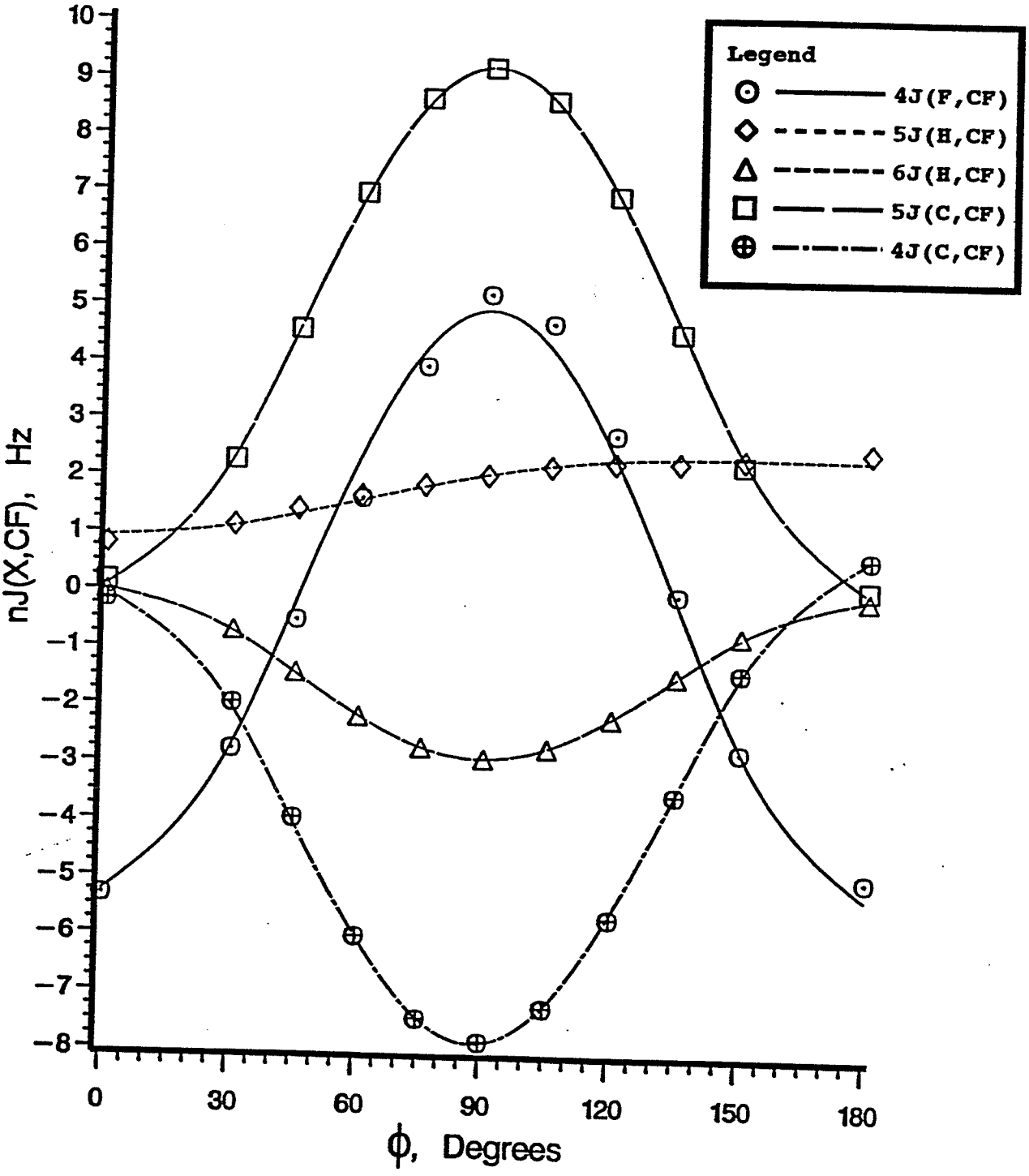

Table 3.4.3 **INDO FPT MO coupling constants for 3,5-difluorobenzyl fluoride (MP2/6-31G** geometries)**

Angle(ϕ)	^4J(H,CF)	^5J(F,CF)	^6J(H,CF)	^5J(C,CF)	^4J(C,CF)
0.0	-3.534	0.658	-0.044	0.278	1.240
30.0	-2.996	0.056	-0.734	2.556	-1.335
45.0	-2.787	-0.813	-1.452	4.956	-3.984
60.0	-2.883	-1.637	-2.170	7.391	-6.440
75.0	-3.099	-2.588	-2.679	9.138	-8.027
90.0	-3.236	-2.700	-2.857	9.753	-8.330
105.0	-3.187	-2.077	-2.679	9.138	-7.474
120.0	-2.894	-0.697	-2.170	7.391	-5.581
135.0	-2.405	0.537	-1.452	4.956	-3.173
150.0	-1.890	1.784	-0.734	2.556	-0.744
180.0	-1.392	2.990	-0.044	0.278	1.690

Least Sqaures Fits (errors in parentheses)

^4J(H,CF) = $-3.13(29)\sin^2\phi - 2.33(32)\cos^2\phi$

^5J(F,CF) = $0.93(14) - 4.47(17)\sin^2\phi + 2.10(17)\sin^2(\phi/2)$

^6J(H,CF) = $-0.04(01) - 2.83(01)\sin^2\phi$

^5J(C,CF) = $0.23(02) + 9.53(03)\sin^2\phi$

^4J(C,CF) = $1.01(13) - 9.85(16)\sin^2\phi + 0.82(17)\sin^2(\phi/2)$

Figure 3.4.3

Least squares fits of INDO FPT MO coupling constants for 3,5-difluorobenzyl fluoride. See Table 3.4.3 for functions.

INDO couplings in 3,5–difluorobenzylfluoride

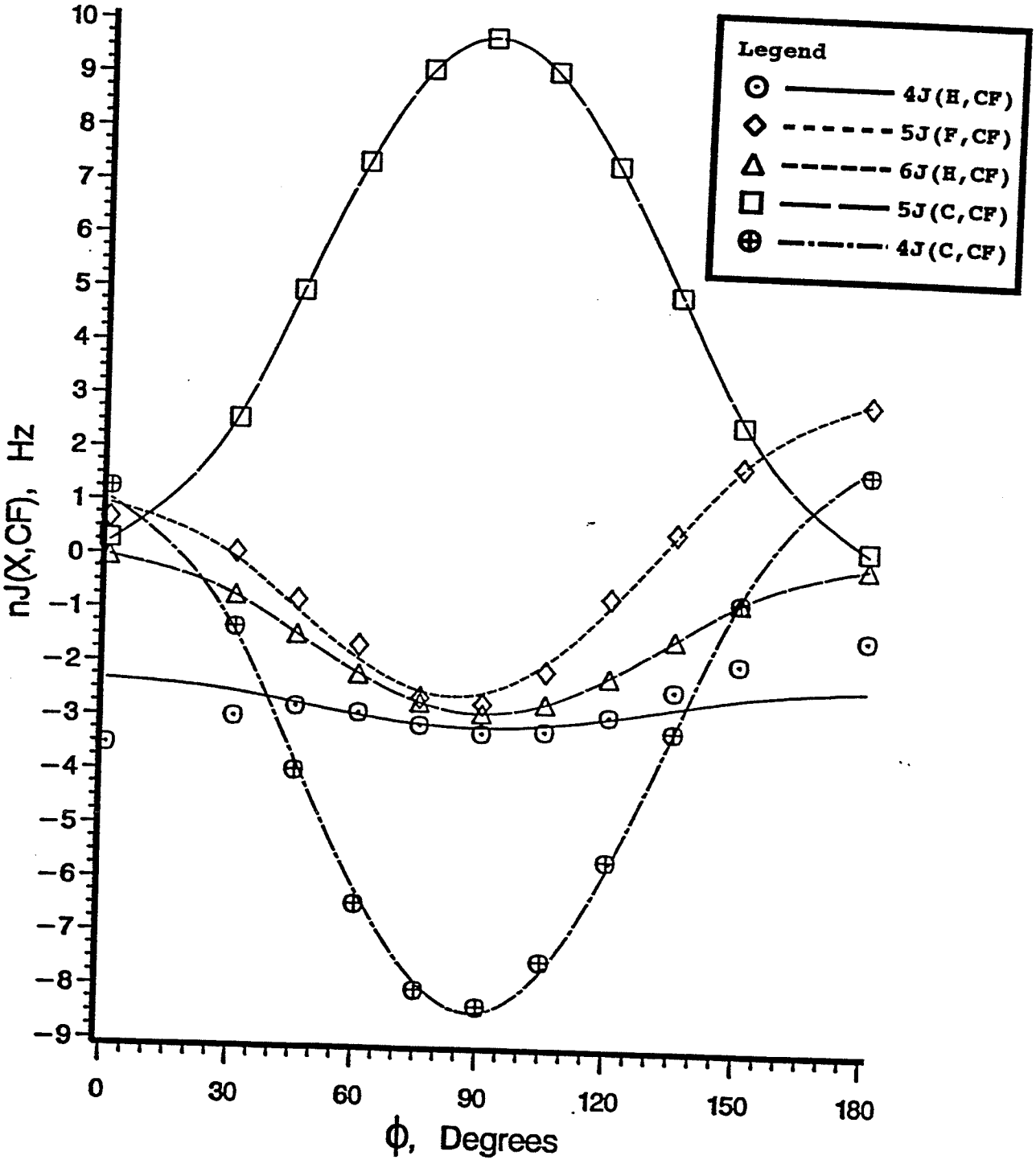

Table 3.4.4 **INDO FPT MO coupling constants for 4-fluorobenzyl fluoride (MP2/6-31G** geometries)**

Angle(ϕ)	^4J(H,CF)	^5J(H,CF)	^6J(F,CF)	^5J(C,CF)	^4J(C,CF)
0.0	-3.427	0.549	-0.355	0.432	0.884
30.0	-2.966	1.016	0.958	2.873	-1.711
45.0	-2.812	1.431	2.311	5.407	-4.315
60.0	-2.964	1.790	3.712	7.951	-6.738
75.0	-3.252	2.055	4.727	9.751	-8.229
90.0	-3.464	2.252	5.098	10.378	-8.575
105.0	-3.461	2.392	4.727	9.751	-7.852
120.0	-3.160	2.438	3.712	7.951	-6.188
135.0	-2.613	2.387	2.311	5.407	-3.936
150.0	-2.020	2.306	0.958	2.873	-1.680
180.0	-1.494	2.407	-0.355	0.432	0.575

Least Sqaures Fits (errors in parentheses)

^4J(H,CF) = $-3.36 \sin^2\phi - 2.31 \cos^2\phi$ **

^5J(H,CF) = $0.67(05) + 0.87(06) \sin^2\phi + 1.52(06) \sin^2(\phi/2)$

^6J(F,CF) = $-0.39(01) + 5.47(02) \sin^2\phi$

^5J(C,CF) = $0.41(02) + 10.01(03) \sin^2\phi$

^4J(C,CF) = $0.59(15) - 9.37(19) \sin^2\phi + 0.14(19) \sin^2(\phi/2)$

** did not converge

Figure 3.4.4

Least squares fits of INDO FPT MO coupling constants for 4-fluorobenzyl fluoride. See Table 3.4.4 for functions.

INDO couplings in 4–fluorobenzylfluoride

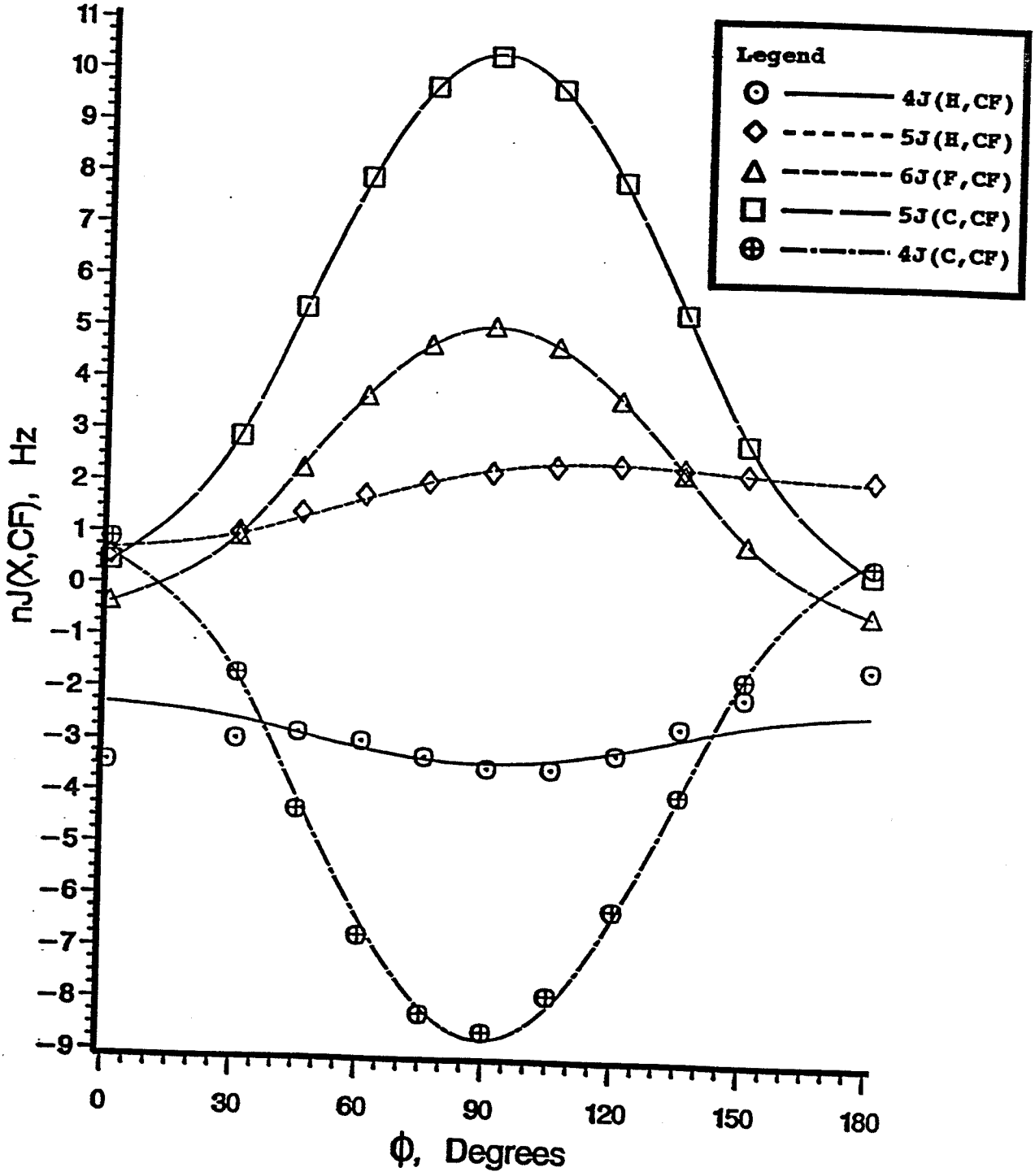

4. Discussion

Discussion

4.1 Six-bond couplings as indicators of internal rotational potentials in benzyl fluoride, 3,5-difluorobenzyl fluoride, and 3,5-dichlorobenzyl fluoride

Application of the *J*-method depends upon the accurate measurement of long-range coupling constants over six formal bonds (or of some other ^{n}J whose angle dependence can be established). Specifically, the coupling ^{6}J is measured from an α-position on the sidechain to the *para*-position on the aromatic ring. Couplings of this nature depend on a σ-π mechanism[13,15,20] and have a $\sin^2\theta$ dependence, where θ is the angle by which the α-substituent twists out of the plane of the aromatic ring. This dependence is given by the equation

$$^{6}J = {}^{6}J_{90}\langle\sin^2\theta\rangle \qquad \textbf{(4.1)}$$

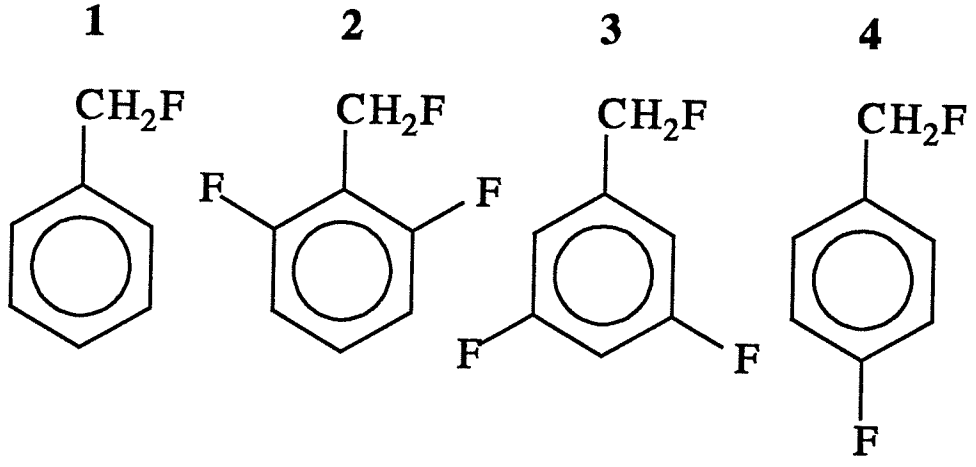

where $\langle \sin^2\theta \rangle$ is the expectation value for $\sin^2\theta$ averaged over hindered rotor states.

In the case of the benzyl fluoride derivatives pictured above, there are two distinct angular dependencies which can be extracted. One is the angular dependence of the ^6J coupling involving the α-proton and *para*-position nucleus, and the other involves benzylic fluorine and the *para*-position nucleus. Two conformers are pictured below in which the benzylic fluorine assumes conformations parallel (**I**) and perpendicular (**II**) to the plane of the aromatic ring. Assuming that maximum coupling occurs when the C-H or C-F bonds are twisted 90° out of the ring plane,

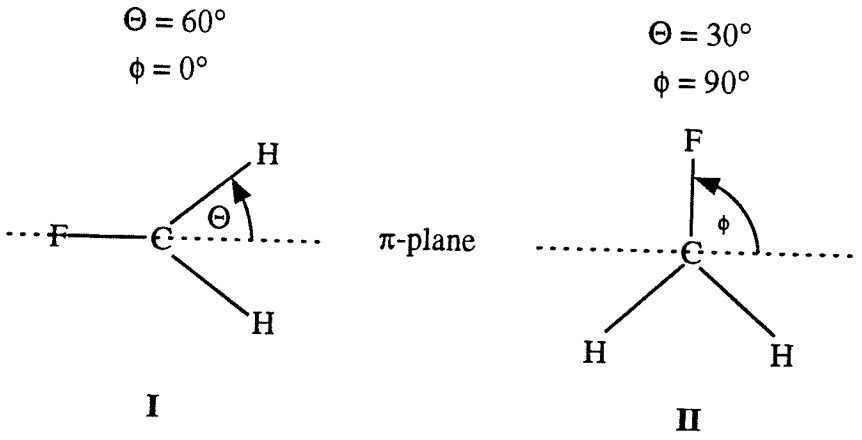

I **II**

one has:

$$^6J(\mathrm{H,CH}) = {}^6J_{90}(\mathrm{H,CH})\langle\sin^2\theta\rangle \quad (4.2)$$

$$^6J(\mathrm{H,CF}) = {}^6J_{90}(\mathrm{H,CF})\langle\sin^2\phi\rangle \quad (4.3)$$

From couplings in two solvents, and the identity (4.4)

$$\langle\sin^2\theta\rangle = 0.75 - 0.5\langle\sin^2\phi\rangle \quad (4.4)$$

a system of two equations in two unknowns can be solved for $^6J_{90}$(H,CH) and $^6J_{90}$(H,CF), from which the expectation values follow.

Table 4.1.1 shows the ^6J values in two solvents, along with the expectation values and internal potentials. Benzyl fluoride was examined in a number of solvents,[23a,58] and the general trend was a decrease in potential when moving from polar to nonpolar solvents, with the minimum in the potential well occurring at $\phi = 90°$. For benzyl fluoride, the most stable conformer is **II**, with a net stabilization of 1.9 kJ mol^{-1} when going from the nonpolar CS_2 solution (0.8 kJ mol^{-1}) to the polar acetone-d6 solution (2.7 kJ mol^{-1}). From values for ^6J(H,CH) of -0.409(2) Hz in acetone-d6, -0.452(2) Hz in CS_2, and values for ^6J(H,CF) of -1.800(2) Hz in acetone-d6 and -1.539(2) Hz in CS_2, values of $^6J_{90}$(H,CH) and $^6J_{90}$(H,CF) are calculated as -0.941(4) and -2.855(4) Hz, respectively. From these values, $\langle\sin^2\phi\rangle$ is found to be 0.631 and 0.539 for acetone-d6 and CS_2, with an energy minimum at $\phi = 90°$ and $\theta = 30°$. The increased polarity of the acetone-d6 solution stabilizes conformer **II**, perhaps enhancing the hyperconjugative interaction between

Table 4.1.1: Barriers to internal rotation as calculated from ^6J couplings

Compound	benzyl fluoride[a]		3,5-difluoro-benzyl fluoride		3,5-dichloro-benzyl fluoride[b]	
Solvent[c]	Acetone-d6	CS_2	Acetone-d6	CS_2	Acetone-d6	CS_2
^6J(H,CH)	-0.409(2)	-0.452(2)	-0.496(1)	-0.533(1)	-0.499(2)	-0.534(2)
^6J(H,CF)[d]	-1.800(2)	-1.539(2)	-1.161(1)	-0.934(1)	-1.256(2)	-1.038(2)
$^6J_{90}$(H,CH)	-0.941(4)		-0.910(2)		-0.934(2)	
$^6J_{90}$(H,CF)	-2.855(4)		-2.832(2)		-2.909(2)	
$\langle\sin^2\theta\rangle$	0.435	0.481	0.545	0.585	0.534	0.572
$\langle\sin^2\phi\rangle$	0.631	0.539	0.410	0.330	0.432	0.357
$V_{2\,d}$	2.7(2)	0.8(2)	1.9(2)	3.8(2)	1.4(2)	3.0(2)

[a] Data from ref. 58
[b] Data from ref. 64
[c] Solvents include small amounts of C_6F_6 and TMS as internal standards. See experimental for details.
[d] Internal potential, in kJ mol^{-1}.

the aromatic π-system and the benzylic C-F bond (charge separation), resulting in a larger barrier in the polar solution.

3,5-dichlorobenzyl fluoride, **3b**, a chlorine analogue of **3**, was previously studied in a number of solvents,[64] and yielded results displaying behaviour opposite to that of **1**. Values of -0.499(1) Hz in acetone-d6 and -0.534(1) Hz in CS_2 for ^6J(H,CH) and -1.256(1) Hz and -1.038(1) Hz for ^6J(H,CF) in acetone-d6 and CS_2, respectively, give values of -0.934(2) Hz for $^6J_{90}$(H,CH) and -2.909(2) Hz for $^6J_{90}$(H,CF), similar to those for **1**. However, calculated expectation values are quite different, with $\langle\sin^2\phi\rangle_{ACETONE}$ = 0.432, and $\langle\sin^2\phi\rangle_{CS2}$ = 0.357. These yield barriers of 1.4(2) kJ mol^{-1} for 3,5-dichlorobenzyl fluoride in acetone-d6 solution, and 3.0(2) kJ mol^{-1} in CS_2. Values of $\langle\sin^2\phi\rangle$ are less than 0.5; thus, **I** is the most stable conformer in both solvents. The lower barrier in acetone-d6 indicates that the perpendicular conformer is stabilized by the polar solvent.

Similar results are obtained for **3**, using the same procedures as above. With $^6J(H,CH)_{ACETONE}$ = -0.496(1) Hz, $^6J(H,CH)_{CS2}$ = -0.533(1) Hz, $^6J(H,CF)_{ACETONE}$ = -1.161(1) Hz, and $^6J(H,CF)_{CS2}$ = -0.934(1) Hz, $^6J_{90}$ values are calculated which correspond very well with the results for **1** and **3b**. Values of $^6J_{90}$(H,CH) = -0.910 Hz, and $^6J_{90}$(H,CF) = -2.832 Hz give values for $\langle\sin^2\phi\rangle$ of 0.410 and 0.330, which in turn give internal potentials of 1.9(2) kJ mol^{-1} and 3.8(2) kJ mol^{-1} in acetone and CS_2, respectively. The formally calculated errors for the barriers are < 0.1 kJ mol^{-1}, but are quoted as ± 0.2

kJ mol^{-1}.

It has been hypothesized that the electronegative chlorine substituents in **3b** enhance the polarity of the *ortho* C-H bonds, thereby causing an increased attraction between the benzylic C^{+}-F^{-} dipole and the *ortho* C^{-}-H^{+} dipole. This interaction stabilizes conformer **I**.[60,64] Since the *meta*-fluorines are more electronegative than the *meta*-chlorines, the *ortho* C-H dipole would become further enhanced, correspondingly intensifying the attraction between the two dipoles and resulting in an increased barrier to internal rotation relative to **3b**.

The *meta*-halogen substituents obviously play a role in determining the low-energy conformer in **3** and **3b**, and the barrier sizes are distinctly different from that in **1**. However, all three molecules experience a stabilization of 1.7 ± 0.2 kJ mol^{-1} of the perpendicular conformer, when going from CS_2 to acetone-d6 solutions.

4.2 $^5J_{90}$(C,F) as an indicator of internal potentials

It is predicted by INDO-FPT-MO calculations that ^5J(C,CF), the coupling between an α-fluorine and the *para*-carbon, displays a $\langle\sin^2\phi\rangle$ dependence (also see INDO calculations in the data section), and is thus a pure σ-π parameter.[23a,81] ^5J(C,CF) can be used as a confirmatory check on the predicted barrier sizes through a comparison of the implied $^5J_{90}$(C,CF) values in **1** and **3** with the $^5J_{90}$(C,CF) from a rigid-model compound, 1-fluoroindan.[51]

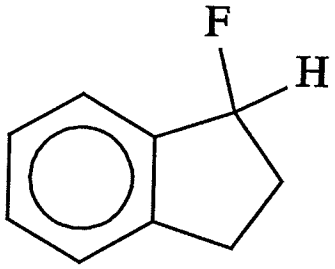

Previously, a comparison was made between the predicted value of $^5J_{90}$(C,CF) in benzyl fluoride, and the calculated result from 1-fluoroindan, which was 5.2(3) Hz.[23a] With reference to Table 4.1.2, $^5J_{90}$(C,CF) = ^5J(C,CF)/$\langle\sin^2\phi\rangle$ = 4.94(3) Hz in acetone-d6 and 5.13(3) Hz for CS_2, acceptable within the given error ranges. For **3**, values of ^5J(C,CF) yield $^5J_{90}$(C,CF) = 5.19(3) Hz in acetone-d6, and $^5J_{90}$(C,CF) = 5.45(3) Hz in CS_2, again within an acceptable range of $^5J_{90}$(C,CF) in 1-fluoroindan. Apparently, ^5J(C,CF) is rather insensitive to ring substitution, even in 4-fluorobenzyl fluoride (see below); it is also easily measurable.

4.3 The barrier to internal rotation in 2,6-difluorobenzylfluoride

The sterically hindered 2,6-difluorobenzyl fluoride, **2**, presents a dilemma when attempting to calculate the $^6J_{90}$'s with the same technique used for **1**, **3**, and **3b**. The unusually small $^6J(H,CH)_{ACETONE}$ of -0.207(1) Hz and the $^6J(H,CH)_{CS2}$ of -0.211(1) Hz, together with the $^6J(H,CF)_{ACETONE}$ of -2.481(1) Hz and the $^6J(H,CF)_{CS2}$ of -2.333(1) Hz, yield the absurd values of -0.365 Hz for $^6J_{90}(H,H)$ and -6.76 Hz for $^6J_{90}(H,CF)$. The average values for $^6J_{90}(H,CH)$ and $^6J_{90}(H,CF)$ in benzyl fluoride and its *meta*-substituted derivatives lie near -0.93 Hz and -2.87 Hz, compelling the belief that the predicted values for **2** are untenable. In benzyl fluoride, the highly electronegative benzylic fluorine polarizes the benzylic C-H bonds, thereby decreasing the hyperconjugative interaction with the aromatic π electrons. It may be that in **2** the polarized C-H bonds are additionally perturbed by the electronegative, proximate *ortho* C-F bonds.[23d]

To obtain a potential in **2**, $^5J_{90}(C,CF)$ is now used. $^5J_{90}(C,CF)$ is 5.18 ± 0.25 Hz (the average of $^5J_{90}(C,CF)$ in **1** and **3**) and yields $\langle\sin^2\phi\rangle_{ACETONE}$ = 0.766 and $\langle\sin^2\phi\rangle_{CS2}$ = 0.737, giving barriers of 6.4(3) and 5.4(3) kJ mol^{-1} in acetone-d6 and CS_2, respectively. The $^6J_{90}(H,CF)$ follow as -3.24 ± 0.16 Hz in acetone-d6 and -3.17 ± 0.15 Hz in CS_2. The *ortho* C-F bonds apparently also perturb $^6J(H,CF)$, though to a lesser degree than $^6J(H,CH)$. The benzylic C-F bond does not approach the *ortho* fluorines as closely as do the α C-H bonds (see **II**), which may account for the perturbation of $^6J_{90}(H,CH)$.

4.4 ^4J(H,CH) and the rotational barrier in 4-fluorobenzyl fluoride

For 4-fluorobenzyl fluoride, $^6J_{90}$(H,CH) is unavailable, of course; however the ^6J(F,CH) and ^6J(F,CF) values (known in two solvents) can be tested as a source of internal barriers. From values of 0.667(1) and 0.778(1) Hz for ^6J(F,CH) in acetone-d6 and CS_2, and values of 5.591(1) and 4.919(1) Hz for ^6J(F,CF), and using the relation given in equation 4.4, one has $^6J_{90}$(F,CH) = 2.121 Hz and $^6J_{90}$(F,CF) = 6.420 Hz. This gives values of $\langle\sin^2\phi\rangle_{\text{ACETONE}} = 0.871$, and $\langle\sin^2\phi\rangle_{\text{CS2}} = 0.766$, and of $V_2 = 11.7(2)$ and $V_2 = 6.3(2)$ kJ mol^{-1} in acetone-d6 and CS_2, respectively. Previously measured barriers for the other benzylfluoride derivatives suggest that these results are too large.

The orthobenzylic coupling, ^4J_o(H,CH), is a monitor of $\langle\sin^2\theta\rangle$ in 3,5-dichlorobenzyl fluoride (**3b**), reproducing experimental ^4J(H,CH) values to within a deviation of 0.002 Hz.[64] For toluene, it has been suggested that $^4J_o(H,CH_3)$ obeys (4.5)[24,82]

$$\begin{aligned} {}^4J_o(H,CH_3) &= {}^4J_{90}^{\pi}\langle\sin^2\theta\rangle + {}^4J^{\sigma}\langle\cos^2\theta\rangle \\ &= -1.08\langle\sin^2\theta\rangle - 0.32\langle\cos^2\theta\rangle \end{aligned} \qquad \textbf{(4.5)}$$

For **3b**, the experimental values of ^4J(H,CH) and $\langle\sin^2\theta\rangle$ are known in six solvents. Assuming a relationship similar to (4.5), one finds $^4J_{90}{}^{\pi}$(H,CH) = -1.23 Hz, and $^4J^{\sigma} < 0.002$ Hz. The σ-component represents a negligible percentage of the four-bond coupling, so that effectively

$$^4J(\mathrm{H,CH}) = {}^4J_{90}(\mathrm{H,CH})\langle\sin^2\theta\rangle \qquad (4.6)$$

Applying this relationship to compounds **1** and **3** yields a $^4J_{90}$(H,CH) of -1.28 ± 0.01 Hz in **1**, of -1.22 ± 0.01 Hz in **3**, and of -1.23 ± 0.01 Hz in **3b**.

Assuming that $^4J_{90}$(H,CH) is -1.28 ± 0.05 Hz in **4**, (the *para*-fluorine is far enough away from the *ortho*-position that its perturbing effect should not be as significant as in **3**), it follows that $\langle\sin^2\theta\rangle_{\mathrm{ACETONE}} = 0.416$, $\langle\sin^2\theta\rangle_{\mathrm{CS2}} = 0.453$, $\langle\sin^2\phi\rangle_{\mathrm{ACETONE}} = 0.668$ and $\langle\sin^2\phi\rangle_{\mathrm{CS2}} = 0.594$. The most stable conformer for **4** is **II**. The barriers extracted from these expectation values are $V_{2(\mathrm{ACETONE})} = 3.6(2)$ kJ mol^{-1}, and $V_{2(\mathrm{CS2})} = 1.9(2)$ kJ mol^{-1}.

These expectation values can be checked by the implied $^5J_{90}$(C,CF) values. From $^5J(\mathrm{C,CF})_{\mathrm{ACETONE}} = 3.47(1)$ Hz, and $^5J(\mathrm{C,CF})_{\mathrm{CS2}} = 3.10(1)$ Hz, one has a $^5J_{90}$(C,CF) of 5.2(3) Hz, in good agreement with $^5J_{90}$(C,CF) values for all of the other derivatives (see Table 4.1.2).

Further, $^6J_{90}$(F,CH) now follow as 1.60 ± 0.06 Hz in acetone-d6 and 1.72 ± 0.07 Hz in CS_2, and $^6J_{90}$(F,CF) as 8.37 ± 0.33 Hz and 8.28 ± 0.34 Hz in acetone-d6 and CS_2, respectively. The predicted perpendicular coupling constants, expectation values and potentials for all of the above compounds are summarized in Table 4.1.2.

Examination of Table 4.1.2 shows that all of the molecules experience a net stabilization of conformer **II** by 1.7 to 1.9 kJ mol^{-1} in the more polar solvent (excepting **2**, in which **II** is stabilized by 1.0 ± 0.1 kJ mol^{-1}). A

Table 4.1.2: Summary of barriers to internal rotation and predicted perpendicular long-range couplings

Compound	benzylfluoride[a]		2,6-difluoro-benzylfluoride		3,5-difluoro-benzylfluoride		3,5-dichloro-benzylfluoride[b]		4-fluoro-benzylfluoride	
Solvent[c]	Acetone-d6	CS_2	Acetone-d6	CS_2	Acetone-d6	CS_2	Acetone-d6	CS_2	Acetone-d6	CS_2
^6J(H,CH)	-0.409(2)	-0.452(2)	-0.207(1)	-0.211(1)	-0.496(1)	-0.533(1)	-0.499(1)	-0.534(1)	---	---
^6J(H,CF)[d]	-1.800(2)	-1.539(2)	-2.481(1)	-2.333(1)	-1.161(1)	-0.934(1)	-1.256(1)	-1.038(1)	0.667(1)	0.778(1)
^6J(F,CF)[e]	---	---	---	---	---	---	---	---	5.591(1)	4.919(1)
$^6J_{90}$(H,CH)	-0.941(4)		-0.56(4)[f]		-0.910(2)		-0.934(2)		---	
$^6J_{90}$(H,CF)[d]	-2.855(4)		-3.2(2)[g]		-2.832(2)		-2.909(2)		1.66(9)	
$^6J_{90}$(F,CF)[e]	---		---		---		---		8.3(4)	
^5J(C_p,CF)	3.11(1)	2.76(1)	3.97(1)	3.82(1)	2.13(2)	1.80(1)	---[h]	---	3.47(1)	3.10(1)
$^5J_{90}$(C,CF)[i]	5.03(4)		5.2(3)[j]		5.33(6)		---		5.2(3)	
^{4}J(H,CH)[k]	-0.560(2)	-0.610(1)	---[l]	---	-0.661(1)	-0.713(1)	-0.608(1)	-0.705(1)	-0.532(1)	0.580(1)
$^4J_{90}$(H,CH)	-1.28(1)		---		-1.22(1)		-1.23(1)		-1.28(5)[m]	
$\langle\sin^2\theta\rangle$	0.435	0.481	0.367	0.382	0.545	0.585	0.534	0.572	0.416	0.453
$\langle\sin^2\phi\rangle$	0.631	0.539	0.766	0.737	0.410	0.330	0.432	0.357	0.668	0.594
V_2[n]	2.7(2)	0.8(2)	6.4(3)	5.4(3)	1.9(2)	3.8(2)	1.4(2)	3.0(2)	3.6(2)	1.9(2)

[a] Data from references 4 and 5.

[b] Data from reference 6.

[c] All samples are 5.0 mol% solutions, with small amounts of internal references TMS (^{1}H) and C_6F_6 (^{19}F).

[d] This refers to $^6J(H_p,F_a)$ for compounds **1** through **3b**. For compound **4**, this is $^6J(F_p,H_a)$, due to the presence of the *para* fluorine.

[e] Exists only for compound **4** (coupling between benzylic and *para* fluorines).

[f] These values are absurd (see text).

[g] Calculated from estimated $^5J_{90}$(C,F). See discussion for details.

[h] Not measured for **3b**.

[i] $^5J_{90}$(C,F) are estimated from ratios of known ^5J(C,F) over predicted expectation values.

[j] Estimated from median in **1** and **3**.

[k] Orthobenzylic four bond proton-proton coupling.

[l] Does not exist for **2**, due to presence of *ortho* fluorines.

[m] Assumed to be the same value as in **1**. Expectation values and barriers calculated from predicted $^4J_{90}$(H,H). See discussion for details.

[n] Internal rotational potential, in kJ mol^{-1}.

possible explanation for the increased barrier size of **4** relative to **1** (by approximately 1.0 kJ mol^{-1}) could be the π-donor effect of the *para*-C-F bond, and the hyperconjugative accepting ability of the benzylic sidechain; the latter is maximal when the benzylic C-F bond lies in the plane containing the $2p_z$ orbitals of the aromatic nucleus. In that case, $^6J_{90}$(F,CF) should be rather larger than expected (8.3 Hz is quite a large coupling). The magnitude of $^6J_{90}$(F,CF) is estimated in an unperturbed system as follows:

From the McConnell formulation of π-electron coupled proton interactions[83] it is predicted that[84]

$$J^{\pi} \propto Q_{CH}Q_{CCH} \qquad (4.7)$$

Q_{CH} and Q_{CCH} are isotropic hyperfine interaction constants representing the interaction between the π-electron on an aromatic carbon orbital and the adjacent aromatic and methyl protons, respectively.[20] Similar expressions can be written for couplings involving fluorine nuclei.[79] Assuming that a π-electron coupling mechanism predominates, one can make quantitative comparisons between the molecules pictured below.

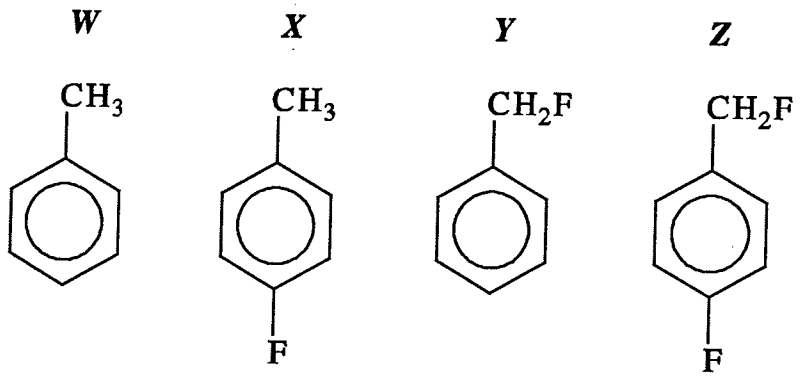

From (4.7), one can write the following equations:

$$\begin{array}{lll} \text{In} & \text{W:} & {}^{6}J(H,CH) \propto Q^{H}_{CH}Q^{H}_{CCH} \\ & \text{X:} & {}^{6}J(F,CH) \propto Q^{F}_{CF}Q^{H}_{CCH} \\ & \text{Y:} & {}^{6}J(H,CF) \propto Q^{H}_{CH}Q^{F}_{CCF} \\ & \text{Z:} & {}^{6}J(F,CF) \propto Q^{F}_{CF}Q^{F}_{CCF} \end{array} \qquad (4.8)$$

${}^{6}J$(H,CH) is -0.60 Hz in toluene [14d]and ${}^{6}J_{90}$(F,CH) is 1.15 Hz in *p*-fluorotoluene.[79] The values for ${}^{6}J_{90}(H,CH)_W$ and ${}^{6}J_{90}(F,CH)_X$ follow as -1.20 Hz and 2.30 Hz, respectively. In benzyl fluoride, ${}^{6}J_{90}(H,CF)_Y$ was previously calculated as -2.855 Hz. Thus, if ${}^{6}J$(F,CF) is "well-behaved" in 4-fluoro-benzyl fluoride, then ${}^{6}J_{90}(F,CF)_Z$ should be

$$\begin{aligned} {}^{6}J_{90}(F,CF)_Z &= {}^{6}J_{90}(H,CF)_Y \times \frac{{}^{6}J_{90}(F,CH)_X}{{}^{6}J_{90}(H,CH)_W} \\ &= -2.855 \times \frac{2.30}{-1.20} = 5.47 \text{ Hz} \end{aligned} \qquad (4.9)$$

The experimental ${}^{6}J_{90}$(F,CF), at 8.3 Hz in **4**, is indeed larger than expected, presumably due to the hyperconjugative effect of the benzylic fluorine and

the concomitant enhanced double-bond character of the *para*-C-F bond.

4.5 ^4J(H,CF) as a monitor of barrier size

Under the assumption that ^4J(H,CF), the four-bond coupling between the benzylic fluorine and the *ortho*-proton, has an angular dependence similar to that of ^4J(H,CH) (see 4.5), it has been shown that values of $\langle\sin^2\phi\rangle$ calculated for **3b** from ^6J(H,CF) reproduce ^4J(H,CF) with an average deviation of 0.004 Hz (in six solvents).[64] ^4J(H,CF)/Hz is written as -3.25_3 $\langle\sin^2\phi\rangle$ -0.134_8 $\langle\cos^2\phi\rangle$. This relationship can be tested for **1**, **3**, and **4** as follows:

Starting with **1**, $\langle\sin^2\phi\rangle$ values calculated from six-bond proton-proton and proton-fluorine couplings are inserted into (4.10)

$$\begin{aligned} {}^4J(\mathrm{H,CF}) &= -1.961 = 0.631\cdot{}^4J_{90}(\mathrm{H,CF}) + 0.369\cdot{}^4J^{\sigma}(\mathrm{H,CF}) \\ {}^4J(\mathrm{H,CF}) &= -1.680 = 0.539\cdot{}^4J_{90}(\mathrm{H,CF}) + 0.461\cdot{}^4J^{\sigma}(\mathrm{H,CF}) \end{aligned} \qquad \textbf{(4.10)}$$

It follows that $^4J_{90}$(H,CF) is -3.09 Hz, and $^4J^{\sigma}$(H,CF) is -0.034 Hz, with the σ component making up only 1.1% of the total coupling. Compounds **3** and **4** give results similar to those for **1** and **3b**, with $^4J_{90}$(H,CF) = -3.08 Hz and $^4J^{\sigma}$(H,CF) = -0.135 Hz in **3**, and $^4J_{90}$(H,CF) = -3.25 Hz and $^4J^{\sigma}$(H,CF) = -0.357 Hz in **4**. If **1**, **3** and **4** were tested in a large number of solvents, it is possible that better correspondence between the predicted $^4J_{90}$(H,CF) would be found. If so, ^4J(H,CF) would become a useful indicator of internal rotational potentials.

4.6 *The coupling mechanism and sign of ^4J(C,CF)*

^4J(C,CF) was previously written as

$$^4J(C,CF) = {}^4J^{\pi}\langle\sin^2\phi\rangle + {}^4J^{\sigma}\langle\sin^2(\phi/2)\rangle \qquad (4.11)$$

where the σ-π component, $^4J^{\pi}$, is negative and the σ electron component is positive.[23a,58] Inserting experimentally determined ^4J(C,CF) and $\langle\sin^2\phi\rangle$ into (4.11) allows one to roughly approximate the σ-π and σ components of ^4J(C,CF) in all of the benzyl fluoride derivatives.

Assuming that ^4J(C,CF) is negative, the components for **1** and **4** follow as $^4J^{\pi}$ = -5.36 Hz and $^4J^{\sigma}$ = 3.93 Hz, and $^4J^{\pi}$ = -6.03 Hz and $^4J^{\sigma}$ = 4.63 Hz, respectively. The ratio of σ-π to σ components is -1.33 ± 0.3 for these two molecules. The ^4J(C,CF) in **1** and **4** are relatively close to one another in size. The difference in magnitude between these couplings may be indicative of the conformational preference of the CH_2F group, as well as the electronic effects of the *para*-fluorine atom.

^4J(C,CF) takes on extreme values in **2** and **3** (See Table 4.1.3). For **2**, $^4J^{\pi}$ = -4.21 Hz and $^4J^{\sigma}$ = 0.56 Hz; the ratio of σ-π to σ components is -7.56. For compound **3**, a negative σ component is calculated, with $^4J^{\pi}$ = -4.21 Hz and $^4J^{\sigma}$ = -0.81 Hz (ratio = 5.19). The σ-π parameter for couplings involving α-fluorines is known to be very substituent dependent.[49,58,81,85] Since aromatic fluorine nuclei in **2** and **3** perturb electron density of carbons residing in the coupling pathway of ^4J(C,CF), the magnitudes and estimated

components of these couplings may reflect intrinsic substituent perturbations on ^4J(C,CF), and not the conformational preference of the sidechain.

In all cases, the σ-π electron contribution is negative due to electron correlation. The spin correlation function for atoms of different classes is negative, and π electron contributions in even alternant molecules alternate in sign.[83] Thus, if positive σ-π components occur at the C_o and C_p positions, the component at C_m should be negative.[81,83] ^4J(C,CF) becomes increasingly negative when moving from nonpolar to polar solvent. This corresponds to an increased negative σ-π parameter resulting from increased hyperconjugation. The sign of ^4J(C,F) is likely negative. INDO FPT MO calculations garner further support for this conclusion (see Tables 3.3.1 - 3.3.4 and discussion).

4.7 Solvent perturbations: qualitative trends for carbon-fluorine couplings. Qualitative comparisons with INDO FPT MO calculations.

Aromatic carbon - benzylic fluorine couplings are summarized in Table 4.1.3. The magnitude of ^4J(C,CF) increases when going from nonpolar to polar solvents in **1** to **4**. The proposed angular dependence of ^4J(C,CF) is consistent with the increased stability of **II** in polar solvents predicted by ^4J(H,CH), ^5J(C,CF), ^6J(H,CH) and ^6J(H,CF).

^3J(C,CF) decreases when moving from nonpolar to polar solvents, except for **2**, where an increase is observed. The anomalous behaviour in **2** is likely due to perturbation of ^3J(C,CF) by the *ortho* fluorine. Substituents in the *meta*- and *para*-positions have little effect on ^3J(C,CF) in benzotrifluorides[81]; thus, similar behaviour is expected for ^3J(C,CF) in the *meta*- and *para*-substituted benzyl fluoride derivatives. Since **II** is stabilized in the polar solvent, the decrease of ^3J(C,CF) in polar solvents is consistent with qualitative INDO FPT MO predictions. INDO computations qualitatively predict the atypical angular dependence of the coupling in **2**.

^2J(C,CF) are positive, and are found to decrease when going from polar to nonpolar solvents. This is also consistent with qualitative trends from INDO computations [though INDO calculations predict the incorrect sign for ^2J(C,F)]. ^1J(C,F) are definitely negative, and become more negative when going from polar to nonpolar solvents. INDO FPT MO calculations predict opposite behaviour, suggesting that additional non-contact

Table 4.1.3: Carbon-fluorine coupling constants in benzyl fluoride derivatives[a]

Compound (solv.)	^{1}J(C,CF)	^{2}J(C,CF)	^{3}J(C,CF)	^{4}J(C,CF)	^{5}J(C,CF)
1 (acetone-d6)[b]	-163.62	16.91	5.74	-1.41[c]	3.11
1 (CS_2)[b]	-170.39	17.46	5.93	-0.92	2.76
2 (acetone-d6)	-163.60	16.81	3.47	-2.94	3.97
2 (CS_2)	-169.20	17.11	3.27	-2.82	3.82
3 (acetone-d6)	-166.88	18.18	7.01	-0.33	2.13
3 (CS_2)	-173.45	18.83	7.23	-0.21	1.80
4 (acetone-d6)	-163.67	17.41	5.46	-1.71	3.47
4 (CS_2)	-170.04	18.05	5.58	-1.27	3.10

[a] Couplings are listed in Hz.

[b] From reference 23a.

[c] ^{4}J(C,CF) are likely negative. See discussion.

contributions should be considered.

It is known that increased hyperconjugative interactions result in the lengthening of C-H bonds.[86] Theoretically, this is observed for the benzylic C-F bond lengths (in **1** to **4**) calculated at the MP2/6-31G* and MP2/6-31G** levels (see Experimental Results, Figure 3.3.2). The maximum hyperconjugative interaction must take place when the benzylic C-F bond is perpendicular to the ring plane.

The CLOPPA (contributions from localized orbitals within the polarization propagator approach)[87] suggests that ^1J(C,F) are negative, since "lone pair" contributions are greater than "bond" contributions.[88] The bond contribution is positive in this case, since the magnetogyric ratios of fluorine and carbon are both positive. Since hyperconjugative interactions increase the bond length, the positive bond contribution is reduced. This trend is reproduced by INDO FPT MO calculations on all four derivatives. ^1J(C,F) becomes more negative when moving from $\phi = 0°$ to $\phi = 90°$, suggesting a reduced positive bond contribution. This reaffirms suspicions that non-contact terms may be involved in ^1J(C,F).

4.8 Molecular orbital calculations

The relative energies, dipole moments, least square fits and classical expectation values for **1** to **4** appear in Tables 3.3.1 to 3.3.24. Potential energy diagrams and molecular geometries at the MP2/6-31G** level appear in Figures 3.3.1 to 3.3.8. All bond lengths and angles were optimized except for the benzene moiety, which was held planar.

Calculated barriers range from 2.99 - 3.76 kJ mol^{-1} for benzyl fluoride, (more than twice the size of the experimental estimate by Schaefer et al. of 1.1(7) kJ mol^{-1}).[23a] Polarized, split-valence basis sets (6-31G*, 6-311G* and 6-31G**) used at the Hartree-Fock level predict **I** as the low energy conformer, opposite to what is observed in solution. Calculations using second-order Møller-Plesset (MP2) perturbation theory (6-31G* and 6-31G** bases) predict low energy conformers at 18.7° and 13.5°, respectively. The components of the theoretical potential, V/kJ $mol^{-1} = \Sigma_n V_n \sin^2(n\phi/2)$, are listed in Table 3.3.6. All basis sets predict symmetrical potentials. In all cases, V_4 contributes negatively to the barrier height, and higher order terms are generally negligible. Errors in these terms are computed to be only as high as ±0.002 kJ mol^{-1}.

Classical expectation values for $\langle \sin^2\phi \rangle$ were evaluated at 300 K with equation (4.12). Exclusion of higher order terms (i.e. V_4 and higher) does not change the values of $\langle \sin^2\phi \rangle$ significantly (changes range from 0.003 to 0.01, in either direction; these are most likely due to the relatively large V_4

$$\langle \sin^2\phi \rangle = \frac{\int_0^{\pi} \sin^2\phi \, \exp[-V(\phi)/RT] \, d\phi}{\int_0^{\pi} \exp[-V(\phi)/RT] \, d\phi} \qquad \textbf{(4.12)}$$

components).

Geometry refinement at the MP2/6-31G** level computes the benzylic C-F bond length, r(C-F), to be 1.395 Å and 1.402 Å for the planar and perpendicular conformers, respectively. Hartree-Fock calculations calculate r(C-F) values around 1.367(4) Å. Both sets of results differ from experimentally determined r(C-F) in ethyl fluoride (1.383(7) Å)[89] and estimated r(C-F) in 3-fluoro-2-methylpropene (1.382(7) Å).[90] Calculated ∠FCH and ∠HCH correspond well with experimentally determined ∠FCH in ethyl fluoride (107.3(4)°)[89] and ∠HCH in benzyl fluoride (108.8°).[63] Aromatic C-H bond lengths, which are underestimated by Hartree-Fock calculations, and slightly overestimated by MP2/6-31G* calculations, are calculated accurately at the MP2/6-31G** level. This is likely due to the combination of electron correlation and the inclusion of *p*-functions on the hydrogen atoms.[91]

Theoretical barriers for 4-fluorobenzyl fluoride range from 1.98 - 2.79 kJ mol^{-1} (Tables 3.3.19 - 3.3.23). Hartree-Fock calculations predict low energy conformers at $\phi = 0°$. MP2 calculations predict energy minima at $\phi = 24.69°$ (6-31G*) and $\phi = 21.10°$ (6-31G**). As in the case of benzyl

fluoride, the isolated molecule appears to prefer the planar conformation (contrary to experimental results in solution); however, molecular orbital calculations do predict the stabilization of **II** in the presence of the *para*-fluorine.

Barriers are two-fold and symmetrical; however, larger V_4 terms (relative to benzyl fluoride) are calculated. Neglect of four-fold and higher components does not alter the calculated expectation values significantly (Table 3.3.24). Calculated dipole moments for **4** do not vary with angle as much as those calculated for **1**.

The apparent internal potentials in 3,5-difluorobenzyl fluoride are significantly larger than those calculated for benzyl fluoride. Barriers are symmetrical, two-fold, and range from 5.35 - 7.24 kJ mol^{-1} (Tables 3.3.13 - 3.3.17). Both Hartree-Fock and MP2 calculations predict the parallel conformer as the most stable, corresponding with experimental results. The barriers are markedly larger than the experimentally derived barriers. Nonetheless, qualitative trends for stabilization of the perpendicular conformer are observed theoretically and experimentally (i.e. conformer **II** is increasingly stabilized moving from **3** to **1** to **4**).

Theoretical internal rotational potentials in **2** range from 10.66 - 12.97 kJ mol^{-1} (Tables 3.3.7-3.3.11). For all basis sets, the potentials are two-fold and symmetrical with the low energy conformer at $\phi = 90°$. Potentials for the isolated molecules are quite large compared to

experimentally determined values.

In general, geometries and potentials calculated at the 6-31G* and 6-31G** levels are very similar. The same holds true for MP2/6-31G* and MP2/6-31G** calculations. 6-311G* results are fairly distinct, possibly due to the description of the outer valence region (a "triple-split") which differs from that in the other basis sets.[91]

4.9 Theoretical study of dielectric solvent effects on rotational barriers

The strong electric field created by neighbouring solvent molecules should modify the electronic structure of a solvated molecule. The approach taken is to consider the medium surrounding the molecule as a continuum characterized by macroscopic dielectric properties.[92,93] This method stems from the Onsager reaction field model[94] in which the solute in placed in a spherical cavity with radius a_0, surrounded by a continuum with dielectric constant ε. A dipole in the solute induces a dipole in the surrounding medium, and the electric field of the solvent interacts with the molecular dipole, leading to net stabilization. In this method, specific solvent-solute interactions and higher order electric moments are not taken into account.

Calculated energies and resulting electronic structure is strongly dependent upon the size and shape of the cavity.[95,96] For simplicity, assume the cavity is spherical. The reaction field, $\boldsymbol{R}$, is proportional to the molecular dipole moment, $\boldsymbol{\mu}$

$$\boldsymbol{R} = g\boldsymbol{\mu} \qquad \textbf{(4.13)}$$

The proportionality constant g, which defines the strength of the reaction field, is given by

$$g = 2(\epsilon - 1)/(2\epsilon + 1)a_0^3 \qquad \textbf{(4.14)}$$

A SCRF-MO (self-consistent reaction field - molecular orbital) technique is used; therefore, the reaction field hamiltonian is written as

$$H_R = H_0 + H' \qquad (4.15)$$

where H_0 is the hamiltonian of the isolated molecule, and H' is the term which defines coupling between the molecular dipole operator and the electric field:

$$H' = -\hat{\boldsymbol{\mu}} \cdot \boldsymbol{R} \qquad (4.16)$$

Additional terms in the Fock matrix account for reaction field effects. The energy of the entire system is given by

$$E = \langle \Psi | H_0 | \Psi \rangle - \frac{1}{2} \boldsymbol{\mu} \cdot \boldsymbol{R} \qquad (4.17)$$

The package SCRFPAC[73,97] allows one to use an ellipsoidal cavity defined by the van der Waals' radii of atoms in the molecule. The "solvent" is chosen by simply selecting the dielectric constant of a particular solvent. Results from calculations at the 6-31G* level on **1** - **4** in acetone and CS_2 are summarized in Tables 3.3.25 - 3.3.33.

The dielectric solvent effects cause profound changes in the calculated relative energies and resulting potential functions. For benzyl fluoride, barriers are calculated as 3.57 kJ mol^{-1} in acetone and 0.727 kJ mol^{-1} in CS_2. The energy minimum in acetone is at 90°, whereas in CS_2 it lies at 30°. These results are comparable to experimentally deduced barriers of 2.7(2) kJ mol^{-1} and 0.8(2) kJ mol^{-1} in acetone-d6 and CS_2, respectively. The functions describing the internal potentials are still fairly symmetrical, but

are no longer exactly two-fold (see Figure 3.3.9).

In 2,6-difluorobenzyl fluoride, barrier sizes are heartily over-estimated, at 16.7 kJ mol^{-1} in acetone and 13.2 kJ mol^{-1} in CS_2. The calculations still qualitatively predict stabilization of **II** in the polar solvent, in agreement with experimental results. The potential functions are predominantly two-fold, with negligible higher order terms.

Barriers in 3,5-difluorobenzyl fluoride are 0.58 kJ mol^{-1} in acetone, and 4.1 kJ mol^{-1} in CS_2. Energy minima are at $\phi = 45°$ in the former and 0° in the latter. Once again, stabilization of the perpendicular conformer in the polar solvent is indicated. An increased barrier to rotation in the nonpolar solvent is predicted, in agreement with experimental results.

Finally, barriers of 4.7 kJ mol^{-1} and 0.74 kJ mol^{-1} are calculated for 4-fluorobenzyl fluoride in acetone and CS_2, respectively. Stable conformers are calculated at $\phi = 90°$ in the polar solvent and $\phi = 45°$ in the nonpolar solvent. Stabilization of the perpendicular conformer by the polar solvent is once again demonstrated.

Experimentally observed trends are qualitatively reproduced by these SCRF calculations for all four derivatives. Correct definition of exact potential shapes and sizes would likely have to take additional effects into account, such as quadrupole effects and hydrogen bonding interactions. Nonetheless, the dielectric properties of the surrounding medium obviously play a large role in determining the geometrical and electronic structures of

molecules.

4.10 INDO FPT MO calculation of spin-spin coupling constants.

Couplings between the benzylic fluorine atom and a number of ring substituents were calculated at the INDO (intermediate neglect of differential overlap) level of approximation.[76,98] Coupling constants and least squares fits for **1** - **4** are tabulated in Tables 3.4.1 - 3.4.4, and plots are shown in Figures 3.4.1 - 3.4.4.

^6J(H,CF) in **1** - **3** and ^6J(F,CF) in **4** are precisely fit to curves of type A + B $\sin^2\phi$. The six-bond couplings are written as

$$\begin{aligned} {}^6J(H,CF)_1 &= -0.07(01) - 3.12(01)\ \langle\sin^2\phi\rangle \\ {}^6J(H,CF)_2 &= \ \ 0.00(01) - 2.90(02)\ \langle\sin^2\phi\rangle \\ {}^6J(H,CF)_3 &= -0.03(01) - 2.83(01)\ \langle\sin^2\phi\rangle \\ {}^6J(F,CF)_4 &= -0.39(01) - 5.47(01)\ \langle\sin^2\phi\rangle \end{aligned} \qquad \textbf{(4.18)}$$

Insertion of experimentally determined expectation values (see Table 4.1.2) yields theoretical couplings. The functions derived from INDO calculations qualitatively predict the observed coupling constants and their solvent dependence in all cases. A comparison of theoretical and experimental couplings is given in Table 4.1.4.

Theoretical and experimental ^6J(H,CF) are of comparable size. INDO calculations predict the correct couplings for **3**, and approach the correct couplings very closely for **1** and **2** (within calculated error ranges). ^6J(F,CF) are overestimated by INDO calculations; qualitatively, the solvent dependence of the coupling is predicted.

Table 4.1.4: A comparison of INDO and experimental proton-fluorine and carbon-fluorine coupling constants (in Hz)

^6J(H,CF)	INDO	EXPT
1A	-2.04(1)	-1.800(2)
1C	-1.75(1)	-1.539(2)
2A	-2.22(6)	-2.481(1)
2C	-2.14(6)	-2.333(1)
3A	-1.19(1)	-1.161(1)
3C	-0.96(1)	-0.934(1)

(see Legend at bottom of page)

^6J(F,CF)	INDO	EXPT
4A	3.26(11)	5.591(1)
4C	2.86(11)	4.919(1)

^5J(C,CF)	INDO	EXPT
1A	6.78(3)	3.11(1)
1C	5.84(3)	2.76(1)
2A	7.10(19)	3.97(1)
2C	6.84(19)	3.82(1)
3A	4.14(3)	2.13(2)
3C	3.38(3)	1.80(1)
4A	7.10(20)	3.47(1)
4C	6.36(20)	3.10(1)

^5J(H,CF)	INDO	EXPT
1A	2.04(7)	1.164(2)
1C	1.97(7)	1.107(2)
2A	1.98(12)	1.233(1)
2C	1.97(12)	1.185(1)
4A	2.01(9)	1.118(1)
4C	1.94(9)	1.055(1)

^5J(F,CF)	INDO	EXPT
3A	0.15(23)	0.219(1)
3C	0.51(23)	0.585(1)

^4J(H,CF)	INDO	EXPT
1A	-2.96(23)	-1.961(1)
1C	-2.86(20)	-1.680(1)
3A	-2.66(18)	-1.344(1)
3C	-2.59(14)	-1.108(1)
4A	-3.01(38)	-2.053(1)
4C	-2.93(34)	-1.786(1)

^4J(F,CF)	INDO	EXPT
1A	2.56(26)	2.733(1)
1C	2.26(26)	2.631(1)

^4J(C,CF)	INDO	EXPT
1A	-5.31(22)	-1.41(1)
1C	-4.42(21)	-0.92(1)
2A	-5.95(18)	-2.94(1)
2C	-5.71(18)	-2.82(1)
3A	-2.62(23)	-0.33(1)
3C	-1.83(22)	-0.21(2)
4A	-5.60(33)	-1.71(1)
4C	-4.91(33)	-1.27(1)

Legend: The first column contains codes designating the number of the compound (1-4) and the solvent (A = acetone-d6, C = CS_2). The second column contains INDO couplings. The third column contains experimental couplings. Errors are in parentheses.

^5J(C,CF) are fit to curves of the form A + B $\sin^2\phi$. In all four derivatives, INDO calculations overestimate the magnitude of ^5J(C,F) by at least 1 Hz.

^5J(H,CF) in **1**, **2**, and **4** are fit to functions of the form A + B $\sin^2\phi$ + C $\sin^2(\phi/2)$. The expectation value of $\langle\sin^2(\phi/2)\rangle = 0.5$ for a two-fold barrier. Insertion of experimental $\langle\sin^2\phi\rangle$ yield ^5J(H,CF) which are overestimated in size, but are qualitatively correct in terms of solvent dependence. ^5J(F,CF) in **3** is fit to a similar function. Insertion of experimental $\langle\sin^2\phi\rangle$ predicts the correct magnitudes of ^5J(F,CF) in both solvents.

^4J(H,CF) are fit to functions of the form B $\sin^2\phi$ + C $\cos^2\phi$. Examination of plots in Figures 3.4.1 to 3.4.4 show that this function does not accurately fit the calculated values. This is likely due to INDO incorrectly calculating ^4J(H,CF) for the parallel conformer. This function overestimates ^4J(H,CF) in all cases; however, qualitative solvent effects on the coupling are once again reproduced.

INDO data points for ^4J(F,CF) in **2** show a strong $\sin^2\phi$ dependence; thus, the values are fit to a function of the form A + B $\sin^2\phi$. Theoretical couplings correspond very well with the experimentally observed ^4J(F,CF).

Finally, ^4J(C,CF) are fit to A + B $\sin^2\phi$ + C $\sin^2(\phi/2)$. In all four derivatives, the magnitude of the coupling constant is overestimated.

Theoretical couplings qualitatively reproduce the solvent dependence

of all of the coupling constants. Unfortunately, INDO calculations do not yield the correct values for most carbon-fluorine couplings and a majority of the fluorine-proton couplings. Surprisingly, and perhaps fortuitously, ^{4}J(F,CF) and ^{5}J(F,CF) are calculated accurately. In the future, accurate rendering of the correct couplings will depend on the re-parameterization of the INDO scheme for calculation of coupling constants, or extension of *ab initio* methods to substituted aromatic systems.

5. Suggestions for future research

Suggestions for future research

This thesis is only a starting point for the study of internal rotational potentials in benzyl fluoride derivatives. Further analyses of the NMR spectral parameters of **2**, **3**, and **4** in a large number of solvents would allow for the estimation of barriers in the vapour phase. The correspondence between theory and experiment in this work is quite remarkable; accordingly, it would be of great interest to extend this study to similar systems. As well, computational work should be continued on the systems described herein.

Methyl substituted benzyl fluoride systems would provide an interesting contrast to the fluorine substituted systems.

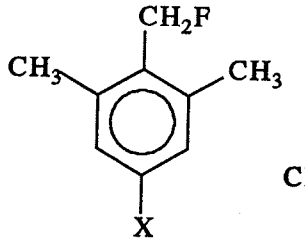

5

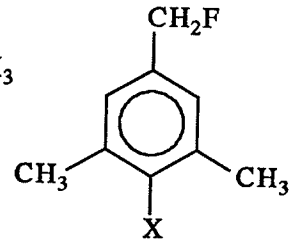

6

Synthesis of the *ortho*-disubstituted benzyl fluoride, **5** (X = H,F), would allow the study of a sterically hindered benzyl fluoride derivative without strongly perturbing fluorine atoms in the *ortho*-positions. Similarly, **6** has methyl groups in the *meta* positions, which would likely have markedly different effects on the shape and size of the internal potential.

The substitution of fluorine atoms in the *para*-position would also have notable effects on the barrier size. Adcock and Abeywickrema suggest a synthesis for **5** (X = H), which could probably be attempted for **6** as well as the *para*-fluorine substituted analogues.[51] Substitution of *t*-butyl groups in *ortho*- and *meta*-positions would also be of interest.

A large factor in the barrier sizes in all of the benzyl fluoride derivatives is the proximity of the benzylic fluorine and C-F bond to the aromatic system. In **2**, steric effects predominate; similarly, electrostatic interactions between *ortho* hydrogens and the benzylic fluorine may play a large role in determining the nature of the internal potential in **3**. It would be of interest to extend the sidechain in such a way that the CH_2F group is distanced from the ring, while still permitting the measurement of long-range couplings between the sidechain and the aromatic system. This could be accomplished by the synthesis of a propynyl system, pictured below.

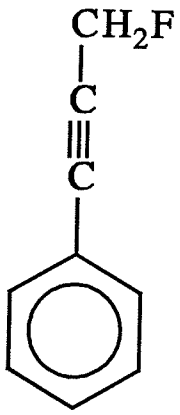

7

The synthesis of this system is potentially quite difficult (strong fluorinating agents may have some effect on the triple bond). If such systems can be synthesized, full spectral analyses would provide further insight into the nature of long-range coupling mechanisms, as well as substituent and solvent effects on rotational barriers. Similar work has been conducted on phenylpropynal and phenylpropyne.[14f]

With the increased computing power now available, further high-level computational studies should be undertaken. MP4 and configuration interaction (CI) calculations should be attempted for all of the derivatives. Computations where the benzene moiety is not constrained would also be of great interest. At the 6-31G* level, preliminary calculations on the un-constrained-planar benzyl fluoride show that the energy difference between planar and perpendicular conformers is not significantly different from the constrained-planar calculations. However, the geometry of the planar conformer shows some twisting of dihedral angles in the aromatic system. Extension of these calculations in greater detail and with larger basis sets may provide additional theoretical information of import.

Preliminary calculations of dielectric solvent effects unambiguously demonstrate the importance of the surrounding medium on the electronic properties of molecules. The qualitative correspondence between theory and experiment is extraordinary. Further calculations with larger basis sets should be attempted.

6. References

1. D.G. Lister, J.N. Macdonald, N.L. Owen. Internal Rotation and Inversion - An Introduction to Large Amplitude Motions in Molecules, Academic Press (1978)

2. W.J. Orville-Thomas. Internal rotation in molecules, John Wiley & Sons Ltd. (1974)

3. W.J. Hehre, J.A. Pople, A.J.P. Devaquet. *J. Am. Chem. Soc.*, **78**, 664 (1976)

4. P.N. Ghosh, T.K. Ha. *J. Mol. Structure (Theochem)*, **206**, 287 (1990)

5. T. Schaefer, R. Sebastian, F.E. Hruska. *Chem. Phys. Lett.*, **189**, 252 (1991)

6. C.R. Quade. *J. Chem. Phys.*, **48**, 5490 (1968)

7. W. Caminati, G. Cazzoli, A.M. Mirri. *Chem. Phys. Lett.*, **31**, 104 (1975)

8. D.G. Lister, N.L. Owen. *J. Chem. Soc. Faraday Trans. II*, **69**, 1304 (1973)

9. D. Schwoch, H.D. Rudolph. *J. Mol. Spectrosc.*, **57**, 47 (1975)

10. J.I. Seeman, J.B. Paine, H.V. Secor, H.S. Im, E.R. Bernstein. *J. Am. Chem. Soc.*, **114**, 5269 (1992)

11. S. Li, E.R. Bernstein, H.V. Secor, J.I. Seeman. *Tetrahedron Lett.*, **32**, 3945 (1991)

12. H.S. Im, E.R. Bernstein, H.V. Secor, J.I. Seeman. *J. Am. Chem. Soc.*, **113**, 4422 (1991)

13. W.J.E. Parr, T. Schaefer. *Acc. Chem. Res.*, **13**, 400 (1980)

14. a) W.J.E. Parr, T. Schaefer. *Can. J. Chem.*, **55**, 557 (1977)

b) T. Schaefer, R.P. Veregin, R. Laatikainen, R. Sebastian, K. Marat, J.L. Charlton. *Can. J. Chem.*, **60**, 2611 (1982)

c) T. Schaefer, L. Kruczynski, W. Niemczura. *Chem. Phys. Lett.*, **38**, 498 (1976)

d) T. Schaefer, R. Sebastian, G.H. Penner. *Can. J. Chem.*, **63**, 2597 (1985)

e) T. Schaefer, R. Sebastian, G.H. Penner, S.R. Salman. *Can. J. Chem.*, **64**, 1602 (1986)

f) T. Schaefer, R. Sebastian, R.W. Schurko. *Can. J. Chem.*, **70**, 2365 (1992)

15. R.A. Hoffman. *Mol. Phys.*, **1**, 326 (1958)

16. M. Barfield, R. Chakrabarti. *J. Am. Chem. Soc.*, **91**, 4346 (1969)

17. H.M. McConnell. *J. Mol. Spectrosc.*, **1**, 11 (1957)

18. T. Schaefer, W. Niemczura, K. Marat. *J. Chem. Soc. Faraday II*, 1526 (1975)

19. J. Hilton, L.H. Sutcliffe. *Progress in Nuclear Magnetic Spectroscopy*, **10**, 27, J.W. Emsley, J. Feeney, L.H. Sutcliffe (ed.), Permagon Press (1975)

20. R. Wasylishen, T. Schaefer. *Can. J. Chem.*, **50**, 1852 (1972)

21. T. Schaefer, C.S. Takeuchi. *Can. J. Chem.*, **67**, 1022-1026 (1989)

22. P.B. Aysbrough, M.S. Brice, R.E.D. McClung. *Mol. Phys.*, **20**, 41 (1971)

23. a) T. Schaefer, C. Beaulieu, R. Sebastian, G.H. Penner. *Can. J. Chem.*, **68**, 581 (1990)

b) T. Schaefer, J. Peeling, G.H. Penner. *Can. J. Chem.*, **61**, 2773 (1983)

c) T. Schaefer, J. Peeling, G.H. Penner, A. Lemire, R. Sebastian. *Can. J. Chem.*, **63**, 24 (1985)

d) T. Schaefer, G.H. Penner. *Can. J. Chem.*, **64**, 2013 (1986)

24. T. Schaefer, C.S. Takeuchi, S.E. Sveinson. *Can. J. Chem.*, **66**, 1490 (1988)

25. C.A. Cupas, J.M. Bollinger, M. Haslanger. *J. Am. Chem. Soc.*, **90**, 5502 (1968)

26. L. Verdonck, G.P. Van der Kelen, Z. Eeckhaut. *Spectrochimica Acta*, **29A**, 813 (1973)

27. N.I. Sadova, L.V. Vilkov, I. Hargittai, J. Brunvoll. *J. Mol. Struct.*, **31**, 131 (1976)

28. K.E. Calderbank, R.J.W. LeFevre, R. Pierens. *J. Chem. Soc. B*, 1463 (1970)

29. J. DeZwaan, J. Jonas. *J. Phys. Chem.*, **77**, 1768 (1973)

30. A.J.M. Reuvers, A. Sinnema, Th. J. Nieuwstad, F. Van Rantwijk, H. Van Bekkum. *Tetrahedron*, **27**, 3713 (1971)

31. T. Schaefer, C.M. Wong, and K.C. Tam. *Can. J. Chem.*, **47**, 3688 (1969)

32. J.B. Rowbotham, A.F. Janzen, J. Peeling, T. Schaefer. *Can. J. Chem.*, **52**, 481 (1974)

33. A.F. Janzen, T.Schaefer. *Can. J. Chem.*, **49**, 1818 (1971)

34. T. Schaefer, J.B. Rowbotham, W.J.E. Parr, K. Marat, A.F. Janzen. *Can. J. Chem.*, **54**, 1322 (1976)

35. E. Gout, C. Beguin, D. Canet, J.P. Marchal. *Org. Mag. Res.*, **7**, 633 (1975)

36. C. Beguin, R. Dupeyre. *Mol. Phys.*, **32**, 699 (1976)

37. C.G. Beguin, R. Dupeyre. *J. Mag. Res.*, **44**, 294 (1981)

38. C. Beguin, E. Gout-Mallaret. *J. Fluorine Chem.*, **8**, 279 (1976)

39. W.J. Hehre, L. Random, J.A. Pople. *J. Am. Chem. Soc.*, **94**, 1496 (1972)

40. M.J. Shapiro. *J. Org. Chem.*, **41**, 3197 (1976)

41. G.A. Crowder, M.J. Townsend. *J. Fluorine Chem.*, **10**, 181 (1977)

42. R.J. Abraham, R.A. Hearman, M. Trætteberg, P. Bakken. *J. Mol. Struct.*, **57**, 149 (1979)

43. R.T.C. Brownlee, D.J. Craik. *Tetrahedron Lett.*, **21**, 1681 (1980)

44. I. Fleming. Frontier Orbitals and Organic Chemical Reactions, John Wiley & Sons (1978) [As cited in reference 43]

45. L. Radom, W.J. Hehre, J.A. Pople, G.L. Carlson, W.G. Fately. *Chem. Comm.*, 308 (1972)

46. D.A.R. Happer, B.E. Steenson, R.H. Newman. *Org. Mag. Res.*, **21**, 252 (1983)

47. G. Distefano, A. Modelli, M. Guerra, D. Jones, S. Rossini. *J. Mol. Struct.*, **174**, 177 (1988)

48. T. Schaefer, W. Danchura, W. Niemczura, J. Peeling. *Can. J. Chem.*, **56**, 2442 (1978)

49. T. Schaefer, W. Niemczura, C.M. Wong, K. Marat. *Can. J. Chem.*, **57**, 807 (1979)

50. T. Schaefer, W.P. Niemczura, R. Sebastian, L.J. Kruczynski, W. Danchura. *Can. J. Chem.*, **58**, 1178 (1980)

51. W. Adcock, A.N. Abeywickrema. *Aust. J. Chem.*, **33**, 181 (1980)

52. W. Adcock, A.N. Abeywickrema. *Tetrahedron Lett.*, **20**, 1809 (1979)

53. W. Adcock, A.N. Abeywickrema. *Aust. J. Chem.*, **34**, 1253 (1981)

54. J.C. Facelli, C.G. Giribet, R.H. Contreras. *Org. Mag. Res.*, **19**, 138 (1982)

55. L. Ernst, S. Pulmann. *Org. Mag. Res.*, **16**, 63 (1981)

56. D.A. Burgess, I.D. Rae. *Aust. J. Chem.*, **30**, 1611 (1977)

57. I.D. Rae, D.A. Burgess, S. Bombaci, M.L. Baron, M.L. Woolcock. *Aust. J. Chem.*, **37**, 1437 (1984)

58. T. Schaefer, J. Peeling, R. Sebastian. *Can. J. Chem.*, **63**, 3219 (1985)

59. For a general description of the anomeric effect: F.A. Carey, R.J. Sundberg. Advanced Organic Chemistry Part A: Structure and Mechanisms, pp. 100-103, Plenum Publishing Corporation, New York (1980)

60. G.H. Penner, T. Schaefer, R. Sebastian, S. Wolfe. *Can. J. Chem.*, **65**, 1845 (1987)

61. S.A. Sorenson, N.S. True. *J. Mol. Struct.*, **263**, 21 (1991)

62. G. Celebre, M. Longeri, J.W. Emsley. *Mol. Phys.*, **64**, 715 (1988)

63. G. Celebre, G. De Luca, M. Longeri, J.W. Emsley. *Mol. Phys.*, **67**, 239 (1989)

64. T. Schaefer, J.R. Mansfield, F.E. Hruska, R. Sebastian. *Can. J. Chem.*, **70**, 1750 (1992)

65. T. Schaefer, R. Sebastian, G.H. Penner. *Can. J. Chem.*, **64**, 1372 (1986)

66. a) W.A. Sheppard, C.M. Sharts (ed.). Organic Fluorine Chemistry, W.A. Benjamin, Inc., New York (1969)

b) R.E. Banks, M.G. Barlow. *Fluorocarbon and Related Chemistry*, **1**, Chapter 5, The Chemical Society, London (1971)

c) R.D. Chambers. Fluorine in Organic Chemistry, John Wiley & Sons (1973)

d) A. Skancke, Fluorine-containing molecules: structure, reactivity, synthesis and applications, J.F. Lieberman, A. Greenberg, W.R. Dolbier (ed.), Chapter 3, VCH Publishers, Inc. (1988)

67. a) J.W. Emsley, L. Phillips, V. Wray. Fluorine Coupling Constants, Pergamon Press (1977)

b) P.E. Hansen, A. Berg, H.J. Jakobsen, A.P. Manzara, J. Michl. *Org. Mag. Res.*, **10**, 179 (1977)

c) W.S. Brey, L.W. Jaques, H.J. Jakobsen. *Org. Mag. Res.*, **12**, 243 (1979)

d) S. Suntioinen, R. Laatikainen. *Mag. Res. Chem.*, **30**, 415-419 (1992)

e) R.E. Wasylishen, M. Barfield. *J. Am. Chem. Soc.*, **97**, 4545 (1975)

68. P.A. Messina, K.C. Mange, W.J. Middleton. *J. Fluorine Chem.*, **42**, 137 (1989)

69. Two very helpful articles on shimming NMR magnets:

a) G.N. Chmurny, D.I. Hoult. *Concepts in Mag. Res.*, **2**, 131 (1990)

b) G.A. Pearson, Shimming an NMR Magnet, University of Iowa, G.A. Pearson © (1993)

70. K. Marat, University of Manitoba (© 1991, 1992, 1993)

71. J.S. Martin, A.R. Quirt, K.E. Worvill. The NMR program library, Daresbury Laboratory, Daresbury, U.K. (Extensively modified by R. Sebastian, University of Manitoba)

72. M. J. Frisch, G. W. Trucks, M. Head-Gordon, P. M.W. Gill, M. W. Wong, J.B. Foresman, B. G. Johnson, H. B. Schlegel, M. A. Robb, E. S. Replogle, R. Gomperts, J. L. Andres, K. Raghavachari, J. S. Binkley, C. Gonzalez, R.L. Martin, D. J. Fox, D. J. Defrees, J. Baker, J. J. P. Stewart, J. A.Pople. Gaussian 92, Revision C, Gaussian, Inc., Pittsburgh PA, (1992)

73. D. Rinaldi, R.R. Pappalardo. SCRFPAC: A Self-Constsitent Reaction Field PACkage, *QCPE*, **622** (1992)

74. a) A.A. Ray (ed.). SAS User's Guide: Statistics, Statistical Analysis System Institute (1985)

b) K.A. Council, J.T. Helwig, (ed.). SAS/Graph User's Guide, Statistical Analysis System Institute (1985)

75. a) Maple V Release 2, Waterloo Maple Software, University of Waterloo (© 1981-1993)

b) B.W. Char, K.O. Geddes, G.H. Gonnet, B.L. Leong, M.B. Monagan, S.M. Watt. First Leaves: A Tutorial Introduction to Maple V, Springer Verlag (1992)

76. a) J.A. Pople, D.L. Beveridge, P.A. Dobosh. *J. Chem. Phys.*, **47**, 2026 (1967)

b) P.A. Dobosh, N.S. Ostlund. *QCPE*, **11**, 281 (1975)

c) J.A. Pople, J.W. McIver, Jr., N.S. Ostlund. *J. Chem. Phys.*, **49**, 2960 (1968)

77. T. Schaefer, R. Sebastian, R.P. Veregin, R. Laatikainen. *Can. J. Chem.*, **61**, 29 (1983)

78. C.W. Haigh, J. Hilton, L.H. Sutcliffe, G.J.T. Tiddy. *J. Mag. Res.*, **18**, 241 (1975)

79. R. Wasylishen, T. Schaefer. *Can. J. Chem.*, **49**, 95 (1971)

80. T. Schaefer, J. Peeling, G.H. Penner. *Can. J. Chem.*, **64**, 2162 (1986)

81. T. Schaefer, K. Marat, J. Peeling, R.P. Veregin. *Can. J. Chem.*, **61**, 2779 (1983)

82. M. Barfield, C.J. Fallick, K. Hata, S. Sternhell, P.W. Westerman. *J. Am. Chem. Soc.*, **105**, 2178 (1983)

83. H.M. McConnell. *J. Chem. Phys.*, **30**, 126 (1959)

84. M.J.S. Dewar, R.C. Fahey. *J. Am. Chem. Soc.*, **85**, 2704 (1963)

85. T. Schaefer, J.B. Rowbotham. *Can. J. Chem.*, **54**, 2243 (1976)

86. A. Pross, L. Radom, N.V. Riggs. *J. Am. Chem. Soc.*, **102**, 2253 (1980)

87. a) A.C. Diz, C.G. Giribet, C.C. Ruiz de Azua, R.H. Contreras. *Int. J. Quantum Chem.*, **37**, 663 (1990)

b) R.H. Contreras, M.C. Ruiz de Azua, C.G. Giribet, G.A. Aucar, R. Lobayan de Bonczok. *J. Mol. Struct. (Theochem)*, **284**, 249 (1993)

88. R.H. Contreras, J.C. Facelli. *Ann. Reports on NMR Spec.*, **27**, 255 (1993)

89. P. Nosberger, A. Bauder, Hs. H. Günthard. *Chem. Phys.*, **1**, 418 (1973)

90. J.R. Durig, H.Z. Qiu, D.T. Durig, M. Zhen, T.S. Little. *J. Phys. Chem.*, **95**, 2745 (1991)

91. Two comprehensive references on molecular orbital theory:

a) W.J. Hehre, L. Radom, P.v.R. Schleyer, J.A. Pople. Ab Initio Molecular Orbital Theory, John Wiley & Sons (1986)

b) J.B. Foresman, A. Frisch. Exploring Chemistry with Electronic Structure Methods: A Guide to Using Gaussian, Gaussian, Inc. Pittsburgh (1993)

92. J.-L. Rivail, D. Rinaldi. *Chem. Phys.*, **18**, 233 (1976)

93. D. Rinaldi, M.F. Ruiz-Lopez, J.-L. Rivail. *J. Chem. Phys.*, **78**, 834 (1983)

94. L. Onsager. *J. Am. Chem. Soc.*, **58**, 1486 (1936)

95. S. Miertus, E. Scrocco, J. Tomasi. *Chem. Phys.*, **55**, 117 (1981)

96. M.W. Wong, M.J. Frisch, K.B. Wiberg. *J. Am. Chem. Soc.*, **113**, 4776 (1991)

97. E. Sanchez-Marcos, R.R. Pappalardo, D. Rinaldi. *J. Phys. Chem.*, **95**, 8928 (1991)

98. J.A. Pople, D.L. Beveridge. Approximate Molecular Orbital Theory, McGraw-Hill, Inc. (1967)